LAPPEENRANTA UNIVERSITY OF TECHNOLOGY
Faculty of Technology
Mechanical Engineering

Minna Salkinoja

THE PLASTIC CAPACITY OF BOILER SUPPORTING HEADERS

Examiners: Professor Timo Björk
M. Sc. (Tech.) Heikki Holopainen

ABSTRACT

Lappeenranta University of Technology
Faculty of Technology
Mechanical Engineering
Steel Structures

Minna Salkinoja

The Plastic Capacity of Boiler Supporting Headers

Master's Thesis

2011

97 pages, 52 figures, 3 tables and 5 appendices

Examiners: Professor Timo Björk
M. Sc. (Tech.) Heikki Holopainen

Keywords: Plastic design, header, virtual work, plasticity

The goal of this thesis was to make a dimensioning tool to determine the plastic capacity of the boiler supporting header. The capacity of the header is traditionally determined by using FE-method during the project phase. By using the dimensioning tool the goal is to ensure the capacity already in the proposal phase.

The study began by analyzing the headers of the ongoing projects by using FE-method. For the analytical solution a plain header was analyzed without the effects of branches or lug. The calibration of parameters in the analytical solution was made using these results.

In the analytical solution the plastic capacity of the plastic hinges in the header was defined. The stresses caused by the internal pressure as well as the normal and shear forces caused by the external loading reduced the plastic moment. The final capacity was determined by using the principle of virtual work. The weakening effect of the branches was taken into account by using pressure areas. Also the capacity of the punching shear was defined.

The results from the FE-analyses and the analytical solution correlate with each other. The results from the analytical solution are conservative but give correct enough results when considering the accuracy of the used method.

TIIVISTELMÄ

Lappeenrannan teknillinen yliopisto
Teknillinen tiedekunta
Konetekniikka
Teräsrakenteet

Minna Salkinoja

Kattilaa kannattelevien kammioiden plastinen kestävyys

Diplomityö

2011

97 sivua, 52 kuvaa, 3 taulukkoa ja 5 liitettä

Tarkastajat: Professori Timo Björk
DI Heikki Holopainen

Hakusanat: Plastinen mitoitus, kammio, virtuaalinen työ, plastisuus
Keywords: Plastic design, header, virtual work, plasticity

Työn tarkoituksena oli laatia mitoitustyökalu, jonka avulla voidaan määrittää voimalaitoskattilaa kannattelevan kammion plastinen kantokyky. Kammioiden riittävä kantokyky on perinteisesti varmistettu projektivaiheessa käyttäen FE-menetelmää. Mitoitustyökalun avulla on tarkoitus saada varmistettua riittävä kammion kestävyys jo tarjousvaiheessa.

Tutkimus aloitettiin analysoimalla yhtiössä käynnissä olevien projektien kammioita FE-menetelmällä. Analyyttistä mallia varten tutkittiin myös yksinkertaistettua kammiota ilman yhteiden tai korvakkeiden vaikutuksia. Näillä tuloksilla pystyttiin kalibroimaan analyyttisen ratkaisun parametreja.

Analyyttisessä ratkaisussa määritettiin kammioon syntyvien plastisten nivelten plastinen momentti. Tätä varten tuli ottaa huomioon sisäisestä paineesta aiheutuvat jännitykset sekä ulkoisesta kuormituksesta aiheutuvat normaali- ja leikkausvoimat. Lopullinen kantokyky määritettiin virtuaalisen työn perusteella. Yhteiden heikentävä vaikutus otettiin huomioon käyttäen painealoja. Myös leikkauskriittinen rakenne määritettiin.

Tulokset FE-malleista sekä analyyttisestä ratkaisusta korreloivat toisiaan. Analyyttisen ratkaisun tulokset ovat konservatiivisia, mutta antavat menetelmän tarkkuuteen nähden riittävän hyviä tuloksia.

PREFACE

I would like to give my special thanks to Professor Timo Björk for the help during the thesis and all my studies. I would also like to thank my supervisor Heikki Holopainen for the ideas and help given for the thesis. Thanks also to the whole Boiler Structural Engineering department for the support in all my work in the company.

My sincere gratitude I give to my parents, brother and sister for the help and support for my studies. Special thanks to Simo Jutila and Ritva Korhonen for proofreading of the thesis.

Many thanks to my dear friends for all the unforgettable years in Lappeenranta. I thank my fiancé for the help during the thesis but especially helping me to put my studies in its true scale.

Varkaus, April 20th 2011
Minna Salkinoja

CONTENTS

ABSTRACT
TIIVISTELMÄ
PREFACE
CONTENTS 5
SYMBOLS AND ABBREVIATIONS 8
1 INTRODUCTION 10
1.1 Goals of the Thesis 11
1.2 Boundaries of the Thesis 11
1.3 Foster Wheeler Energy Oy Group 11
2 PLASTICITY 12
2.1 Yield Criterion 12
2.1.1 Principal Stresses 12
2.1.2 Tresca's Yield Criterion 15
2.1.3 Von Mises' Yield Criterion 16
2.1.4 Comparing the Yield Criterions 16
2.2 Material Models 17
2.3 True Stress – True Strain Relation 20
2.4 Loading Criterion and Flow Rule 21
2.5 Factor of Safety 23
3 PLASTIC DESIGN 25
3.1 Evaluation of the Fully Plastic Moment 26
3.1.1 Effect of Normal Force 28
3.1.2 Effect of Shear Force 29
3.2 Principle of Virtual Work 30
3.3 Yield Line Theory of Plates 31
4 BASICS OF FINITE ELEMENT METHOD 32
4.1 Linear Analysis 33
4.2 Nonlinear Analysis 33
4.2.1 Geometric Nonlinearity 34
4.2.2 Boundary Nonlinearity 35

4.2.3 Material Nonlinearity 36
5 HEADERS IN STANDARDS 37
5.1 Design Stress 37
5.2 Structural Attachments 38
5.3 Design by Analysis 41
5.3.1 Design by Analysis According to EN 12952-3 and EN 13445-3 41
5.3.2 DBA According to ASME 2010 Section VIII 43
5.3.3 Conflicts in Standards 44
6 ANALYSES 45
6.1 Finite Element Analysis 46
6.1.1 Material Model 46
6.1.2 Safety Factors for Loads 46
6.1.3 Design Stress 48
6.1.4 Boundary Conditions and Mesh 51
6.2 Analytical Solution 55
6.2.1 Stresses caused by Internal Pressure 56
6.2.2 Circumferential Strength and the Effects of Normal and Shear Forces 57
6.2.3 Plastic Moment 62
6.2.4 Principle of Virtual Work 65
6.2.5 Effect of Branches 67
6.2.6 Punching Shear 69
7 RESULTS 71
7.1 Results from the Finite Element Analyses 72
7.1.1 Plain Header 72
7.1.2 Header with Wall Panel and Roof Panel 75
7.2 Results from Analytical Solutions 78
7.2.1 Variable Length of the Plastic hinge 78
7.2.2 Constant Length of the Plastic Hinge 80
7.2.3 Punching Shear 82
7.2.4 Header with Roof and Wall Panels 83
8 DISCUSSION 86
8.1 Analyzing Headers According to Standards 86

8.2 Differences in the FE-models and Analytical solution 87
8.2.1 Differences in Analyzing Plain Header 87
8.2.2 Differences in punching shear. 88
8.2.3 Effect of Branches 89
8.3 Suggestions for Further Research 89
9 CONCLUSIONS 91
10 SUMMARY 93
REFERENCES 95
APPENDIX I. EXAMPLE CALCULATIONS ACCORDING TO EN 12952-3, CHAPTER 11.5
APPENDIX II. DEDUCION OF PLASTIC MOMENT
APPENDIX III. PRINCIPLE OF WIRTUAL WORK
APPENDIX IV. THE EFFECT OF BRANCHES
APPENDIX V. PUNCHING SHEAR

SYMBOLS AND ABBREVIATIONS

a	constant
A	cross-sectional area
b	constant
B	auxiliary variable
c_1	minus tolerance on the ordered nominal wall thickness
d	diameter
e	wall thickness
E	Young's modulus
E_t	Tangent modulus
f	calculation strength
f_φ	circumferential strength after shear and pressure reductions
f_{MAWS}	maximum allowed working stress
k	constant
L	length
L_H	length of plastic hinge
M	bending moment
M_p	plastic moment
n	constant
p_c	calculation pressure
R	bending radius of a curved beam
R_m	tensile stress
$R_{p0.2/t}$	yield stress
$R_{p0.1/T/t}$	creep strain
$R_{m/T/t}$	creep rupture
α	angle of roof
γ	safety factor
δ	displacement
ε	strain
θ	angle variable
λ	scalar to be determined
σ	stress

σ_0	yield stress
σ_1, σ_2, σ_3	principal stresses, so that $\sigma_1 > \sigma_2 > \sigma_3$
σ_r	radial stress caused by internal pressure
σ_z	longitudinal stress caused by internal pressure
σ_φ	circumferential stress caused by internal pressure
τ	shear stress
τ_0	yield stress in pure shear
DOF	degree of freedom
E.A.A	equal area axis
FEM	finite element method
N.A	neutral axis

Subscripts not determined earlier

a	actual value
b	refers to branch generally
i	inside
m	mean value
M	refers to bending moment
max	maximum value
min	minimum value
n	nominal value
N	refers to normal force
o	outside
p	refers to connecting pipe
r	refers to roof tube
s	refers to header
T	lifetime
t	temperature
w	refers to wall tube
τ	refers to shear

1 INTRODUCTION

Temperatures reach several hundred degreed in large boilers, thus thermal expansion is significant. This is why the furnace, the convection cage and some other parts of the boiler are usually supported from the top and they are hanging from the steel structure. Figure 1-1 shows an example of a hanger rod supported furnace. Loads go from the hanger rod through the lugs and the header to the wall panel. Dimensioning of the wall panel, the hanger rod and the lugs are relatively simple but ensuring the capacity of a header is more complicated. Previously this design check has been made with finite element method (FEM) but this process needs simplification, thus a dimensioning tool was created.

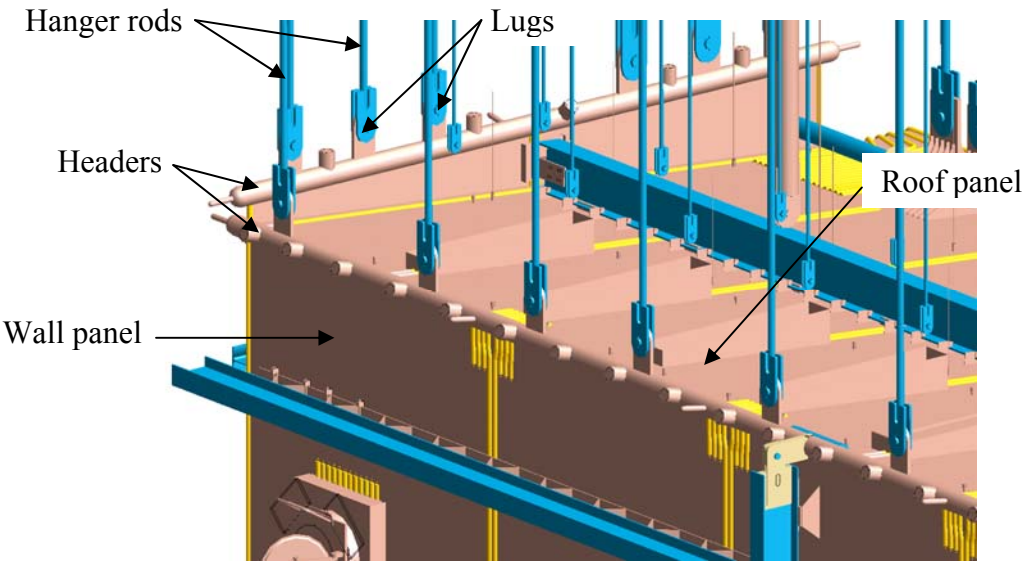

Figure 1-1. A furnace supported with hanger rods.

A header is basically a relatively large and thick walled pipe with different size of branches. Its purpose is to distribute or gather water and steam from the wall panel to the connecting pipes or the other way around. Hanging from the header is basically a secondary purpose, although a very essential purpose considering the header as a load carrying structure.

1.1 Goals of the Thesis

The main goal in this thesis is to create a dimensioning tool that is quicker to use than finite element analysis. The internal pressure alone may cause plastic deformations in a header and in these cases elastic dimensioning is conservative. This is the main reason why plastic capacity is taken under consideration. If a FE-model is to be made, plastic capacity will be used.

The dimensioning tool is supposed to be simple to use so that no more FE-analysis will be needed in basic situations. Therefore the header's capacity can be checked in early proposal phase and possible changes in material orders will not be needed during the project phase.

1.2 Boundaries of the Thesis

Because the main goal is to make a dimensioning tool, research is needed and results from hand calculations are calibrated with the FE-analysis.

Design checks for the hanger rod and the lugs' capacities are not included in this thesis. The panel hanging capacity is checked in the FE-models, because the panel is modeled and checking is natural, but the design check is bounded out from the final dimensioning tool. The focus is in the steels other than austenitic because they are commonly used. Thus austenitic steels are bounded out.

The FE-analysis is still used in earthquake projects and those special cases are therefore not included in this thesis.

1.3 Foster Wheeler Energy Oy Group

This Master's Thesis was made for Foster Wheeler Energy Oy in Varkaus. The Foster Wheeler Energy Oy Group (FWEOY Group) is a specialist in eco-aware energy generation and an expert in power and industrial boilers and boiler maintenance and service.

A high-efficiency, low-emission fluidized bed technology – and in particular the circulating fluidized bed (CFB) – lie at the heart of the company's know-how. Foster Whee-

ler is the world's leading supplier of CFB boilers, with approximately 40% share of the market.

The FWEOY Group operates in Finland, at Espoo and Varkaus, and has subsidiaries in Sweden and Germany. The Group employs around 520 people, of which some 500 are based in Finland. In 2008 net sales totaled 340 million Euros and were generated by 26 projects in 14 countries.

2 PLASTICITY

General concepts of plasticity are discussed in this chapter. For example the concepts of yield criteria are covered. Material behaviors, flow rule and safety factors are also discussed.

2.1 Yield Criterion

Suppose that an element of material is subjected to a system of stresses. The stresses are gradually increasing magnitude. The initial deformation of the element is entirely elastic and the original shape of the element is recovered after complete unloading. For certain combinations of applied stresses, plastic deformation first appears in the element. This limit is called the yield criterion, a law defining the limit of elastic behavior under any possible combination of stresses. In developing mathematical theory, it is necessary to take into account a number of idealizations such as, the material is assumed to be isotropic, so that its properties are the same at all points. (Chakrabarty 1987, p. 55.)

2.1.1 Principal Stresses

Stress is simply a distributed force on an internal or external surface of a body. Consider a stress element shown in Figure 2-1, where the surfaces on which the distributed load affects are selected to be mutually perpendicular. (Young, Budynas 2002, p. 9, 12.)

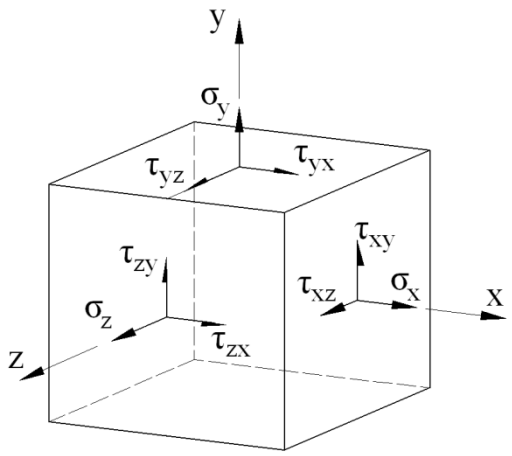

Figure 2-1. Stress element relative to *xyz*-axis (Young, Budynas 2002, p. 18).

This state of stress can be written in a matrix form

$$\sigma = \begin{bmatrix} \sigma_x & \tau_{xy} & \tau_{xz} \\ \tau_{yx} & \sigma_y & \tau_{yz} \\ \tau_{zx} & \tau_{zy} & \sigma_z \end{bmatrix}, \tag{1}$$

where σ is the stress matrix, σ is normal stress and τ is shear stress. (Young, Budynas 2002, p. 13.)

In many practical problems the stresses in one direction are zero. This case is called plane stress. If the z-direction is chosen to be stress free with $\sigma_z = \tau_{xz} = \tau_{zx} = 0$. The stress matrix can be written as

$$\sigma = \begin{bmatrix} \sigma_x & \tau_{xy} \\ \tau_{yx} & \sigma_y \end{bmatrix} \quad . \tag{2}$$

The corresponding stress element is shown in Figure 2-2. (Young, Budynas 2002, p. 13.)

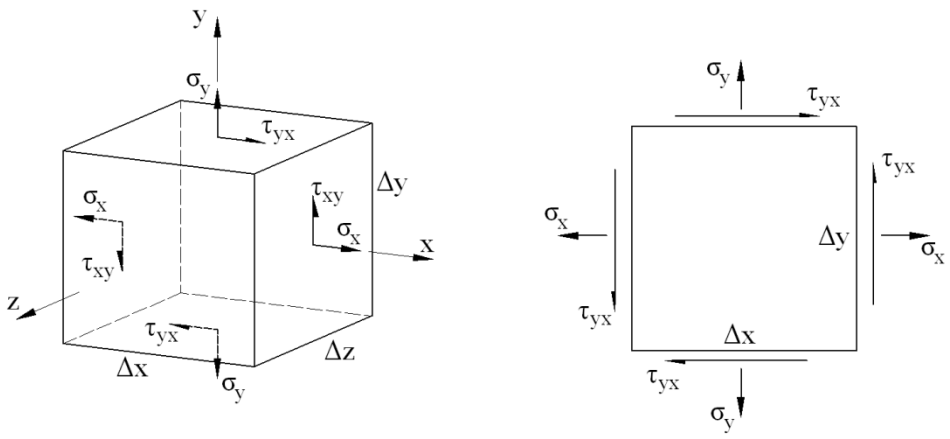

Figure 2-2. Plane stress element (Young, Budynas 2002, p. 14).

In general the minimum and maximum values of normal stresses occur on surfaces where the shear stresses are zero. These stresses are called the principal stresses and they are actually the eigenvalues of the stress matrix:

$$\begin{bmatrix} \sigma_x - \sigma_p & \tau_{xy} & \tau_{xz} \\ \tau_{yx} & \sigma_y - \sigma_p & \tau_{yz} \\ \tau_{zx} & \tau_{zy} & \sigma_z - \sigma_p \end{bmatrix} = 0 \quad , \tag{3}$$

where σ_p is a principal stress. Three principal stresses exist, σ_1, σ_2 and σ_3, and they are commonly ordered $\sigma_1 \geq \sigma_2 \geq \sigma_3$. Principal stresses in a stress element are shown in Figure 2-3. (Young, Budynas 2002, p. 24.)

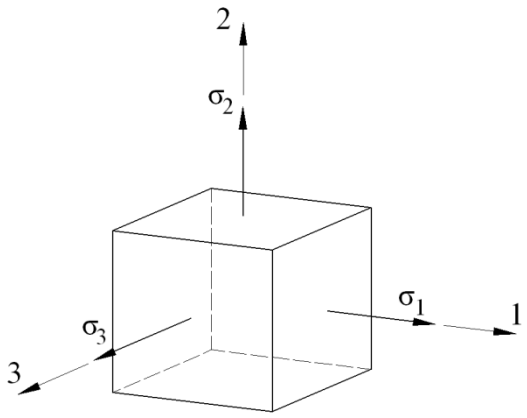

Figure 2-3. Principal stresses (Young, Budynas 2002, p. 29).

When principal stresses have been determined using the methods described for example by Young and Budynas (2002), in a plane stress case i.e., $\sigma_1 \neq 0$, $\sigma_2 \neq 0$, $\sigma_3=0$ and $\sigma_1 \geq \sigma_2$, the maximum shear stress is on surface ±45° from the two principal stresses. On these surfaces, the maximum shear stress would be one-half of the difference of the principal stresses. Considering the three principal axes, the three maximum shear stresses would be referred to as the principal shear stresses. Since the principal stresses are commonly ordered $\sigma_1 \geq \sigma_2 \geq \sigma_3$, the maximum shear stress is given by the difference of the maximum and minimum of the principal stresses. The equation is written as

$$\tau_{\max} = \frac{\sigma_1 - \sigma_3}{2} \quad . \tag{4}$$

(Young, Budynas 2002, p. 29-30.)

2.1.2 Tresca's Yield Criterion

Tresca (1864) found out that plastic deformation starts to occur in metals when the maximum shear stress reaches the value of yield stress in pure shear, i.e. using equation (4), if

$$|\tau_{\max}| = \frac{1}{2}|\sigma_1 - \sigma_3| = \tau_{0.\mathrm{Tresca}} \quad , \tag{5}$$

where $\tau_{0.\mathrm{Tresca}}$ is the yield stress in pure shear. This theory is also called the maximum shear stress theory. In the principal stress plane σ_1–σ_2 this represented by a hexagon shown in Figure 2-4. (Kaliszky 1989, p. 65-66.)

The material constant may be determined by a simple tension test, then

$$\tau_{0.\mathrm{Tresca}} = \frac{\sigma_0}{2} \quad , \tag{6}$$

where σ_0 is the yield stress. The material yields also if one of the principal stresses reaches the yield stress. (Chen, Han 1988, p. 74.)

Generally, if the principal stresses are not in order $\sigma_1 \geq \sigma_2 \geq \sigma_3$, combining the equations (5) and (6) the Tresca's yield criterion can be written as

$$\sigma_0 = MAX\ [|\sigma_1|, |\sigma_2|, |\sigma_3|, |\sigma_1 - \sigma_2|, |\sigma_2 - \sigma_3|, |\sigma_1 - \sigma_3|] \ . \tag{7}$$

2.1.3 Von Mises' Yield Criterion

Huber (1904), von Mises (1913) and Hencky (1924) independently proposed a yield criterion that yield will occur when the specific elastic distortion energy reaches the value $\tau_0^2/(2G)$, where G is the shear modulus. This theory is called distortion energy theory and is commonly known as von Mises' yield criterion. Yield criterion can be expressed as

$$\frac{1}{6}[(\sigma_1 - \sigma_2)^2 + (\sigma_2 - \sigma_3)^2 + (\sigma_1 - \sigma_3)^2] - \tau_{0.\text{Mises}}^2 = 0 \ . \tag{8}$$

Now $\tau_{0.\text{Mises}}$ is the yield stress in pure shear and is determined as

$$\tau_{0.\text{Mises}} = \frac{\sigma_0}{\sqrt{3}} \ . \tag{9}$$

In stress plane σ_1–σ_2 the yield surface is an ellipse shown in Figure 2-4. (Kaliszky 1989, p. 63-65.)

2.1.4 Comparing the Yield Criterions

From a theoretical point of view, the main difference between the von Mises' and the Tresca's yield criterions is that in the von Mises' criterion all three principal stresses play equal roles, while in the Tresca's criterion the intermediate principal stress has no effect on yielding. A large number of experimental studies can be found in the literature that studies the difference between these yield criteria. For example Lode (1926) found out that experimental results favor the von Mises' criterion. The both yield criteria are used in the theory of the plasticity and in the engineering practice. The advantage of the von Mises' yield criterion is that it can be determined by a single function, but the dis-

advantage is that the function is not linear. The Tresca's yield criterion can be determined only by three different functions, which are, however, linear. Using three functions causes difficulties in analytical solutions. There are special problems where the orientations of the principal stresses at each point are known, and then the Tresca's yield criterion involves relatively simple calculations. (Kaliszky 1989, p. 66-67.)

Note that the yield stress in pure shear (τ_0) is defined differently in the von Mises' yield criterion and in the Tresca's yield criterion, see equations (6) and (9). If the two criteria are made to agree for a simple tension yield stress σ_0, the ratio of the yield stress in shear between the von Mises' and the Tresca's yield criteria is $2/\sqrt{3} \approx 1.15$. Graphically the von Mises' ellipse circumscribes the Tresca's hexagon as shown in Figure 2-4. (Chen, Han 1988, p. 78.)

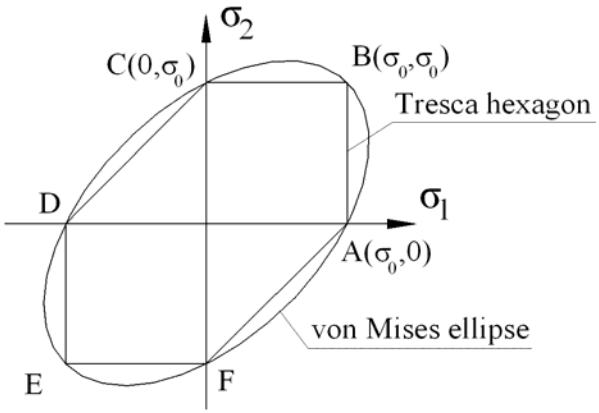

Figure 2-4. Yield criteria in stress plane $\sigma_1 - \sigma_2$ ($\sigma_3 = 0$) (Chen, Han 1988, p. 75).

2.2 Material Models

The simplest type of loading is represented by a simple tension test, for which $\sigma_1 > 0$, $\sigma_2 = \sigma_3 = 0$ (Chen, Han 1988, p. 7). Figure 2-5 shows a typical stress-strain curve response from a simple tension test. The upper yield stress has little practical significance and it is difficult to determine, therefore it is ignored in design calculations. (Davies, Brown 1996, p. 1.)

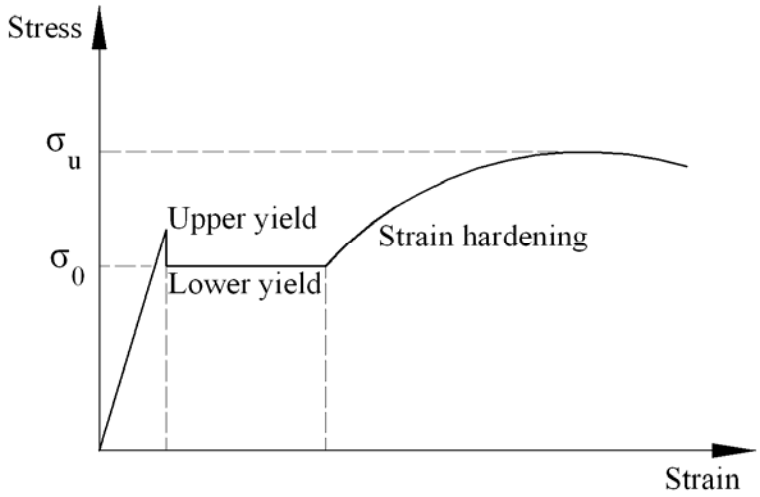

Figure 2-5. Typical stress-strain curve for mild steel (Davies, Brown 1996, p. 2).

Above the yield point, the behavior of the material is nonlinear. The response of the material is both elastic and plastic. The slope of the curve decreases steadily and monotonically. The effect of the material being able to carry a greater stress after yielding is called work hardening, i.e. the material gets stronger the more it is strained. Eventually failure occurs. A ductile material is able to incur large strains without failure, while a brittle material fails after very little straining. (Chen, Han 1988, p. 8-9.)

It is necessary to idealize the stress-strain curve, in order to obtain a solution to a deformation problem. One model is called an elastic-perfectly plastic model. The effect of work hardening is neglected and it is assumed that the plastic flow occurs when the stress has reached the yield stress σ_0. This model is shown in Figure 2-6(a). The uniaxial tension stress strain relation can be expressed as

$$\begin{aligned} \varepsilon &= \frac{\sigma}{E} && \text{for } \sigma < \sigma_0 \\ \varepsilon &= \frac{\sigma}{E} + \lambda && \text{for } \sigma = \sigma_0, \end{aligned} \tag{10}$$

where ε is strain, E is Young's modulus and λ is a scalar to be determined and $\lambda > 0$. (Chen, Han 1988, p. 11-12.)

Note that when the yield stress is reached, the corresponding strain is undefined. The magnitude of the strain can be determined in a partially elastic and partially plastic structure only by the surrounding elastic material restricting the plastic flow. (Chen, Zhang 1991, p. 6.)

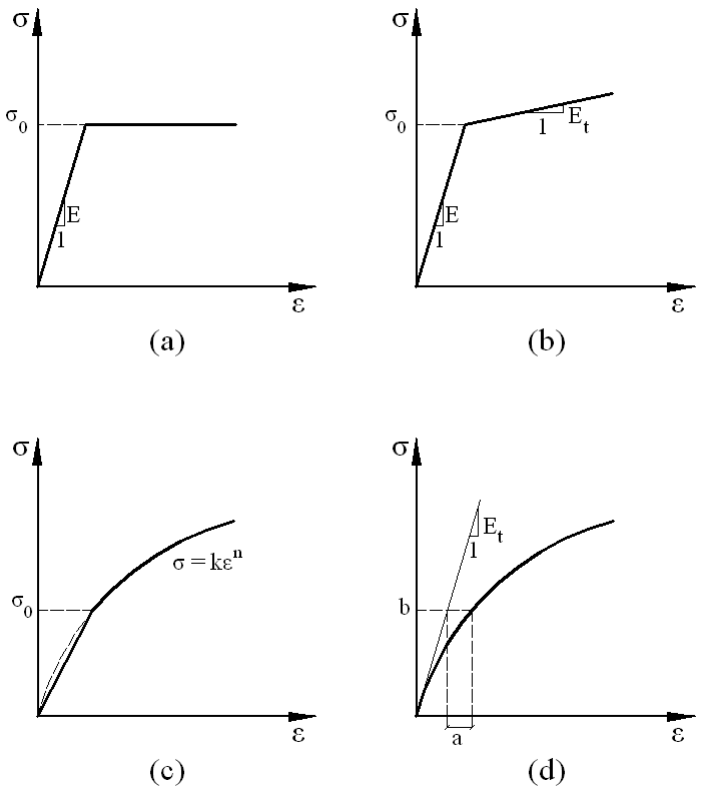

Figure 2-6. Idealized stress-strain curves: (a) Elastic-perfectly plastic model, (b) Elastic-linear work hardening model, (c) Elastic-exponential hardening model and (d) Ramberg-Osgood model (Chen, Han 1988, p. 11).

In the elastic-linear hardening model the continuous curve is approximated by two linear lines, see Figure 2-6(b). The stress-strain relation has the form

$$\begin{aligned} \varepsilon &= \frac{\sigma}{E} && \text{for } \sigma \leq \sigma_0 \\ \varepsilon &= \frac{\sigma}{E} + \frac{1}{E_\mathrm{t}}(\sigma - \sigma_0) && \text{for } \sigma > \sigma_0 . \end{aligned} \tag{11}$$

The first straight line has a slope of Young's modulus and ends at the yielding point. The second line represents an idealized fashion of the work-hardening range and has a slope of Tangent modulus $E_t < E$. (Chen, Han 1988, p. 12.)

The elastic-exponential hardening model can be considered with a power expression of the type

$$\begin{aligned} \sigma &= E\varepsilon \qquad \text{for } \sigma \leq \sigma_0 \\ \sigma &= k\varepsilon^n \qquad \text{for } \sigma > \sigma_0 , \end{aligned} \tag{12}$$

where k and n are two characteristic constants of the material to be determined to best fit into the experimentally defined curve. The curve is plotted in Figure 2-6(c). The latter equation (12) should be used only in the strain-hardening range. (Chen, Han 1988, p. 12.)

The nonlinear Ramberg-Osgood curve as shown in Figure 2-6(d) has the form

$$\varepsilon = \frac{\sigma}{E} + a\left(\frac{\sigma}{b}\right)^n , \tag{13}$$

in which a, b and n are material constants. The curve has an initial slope of Young's modulus and decreases monotonically with increasing loading. The model allows for a better fit of real stress-strain curves because it has three parameters. (Chen, Zhang 1991, p. 6.)

2.3 True Stress – True Strain Relation

Constructing a simple stress-strain curve, the tensile load is usually divided by the initial cross-sectional area A_0 of the specimen in order to obtain the conventional unit stress. For large stretching there will be a considerable reduction in the cross-sectional area. To obtain the true stress, the actual area A, instead of A_0, should be used. If the volume of the specimen is constant the true stress is

$$\sigma_{\text{true}} = \sigma_{\text{eng}}(1 + \varepsilon_{\text{eng}}) \ , \tag{14}$$

where σ_{true} is the true stress, σ_{eng} is the engineering (nominal) stress and ε_{eng} is the engineering strain. The true strain $\varepsilon_{\text{true}}$ is

$$\varepsilon_{\text{true}} = ln(1 + \varepsilon_{\text{eng}}) \ . \tag{15}$$

(Timoshenko 1956, p. 426-428.)

A comparison of the two types of the stress-strain curves is shown in Figure 2-7. In the true stress-strain curve the curve increases continuously up to the fracture. (Pilkey 2005, p. 158)

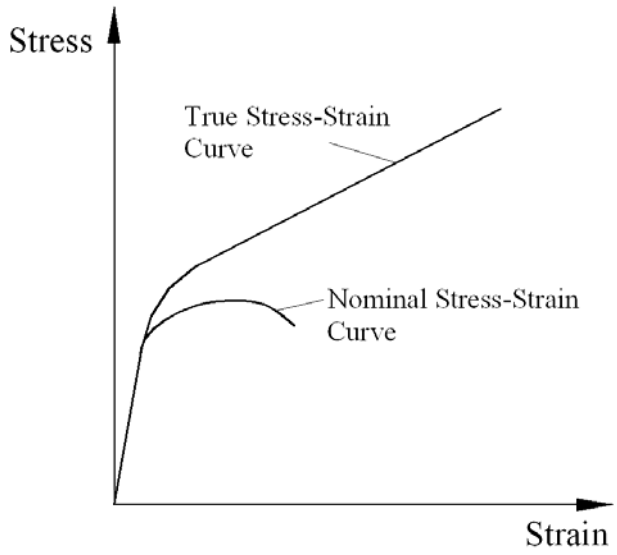

Figure 2-7. Comparison of the engineering (nominal) stress-strain curve with the true stress-strain curve for mild steel (Pilkey 2005, p. 158).

2.4 Loading Criterion and Flow Rule

If the material is idealized as perfectly plastic, as in equation (10), the effect of the strain-hardening is neglected. The elastic-perfectly plastic stress-strain relationship can be expressed in the incremental form as

$$\mathrm{d}\sigma_{\mathrm{ij}} = C_{\mathrm{ijkl}}\mathrm{d}\varepsilon_{\mathrm{ij}}^{\mathrm{e}} = C_{\mathrm{ijkl}}(\mathrm{d}\varepsilon_{\mathrm{ij}} - \mathrm{d}\varepsilon_{\mathrm{ij}}^{\mathrm{p}}) , \tag{16}$$

where $\mathrm{d}\sigma_{\mathrm{ij}}$, is the stress increment tensor, $\mathrm{C}_{\mathrm{ijkl}}$ is the elastic stiffness tensor, $\mathrm{d}\varepsilon_{\mathrm{ij}}$ is the total strain increment tensor, $\mathrm{d}\varepsilon_{\mathrm{ij}}^{\mathrm{e}}$ is the elastic strain increment tensor and $\mathrm{d}\varepsilon_{\mathrm{ij}}^{\mathrm{p}}$ is the plastic strain increment tensor. The strain increment tensors are in relation to each other

$$\mathrm{d}\varepsilon_{\mathrm{ij}} = \mathrm{d}\varepsilon_{\mathrm{ij}}^{\mathrm{e}} + \mathrm{d}\varepsilon_{\mathrm{ij}}^{\mathrm{p}} \quad . \tag{17}$$

The yield function $f(\sigma_{\mathrm{ij}}) = 0$ determines whether the material is in an elastic state or in a plastic state. If it is in a plastic state, it can be determined by the loading criterion whether a stress increment will constitute plastic loading or elastic unloading. If it is a plastic loading, the direction of the corresponding plastic strain increment vector can be determined by the flow rule. (Chen, Zhang 1991, p. 159-160.)

For a perfectly plastic material, the yield surface $f(\sigma_{\mathrm{ij}}) = 0$ is a fixed surface in the stress space and the plastic deformation occurs if the current stress point σ_{ij} is on the surface. After the addition of the stress increment, the resulting stress state $\sigma_{\mathrm{ij}} + \mathrm{d}\sigma_{\mathrm{ij}}$, must remain on the surface in order to maintain the plastic flow that is known as loading. On the other hand, if the resulting stress state moves inside the surface, no further plastic deformation occurs. This is called unloading. The loading criterion can be expressed as

$$\text{Loading:} \quad \begin{aligned} f(\sigma_{\mathrm{ij}} + d\sigma_{\mathrm{ij}}) &= 0 \\ \mathrm{d}f = \frac{\partial f}{\partial \sigma_{\mathrm{ij}}} d\sigma_{\mathrm{ij}} &= 0 \end{aligned} \tag{18}$$

$$\text{Unloading:} \quad \begin{aligned} f(\sigma_{\mathrm{ij}} + \mathrm{d}\sigma_{\mathrm{ij}}) &< 0 \\ \mathrm{d}f = \frac{\partial f}{\partial \sigma_{\mathrm{ij}}} \mathrm{d}\sigma_{\mathrm{ij}} &< 0 \quad . \end{aligned} \tag{19}$$

The yield function is also called the loading function, since it is also used here as a criterion of loading. (Chen, Zhang 1991, p. 160.)

The flow rule specifies the direction or the ratio of the components of the plastic strain increment tensor $d\varepsilon_{ij}^{p}$ in the strain space ε_{ij}. A plastic potential function, $g(\sigma_{ij})$, is a scalar function of the stress tensor and is often employed to describe a flow rule. The plastic strain increment vector corresponding to a given stress tensor σ_{ij} is specified as a vector normal to the potential function,

$$d\varepsilon_{ij}^{p} = d\lambda \frac{\partial g}{\partial \sigma_{ij}} \quad , \tag{20}$$

where $d\lambda$ is a positive scalar and has a non-zero value during plastic loading. This is referred as non-associated flow rule. If the yield functions is used as the potential function, $g = f$, the equation (20) becomes

$$d\varepsilon_{ij}^{p} = d\lambda \frac{\partial f}{\partial \sigma_{ij}} \quad . \tag{21}$$

This is generally referred to the associated flow rule. It can be proven that the solution of an elastic plastic boundary problem is unique for the materials with the associated flow rule. (Chen, Zhang 1991, p. 160-161.)

2.5 Factor of Safety

The strength of a material can be assumed to be normally distributed for example for different melting batches. The allowable stress σ_R^{*} is smaller than the stress basis σ_R^{0}, as shown in Figure 2-8. The index R refers to the resistance of a material, * refers to the minimum value of the normal distributed resistance of the material and 0 refers to the average value of the normal distribution. To study the unreliability in structural design, the resistance factor can be defined as

$$\gamma_R = \frac{\sigma_R^0}{\sigma_R^*} > 1 . \quad (22)$$

Also the loading can be assumed to be normally distributed for example for different loading situations during structure's life time. Now $\sigma_L{}^0$ is the average of the normal distribution and $\sigma_L{}^*$ is the maximum value of loading. The load factor can be determined as

$$\gamma_L = \frac{\sigma_L^*}{\sigma_L^0} > 1 . \quad (23)$$

This represents the margin between applied stress basis $\sigma_L{}^0$ and design stress $\sigma_L{}^*$. The factor of safety should be understood as a safety margin between the external load and resistance of a material. The factor of safety does not mean a measure of safety. The safety margin γ is generally defined as

$$\gamma = \frac{\sigma_R^0}{\sigma_L^0} > 1 \quad . \quad (24)$$

The safety margin corresponds to the partial safety factor design. (Ohnami 1988, p. 38)

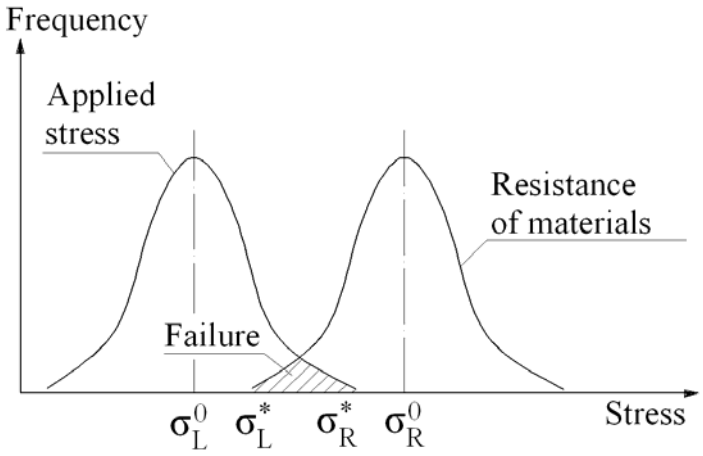

Figure 2-8. Material degradation of structural material in service and occurrence of unreliable region (Ohnami 1988, p. 38).

In literature terms safety factor, load factor and partial safety factor are all used in the same meaning. For example EN 13445-3 uses the term partial safety factor while ASME 2010 VIII-2 uses the term load factor, for the same case.

3 PLASTIC DESIGN

A complete elastoplastic analysis is generally quite complicated. It is necessary to carry out an analysis in an iterative and incremental manner. Limit analysis can be used to obtain the collapse load of a structural problem in a simple manner without recourse to an iterative and incremental analysis. Limit analysis leads to an estimate of the collapse load of a structure. (Chen, Han 1988, p. 409.)

Study a simply supported rectangular beam subjected to a uniformly distributed load q, shown in Figure 3-1(a). The material of the beam is elastic-perfectly plastic. As the load q gradually increases starting from zero, the stress distribution on the cross-section of the beam is elastic and linear. When the applied load reaches the elastic limit load $q = q_e$, the stresses at the upper and lower edges of the center cross-section have just reached the yield stress σ_0, see Figure 3-1(b). Further increase of the applied load will cause the yield zone to spread and the plastic flow in the yield zones is still contained by the surrounding elastic regions, see Figure 3-1(c). This type of elastic-plastic behavior is called contained plastic flow. As the load is increasing at $q = q_c = 1.5q_e$, the upper and lower plastic regions meet to form a plastic hinge and the yielding has spread to such an extent that the remaining elastic material plays an insignificant role in sustaining the load. This is called uncontained or unrestricted plastic flow. The structure becomes a mechanism and reaches its collapse or limit state. The ultimate load q_c is referred to the limit load or collapse load. (Chen, Han 1988, p. 409.)

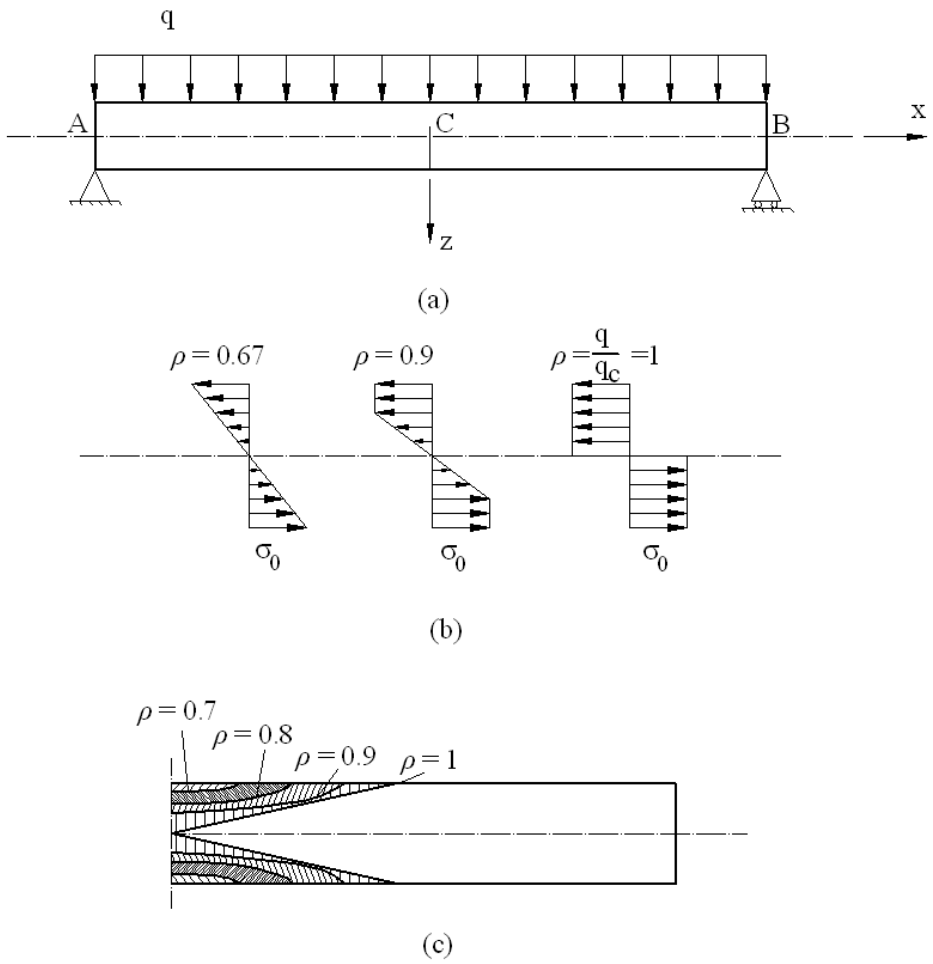

Figure 3-1. An illustration of a collapse process: (a) a simply supported rectangular beam, (b) stress distributions of the cross-section at C, (c) spreading of the yield zone (Chen, Han 1988, p. 410).

The collapse load as calculated in the limit analysis is different from the actual plastic collapse load that occurs in a real structure. At an ideal structure the deformation of the structure can increase without a limit while the load is held constant. This rarely happens in a real structure. The ideal model does not include the work hardening or significant changes in geometry. (Chen, Han 1988, p. 410.)

3.1 Evaluation of the Fully Plastic Moment

Fully plastic moment M_p is the maximum moment that can be applied to a cross-section. Consider a general cross-section with a vertical axis of symmetry Y-Y, see Figure 3-2(a). The section will be subject to a pure bending moment with no axial load.

Figure 3-2(b) shows the stress distribution in the elastic range of the loading. It is linear and has a zero value at the neutrals axis and a maximum value at one of the outer fibers. As the bending moment increases, the yielded zone starts to spread and yield takes place in the region of the maximum stress. The stress distribution when the uppermost fibers have just reached the yield stress is shown in Figure 3-2(c). There is a yielded zone in the lower part of the cross-section. When the moment increases, the yielded zones meet, as shown in Figure 3-2(d). The section is fully plastic and the bending moment is equal to a fully plastic moment M_p. The stress distribution consists of a compressive stress block in the upper part of the cross-section and a tensile stress block in the lower part. Both blocks are at yield stress σ_0. (Davies, Brown 1996, p. 9-10.)

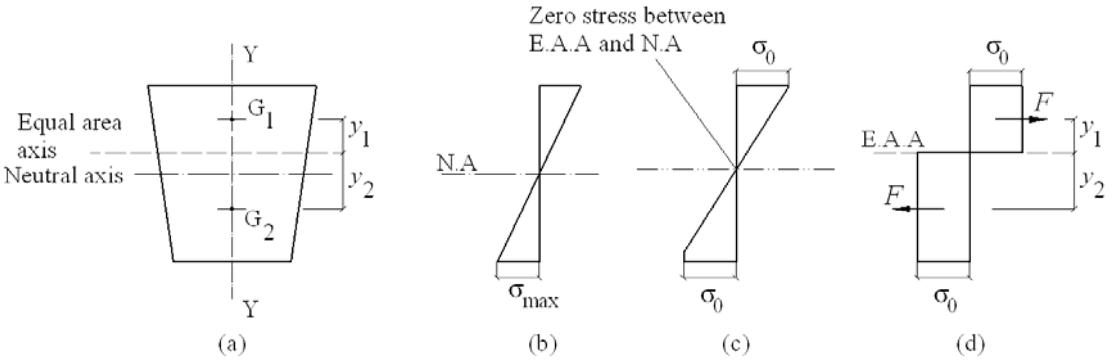

Figure 3-2. Illustrating the development of full plasticity in a singly symmetrical cross-section (Davies, Brown 1996, p. 9).

The forces F associated with each stress block must be equal, because no axial forces were subjected. If the cross-section area is A, the force F is

$$F = \sigma_0 \frac{A}{2} \ . \tag{25}$$

The zero stress axis divides the cross-section into two equal areas and it is usually termed the equal area axis (E.A.A), see Figure 3-2(d). If y_1 and y_2 are distances from E.A.A to the centers of the individual stress blocks, the fully plastic moment can be given by

$$M_{\mathrm{p}} = \sigma_0 \frac{A}{2}(y_1 + y_2) \ . \tag{26}$$

If the cross-section is considered to be divided into a number of elementary areas A_{i} each having a center distance y_{i} from the EAA, the fully plastic moment is

$$M_{\mathrm{p}} = \sigma_0 \sum_i A_i \, y_i \ . \tag{27}$$

There is a dimensionless section property called the shape factor. It is determined as

$$\alpha = \frac{M_{\mathrm{p}}}{M_{\mathrm{y}}} \ , \tag{28}$$

where M_{y} is the moment when the outer fibers have just reached the yield stress σ_0. (Davies, Brown 1996, p. 10.)

3.1.1 Effect of Normal Force

The previously considered beam was subjected only to pure bending. If an axial tension or compression is added, the fully plastic moment reduces. Consider the rectangular cross-section shown in Figure 3-3(a). The cross-section is assumed to be fully plastic under the combination of a compressive force P and a bending moment M_{p}' which is less than the full plastic moment M_{p}. The stress blocks are shown in Figure 3-3(b). The compression block is divided into a shaded portion resisting the moment and an un-shaded portion of depth a resisting the axial force P, so that

$$P = \sigma_0 b a \ . \tag{29}$$

The effective plastic areas are shaded. The effective plastic moment M_{p}' can be written as

$$M_{\mathrm{p}}{}' = \sigma_0 \cdot 2b\left(\frac{d-a}{2}\right)\left(\frac{d+a}{4}\right) , \tag{30}$$

where d is the height of the beam and b is the width of the beam. (Davies, Brown 1996, p. 12-13.)

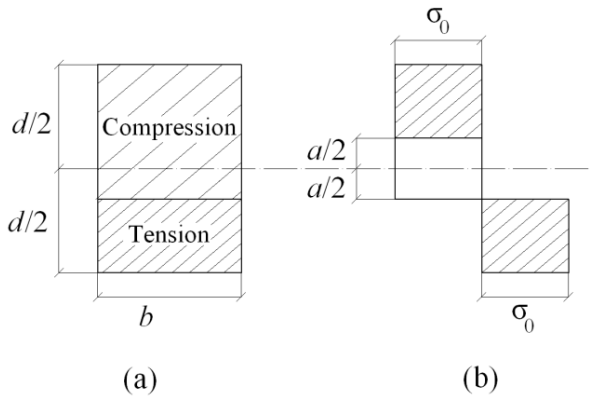

Figure 3-3. Rectangular cross-section subject to moment and axial force; (a) cross-section, (b) stress blocks (Davies, Brown 1996, p. 13).

3.1.2 Effect of Shear Force

The influence of shear force is usually neglected in determining the full plastic moment of the cross-section (Davies, Brown 1996, p. 16). A question is what shear force may reduce the plastic moment of resistance. It might at first be expected that, for any cross-section, the reduction of the plastic moment would be related uniquely to the ratio of applied shear force and maximum resistance of shear. However, this is not the case for beams. Maximum shear force and maximum moment can only occur together at the end of a beam where plastic deformation is affected by the type of the connection between the beam and surrounding members. Plastic moment capacity in the presence of shear force therefore depends on the detailed geometry and loading of the member considered – it is not a simple property of the cross-section of the member. (Horne, Morris 1981. p. 121-122.)

Fortunately, the effect if shear on plastic moment is of secondary importance and safe approximate results, based on behavior at a single cross-section, may be used. Consider a symmetrical I-section subjected to a shear force acting in the plane of the web, to-

gether with a bending moment. It is assumed that the actual applied shear force is resisted by uniform shear stress τ_w over the net depth of the web. The flanges are stresses to the fully yield values $\pm \sigma_0$ but the longitudinal stresses in the web are reduced to $\pm \sigma_w$. Using von Mises' yield criterion the longitudinal stress resistance of the web becomes

$$\sigma_w = \sqrt{\sigma_0^2 - 3 \cdot \tau_w^2} \quad . \tag{31}$$

The "lost" moment capacity due to the reduction of the longitudinal web stresses from $\pm \sigma_0$ to $\pm \sigma_w$ represents the difference between original moment capacity and reduced moment capacity. (Horne, Morris 1981. p. 122.)

3.2 Principle of Virtual Work

The basis of plastic design is that structures are assumed to collapse by the formation of sufficient plastic hinges to create a collapse mechanism. The main problems of plastic design are prediction of the correct collapse mechanism and determination of the maximum load that the structure can be subjected to. There are three conditions that must be satisfied

1. Equilibrium condition: The bending moments must represent a state of equilibrium between the applied loads and the internal forces in the structure.
2. Mechanism condition: At collapse, the bending moment must be equal to the full plastic moment of the cross-section at the sufficient number of sections of the structure for the associated plastic hinges to constitute a mechanism involving the whole structure.
3. Yield condition: At every cross-section of the structure, the bending moment must be less than, or equal to, the full plastic moment. (Davies, Brown 1996, p. 22-23.)

One method to study a plastic design problem is to use the principle of virtual work. The principle states that if a body is in equilibrium, the work done by the external loads on an arbitrary set of small external displacements is equal to the work done by the

internal forces on the corresponding internal displacements. In other words external loads times corresponding displacements equals hinge moments times rotations (Davies, Brown 1996, p. 25). It is assumed that the external loads are supported by the bending resistance of the members. The principle of virtual work completes the equilibrium and the mechanism conditions. When internal moment reaches the fully plastic moment, the yield condition is completed. (Chakrabarty 1987, p. 239.)

3.3 Yield Line Theory of Plates

One analytical approach to ultimate load design of plates is a yield line theory. Yield lines are two dimensional counterparts of plastic hinges. The yield line analysis seeks out of all possible failure patterns the one that corresponds to the smallest failure load. When a laterally loaded plate is on the verge of collapse, yield lines are formed at the locations of the maximum positive and negative moments, see Figure 3-4. Yield lines subdivide the plate into plane segments. The lateral deflection along the yield lines are large, the segments rotate as rigid bodies. The critical load can be obtained for example by the principle of virtual work. (Szilard 2004, p. 745.)

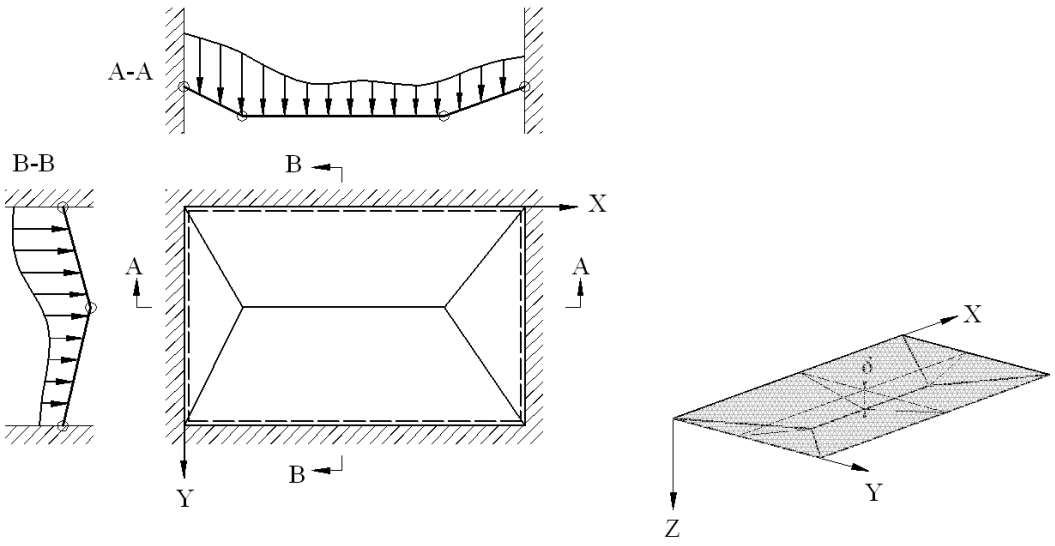

Figure 3-4. Failure mechanism of rectangular plate (Szilard 2004, p. 746).

Yield line analysis requires the following assumptions:

1. Yield lines are developed at the location of the maximum moments.
2. The yield lines are straight lines.
3. Constant ultimate moments are developed along the yield line
4. The elastic deformations are negligible in comparison with the rigid body motion created by the large deformations along the yield lines.
5. Only the pattern pertinent to the lowest failure load is important. This is so called optimum yield line.
6. When yield line pattern is optimum only ultimate bending moments, but not twisting moments or transverse shear forces, are present along the yield lines. (Szilard 2004, p. 745-746.)

4 BASICS OF FINITE ELEMENT METHOD

When a structure is subjected to external loads, the loads are transferred to the supports maintaining equilibrium with the reaction forces. The body deforms in a unique manner which is called the equilibrium state. In finite element method (FEM), a structure is distributed into structural parts called finite elements. The points where the finite elements are interconnected are called nodes. The process in specifying the nodes is called modeling and the collection of elements is called a mesh. The deformed configuration of the element is subjected to the given loads and it can be defined using the nodal displacement and forces. (Spyrakos, Raftoyiannis 1997, p. 2-3.)

The system of equilibrium equations can be formulated in a matrix form for the whole structure

$$\bar{\mathrm{F}} = \mathbf{K}\bar{\mathrm{U}} \ , \tag{32}$$

where $\bar{\mathrm{F}}$ is the nodal force vector, $\mathbf{K}$ is the stiffness matrix and $\bar{\mathrm{U}}$ is the nodal displacement vector. (Spyrakos, Raftoyiannis 1997, p. 3.)

These equations can be determined using different methods such as; equilibrium, principle of virtual work and total potential energy principle. A direct method i.e. equilibrium, can be used in cases of one dimensional elements. In two- and especially in three-dimensional cases using the direct method is not possible or it is possible only in very simple cases, so energy methods i.e. the principle of virtual work and the total potential energy principle must be used. (Hakala 1980, p. 161.)

Solving a finite element model can be divided into five steps (Spyrakos, Raftoyiannis 1997, p. 17-23)

1. Develop a suitable model and select the proper type of finite elements.
2. Compute the global stiffness matrix **K**.
3. Impose the boundary conditions.
4. Solve the equation (32).
5. Calculate stresses and strains using the nodal displacements computed at step 4. (Spyrakos, Raftoyiannis 1997, p. 17-23)

4.1 Linear Analysis

Linear finite element analysis assumes that the material behaves linear-elastically with small deformations theory. The principle of superposition is valid. The results of different load cases can be factored and combined. (Spyrakos, Raftoyiannis 1997, p. 391.)

4.2 Nonlinear Analysis

The majority of structural systems are analyzed by using the linear theory. In some cases the structural behavior is mainly characterized by the nonlinear effects that must be included in the analysis. For example the material may have a nonlinear behavior, large deflections exist or boundary conditions may change for various load levels. These nonlinear effects are called material nonlinearity, geometric nonlinearity and boundary nonlinearity. When a nonlinear behavior is present in a structural system, the linear analysis could lead to completely erroneous results. The nonlinear analysis is common for example in design for ultimate carrying capacity of structures or evaluation of structural safety due to damage, corrosion and loads not foreseen at the design. (Spyrakos, Raftoyiannis 1997, p. 391-392.)

The principle of superposition is not valid in nonlinear analysis. Only one load case can be treated at a time. The loading history depends on the sequence of load applications and the presence of initial stress such as residual stress. (Spyrakos, Raftoyiannis 1997, p. 392.)

4.2.1 Geometric Nonlinearity

Geometric nonlinearity can be considered with an example of the rigid cantilever beam of length L shown in Figure 4-1(a). A rotational spring with elastic constant k constrains free rotation of the beam. A force F is added in the free end of the beam. (Spyrakos, Raftoyiannis 1997, p. 397.)

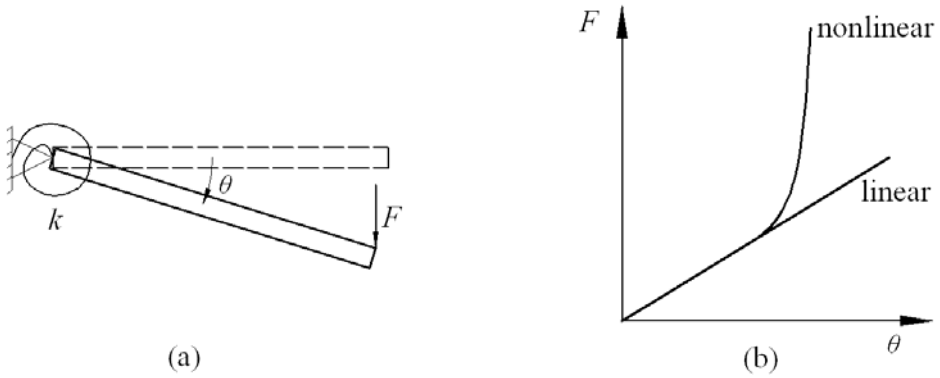

Figure 4-1. (a) Rigid cantilever beam and (b) Force-rotation relations (Spyrakos, Raftoyiannis 1997, p. 397).

Force F causes a rotation θ and produces a moment M at the support and the rotational spring develops a support reaction.

The force-rotation dependences are drawn in Figure 4-1(b), which shows clearly that for small rotations the two curves coincide, while for large rotations the two curves are different. This simple model shows that the source of nonlinearity attributes to change in geometry that affects the equilibrium equations. (Spyrakos, Raftoyiannis 1997, p. 397-398.)

4.2.2 Boundary Nonlinearity

Boundary nonlinearity can be discussed with an example of the cantilever beam shown in Figure 4-2(a). The beam has length *L* and bending stiffness *EI*. The left end is fixed and at the right end an axial spring with stiffness *k* is placed. When the system is unloaded, a small gap of length *d* exists between the spring and the free end of the beam. The following studies the behavior of the cantilever when a force *F* applied at the free end. (Spyrakos, Raftoyiannis 1997, p. 398.)

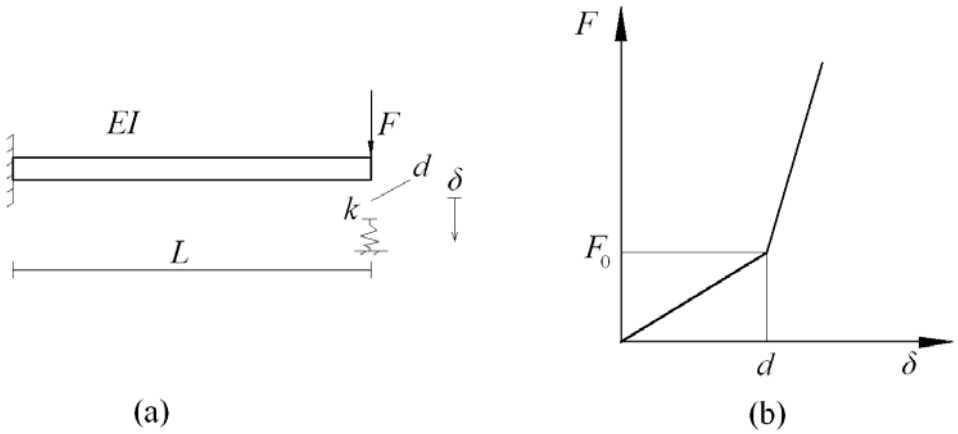

Figure 4-2. (a) Cantilever with spring and (b) Force-displacement curve (Spyrakos, Raftoyiannis 1997, p. 399).

For small values of the force *F* there is no contact between the free end and the spring. Only the bending stiffness of the beam enters to the force-displacement relations. When the applied force reaches the value F_0, where the gap is closed and the beam comes in contact with the spring. For higher values of the applied force than F_0, both bending stiffness of the beam and the axial stiffness of the spring enter to the force displacement relation.

The force-displacement relation is shown to include two linear parts in Figure 4-2(b). The first part corresponds to only the stiffness of the beam while the second part corresponds to the combined effects of the stiffness of the beam and the spring. The modification of the boundary conditions of the system causes the change in stiffness, once

the gap between the free end and the spring is closed. (Spyrakos, Raftoyiannis 1997, p. 399.)

4.2.3 Material Nonlinearity

In this thesis the most interesting nonlinearity is material nonlinearity. This type can be considered with an example of the cantilever shown in Figure 4-3(a). The beam is fixed at the left end and a force F is applied to the right, free end. The cross-section is orthogonal. The load is increased causing stresses at the fixed end beyond the elastic limit. The complete structural response is studied. The material of the beam behaves as an elastic-perfectly plastic. The yield stress σ_0 is the maximum stress that can be undertaken by the material. To simplify the model, only normal stresses are considered in the analysis. (Spyrakos, Raftoyiannis 1997, p. 394.)

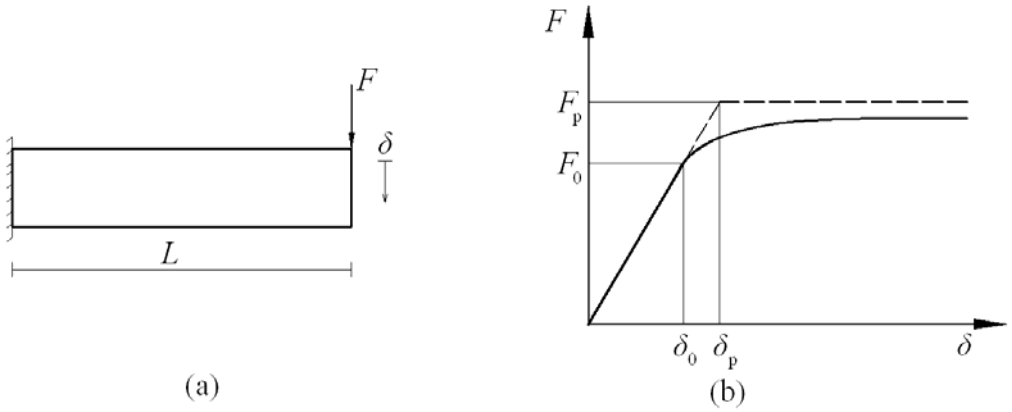

Figure 4-3. (a) Cantilever beam and (b) nonlinear force-displacement relation (Spyrakos, Raftoyiannis 1997, p. 394, 397).

The cantilever behaves similarly as the beam in Figure 3-1. When the applied force F is small, the beam behaves elastically and the stress distribution is linear over the cross-section. When the applied force is increased to the value $F = F_0$, the outermost fibers yields and a plastic hinge starts to develop in the left end of the beam. Finally when the force reaches the value $F = F_p$, the whole cross-section has reached yield stress and the displacement at the end of the beam increases. (Spyrakos, Raftoyiannis 1997, p. 395-396.)

The force-displacement relation is plotted in Figure 4-3(b). The δ_0 and δ_p are the vertical displacement at the tip of the beam corresponding respectively to F_0 and F_p. (Spyrakos, Raftoyiannis 1997, p. 397.)

5 HEADERS IN STANDARDS

When the designing and dimensioning of pressure parts are made according to EN 12952-3, the wall thickness and other dimensions are sufficient to withstand the calculation pressure at the calculation temperature for the design lifetime using materials in accordance with EN 12952-2. When designing a header also the effect of the following loadings shall be determined:

- the bending of a header as a beam under self weight and imposed loads;
- local loading of header by structural attachment. (EN 12952-3:2002, chap. 5.2)

There are requirements for the strengths of the pressure parts. The strengths shall withstand loads:

- internal pressure;
- the weight of all pressure parts and their contents, the weight of components suspended from them and any superimposed slag, fuel, ash or dust;
- loads caused by gas pressure differentials over the boiler furnace and flue gas passes
- loads arising at connections between the boiler system and other parts. (EN 12952-3:2002, chap. 5.3)

5.1 Design Stress

The principal to determine the design stress of components primarily subjected to static loading shall be the lowest value obtained from following

$$f_{\mathrm{MAWS}} = \frac{K}{\gamma}, \tag{33}$$

where f_{MAWS} is the maximum allowed working stress, K is the material strength value and γ is the safety factor (EN 12952-3:2002, chap. 6.3.1). Some safety factors for material strength values are presented in Table 5-1.

Table 5-1. Safety Factors for Material Strength Values.

		EN 12952-3	EN 13345-3	ASME 2010 Sec. II
Yield Stress	$R_{p0.2/t}$	1.5	1.5	1.5
Tensile Stress	R_m	2.4	2.4	3.5
Creep Rupture	$R_{m/T/t}$	1.25	1.5	1.5 *
Creep Strain	$R_{p1.0/T/t}$	-	1.0	1.0 **

* Based on $R_{m/100000h/t}$ values.
If the designed lifetime is 200 000 h the level of safety is 1.25

** Creep strain values only for 1000 h

(EN 12952-3:2002, Table 6.3-1; EN 13445-3:2009, Table 6-1 and chap. 19.5.1.1; ASME 2010 Sec. II-D, Table 1-100)

When load is at the right angle to a weld seam and the creep properties of the welded connection are known, the smallest of the design stresses of the welded connection and the two joined materials shall be used. When the creep properties of the welded connections are not known, but those of the filler material are known, the design stress shall be reduced by 20 %. When the creep strength of the material is not known, the joint design stress shall be reduced by a further 20 %. These reductions are not required when the load is parallel to the weld seam. (EN 12952-3:2002, chap. 6.3.2.)

5.2 Structural Attachments

In the standard EN 12952-3 in chapter 11.5.2 is said that "Where attachments are welded on straight tubes the length of the attachment, measured along the axis of the tube, shall comply with 11.5.4 and 11.5.5, or shall be determined by stress analysis conforming to the criteria of prEN 13445 or prEN 13480 or justified by documented

evidence of previous satisfactory operating experience with similar designs". The thickness of the attachment section, measured in the tube circumferential direction, shall not be more than one-quarter of the tube diameter at the point of attachment, see Figure 5-1. (EN 12952-3:2002, p. 131, 135.)

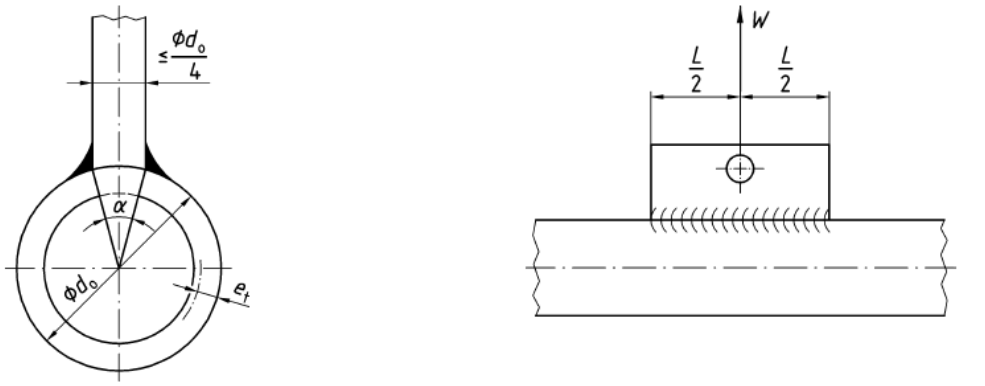

a) Structural attachment welded to tube (section)

b) Horizontal tube vertical symmetrical support

Figure 5-1. Typical structural attachment (EN 12952-3:2002, chap. 11.5.1).

The chapters 11.5.4 and 11.5.5 commit only the length of the attachment. The problem is that if the length is relatively long, the real force distribution is not linear over the length of the attachment. The maximum value of the intensity of radial loading is given in Figure 5-2.

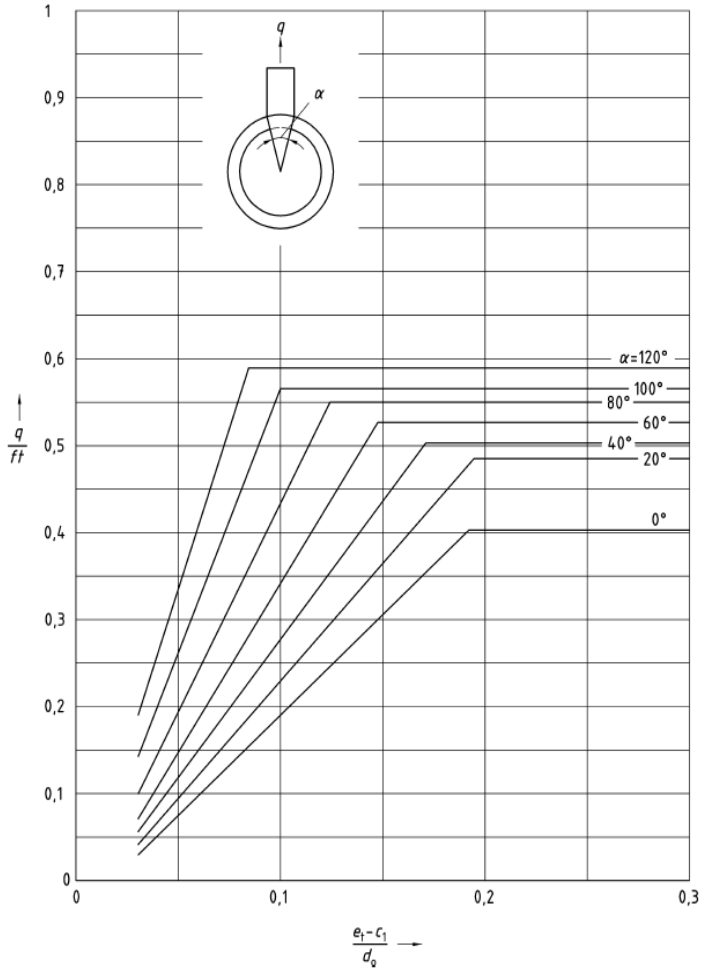

Figure 5-2. Allowable tensile loading of the attachment (EN 12952-3:2002, chap. 11.5.4).

There is a typing error in term q/ft that should be $q/(e_t\text{-}c_1)$ (prEN 12952-3:2008 chap. 11.5.4). There is also one significant difference compared to other rules of dimensioning; this chapter does not oblige the use or corrosion allowance. Also the effect of the utilization rate of the internal pressure is not included in this chapter.

For example consider a header dimensions; outside diameter d_o = 216.1 mm, wall thickness e_t = 45 mm, under tolerance c_1 = 5.625 mm. Lug's dimensions are width w_{lug} = 200 mm and wall thickness e_{lug} = 40 mm. The design stress of the tube material is MAWS = 100 N/mm^2. Calculations are made according to EN 12952-3 chapter 11.5 and are presented in Appendix I. As a result the maximum load is 555 kN. As compari-

son the FE-method gives a header with same dimensions the maximum load from 280 kN to 2080 kN depending on the internal pressure.

The indetermination of this method is the reason why this method is no used and headers are dimensioned using design by analysis (DBA).

5.3 Design by Analysis

Design by analysis (DBA) means that dimensioning and design checks are made for example using finite element method and it is an alternative to design by formulas (DBF). Standards give some limitations and guidelines when using this method. In the following chapters are compared DBA in the European standards EN 12952-3 and EN 13445-3 and ASME 2010 Section VIII, Division 2.

Design by analysis is included in the standard EN 13445-3 as a complement to the common design by formulas (DBF) for cases not covered by the DBF route, but also as an allowed alternative. It may be used as a complement to DBF for cases where superposition with environmental actions is required or for cases where manufacturing tolerances are exceeded. (Baylac, Koplewicz 2004 p. 86.)

When a header is dimensioned using design by analysis, i.e. using finite element method, norms require the use of partial safety factors. ASME uses the term load factor, which has the same meaning. For the sake of clarity, this thesis uses the term safety factor.

5.3.1 Design by Analysis According to EN 12952-3 and EN 13445-3

EN 12952-3 refers to EN 13445-3, which gives guidelines for the failure modes of gross plastic deformation (GPD) and creep rupture (CR). In the gross plastic deformation analysis an elastic-perfectly plastic material model shall be used. Partial safety factors shall be added to load and to material strength to find the design stress. The Tresca's yield criterion and associated flow rule shall be used. If the von Mises' yield criterion is used instead of Tresca's, the design stress parameter shall be multiplied by

$\sqrt{3}/2$, see equation (9). (EN 12952-3:2002, chap. 11.5.3; EN 13445-3:2009, chap. B.8.2 and B.9)

The safety factor for permanent load and pressure is $\gamma_G = \gamma_P = 1.2$. And the safety factor for material is given as

$$\begin{aligned} \gamma_R &= 1.25, && \text{for } \frac{R_{p0.2/t}}{R_{m20°C}} \leq 0.8 \\ \gamma_R &= 1.5625 \cdot \frac{R_{p0.2/t}}{R_{m20°C}}, && \text{otherwise.} \end{aligned} \tag{34}$$

The combined effect of the safety factors for load and material is commonly

$$\gamma = \gamma_R \cdot \gamma_G = \gamma_R \cdot \gamma_P = 1.5, \tag{35}$$

excluding the parameter needed if von Mises' yield criterion is used. The maximum allowed absolute value of the principal structural stains is less than 5 % in normal operating load cases and less than 7 % in testing load cases. (EN 13445-3:2009, chap. B.8.2)

The creep rupture design check is presented in EN 13445-3 in chapter B.9. The CR design check proceeds basically like the gross plastic deformation analysis, there are only some differences. The von Mises' yield criterion shall be used and the maximum absolute value of the principal structural strain is 5 %. The safety factor for materials is defined as

$$\begin{aligned} \gamma_R &= 1{,}25, && \text{for } \frac{R_{m/T/t}}{R_{p1.0/T/t}} \leq 1.5 \\ \gamma_R &= \frac{1}{1.2} \cdot \frac{R_{m/T/t}}{R_{p1.0/T/t}}, && \text{otherwise.} \end{aligned} \tag{36}$$

1.0 % proof strength ($R_{p1.0/T/t}$) values are not included in standard EN 10216-2 for pipes, but are in standard EN 10028-2 for plates. This makes the use of safety factor determined as in latter equation (36) impossible when dealing with pipes.

5.3.2 DBA According to ASME 2010 Section VIII

In ASME 2010 Section VIII the method of design by analysis is considered in chapter 5. The most important is the method of the limit-load analysis, described in chapter 5.2.3. The limit load analysis addresses the failure modes of ductile rupture and gross plastic deformation occurs in the structure. The material model shall be an elastic-perfectly plastic and the yield strength defining the plastic limit shall be yield stress of the material. The Von Mises' yield criterion and associated flow rule should be utilized. The small displacement theory shall be used. The idea is to calculate different load combinations and check if the model still converges. If not, thickness or other properties shall be modified.

There are two dominating load cases for headers. The first includes pressure and so called dead load, which includes for example the weight of the vessel and its contents and refractory and insulation. The second adds thermal loads and live load, which is for example the effect of fluid momentum steady state and transient states. Loads are factored as follows:

- Load case 1: 1.5 for pressure and dead load;
- Load case 2: 1.3 for pressure, dead load and thermal load; 1.7 for live load.

Thermal loads should be considered in cases where elastic follow-up causes stresses that do not relax sufficiently to distribute the load without excessive deformation.

These load factors are greater than in EN 13445-3, but the yield stress is not divided by a safety factor. This means that all safety is transferred to the load and the material yields on its real yield stress. This load case 1 gives the same level of safety than EN 12952-3 for yield stress.

5.3.3 Conflicts in Standards

Probably the most critical conflict in EN-standards is that when a structure is first designed by formulas according to EN 12952-3 and then a more precise analysis is made with FE-method according to EN 13445-3, more safety is required. Also the safety factor is different either creep rupture or yield stress is dominating due to the $\sqrt{3}/2$–factor that EN 13445-3 requires for yield stress but not for creep rupture when von Mises' yield criterion is used.

In EN 13445-3 for gross plastic deformation design check the Tresca's yield criterion was specified for safety reasons, but especially to guarantee the calibration between DBA and DBF. This standard allows von Mises' yield criterion to be used for progressive plastic deformation (PD), instability (I) or creep rupture (CR). An explanation to the fact that Mises' yield criterion is allowed for PD is the fact that, because of material hardening, a less stringent criterion is deemed to be justified. (Baylac, Koplewicz 2004 p. 90-91; EN 13445-3:2009 chap. B.8.3, B.8.4, B.9.4.)

When von Mises' yield stress is multiplied by $\sqrt{3}/2$ – i.e. reducing by 15.5 %, the von Mises' yield line inscribes the Tresca's yield line instead of circumscribing it as shown in Figure 5-3.

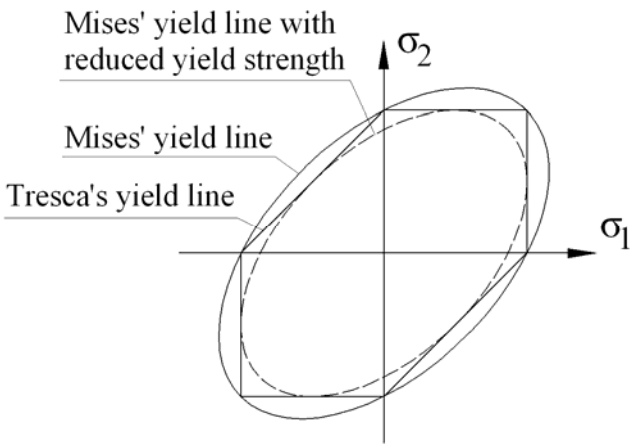

Figure 5-3. The reduction of von Mises' yield stress.

Other conflict is that EN 12952-3 requires the safety factor 1.25 for creep rupture but EN 13445-3 requires the safety factor 1.5. The same problem occurs here that more safety is required when a more accurate analysis is made. A possible reason why EN 12952-3 requires smaller safety factor for creep rupture, is that the writers of this standard have thought that damages caused by creep occur during long period of time and these structures are overseen during shutdowns of boilers (Häkkilä 2011).

The reason for design by analysis route is to have an alternative and a complement to design by formulas route. But it is possible that – in a borderline case – DBF allows a structure but DBA does not. This seems not to have any practical sense. This is why it is not practical to reduce yield strength by $\sqrt{3}/2$ when a more accurate analysis is made. For same reason it is not reasoned to use the safety factor 1.5 for creep rupture in DBA when it is not required in DBF.

Other conflict in EN 13445-3 is acceptance criteria for testing loads (7 %) and normal use (5 %). A probable reason for this difference is that safety factors are different for testing conditions and for a normal use. The required safety factor for testing conditions is 1.05 (EN 13445-3:2009, chap. 6.4.2). The ratio of safety factors 1.05/1.5 is approximately the same that the ratio of accepted plastic strains 5 % / 7 %. This way of thinking is acceptable when it is considered linearly but plastic dimensioning is nonlinear and the principle of superposition is not valid. Besides, the load carrying capacity does not much differ much wheter the acceptance criterion is 5 % or 7 % due to the reason that material is ideal-plastic.

6 ANALYSES

Headers are analyzed by using finite element analysis. Then the analytical solution is compared and parameters are adapted so that the analytical solution fits enough to the results gained from the finite element analysis.

6.1 Finite Element Analysis

Easiest approach to headers' plastic capacity is to use finite element analysis. Probably the most critical source of error is boundary conditions. The material model and safety factors are chosen to fit best with the requirements in norms.

Effect of the branches is examined beginning with single header without any branches. Formulas are calibrated to fit first just a plain header and then the wall panel and later on the roof panel will be added. These studies are made both analytically and using FE-method. The main goal was to sort out how the width of the force affected on the capacity of the header.

6.1.1 Material Model

Both norms EN 13445-3 and ASME 2010 Section VIII require the use of the perfectly plastic material model. This material model can be numerically unstable when finite element analysis is used. Due to this reason the bilinear work hardening material model is chosen. The tangent modulus is set to be E_t = 1 MPa. This means that if plastic strain reaches the value ε_p = 5% the plastic increase in stress is 0.05 MPa. This is close enough to be the perfectly plastic material model and at the same time it is not unstable.

True stress–true strain relation is not used because the norms require the use of perfectly-plastic models.

6.1.2 Safety Factors for Loads

Due to the disorder and conflicts in standards, the used safety factors are collected in this chapter. FE-analyses are divided into five load cases that are

1. Normal load case
2. Abnormal load case
3. Yielding order load case
4. Pressure adjustment
5. Maximum load.

The normal load case is used for normal loads. These kinds of loads are internal pressure and the weight of pipes and other steel, water, refractory, insulation and normal amount of ash and sand. The loading is long term and possible creep is dominant. Another name for these loads are dead loads since they may be considered as constant.

The abnormal load case covers abnormal and short term situations such as accumulation of ash and sand resultant from blockage or abnormal operation of the boiler. The same dead load effects as in the normal load case but live load is added. Abnormal amounts of sand and ash are live load. There may be several abnormal situations but the worst case is calculated. Dimensioning may be based for yield stress instead of creep rupture due to the short term of the abnormal situation.

The yielding order load case covers the maximum load that the hanging rod is able to carry. The goal of this load case is to assure the load carrying capacity of the header and the panel underneath it if the hanger rod is tightened too much. If the header and the panel are strong enough, the plastic deformation develops in the hanger rod that has more deformability than the header.

Pressure adjustment is used only to raise pressure for the last load case. The last load case is to find out the maximum load carrying capacity of the header and the panel underneath it. These two load cases are for the research purpose and to compare results with the results gained from analytical solutions.

Accidental loads are not discussed in this thesis, because they are unusual and challenging to calculate analytically. Accidental loads are for example earthquakes. The yielding order covers loads other than those parallel to the header. The loads parallel to the header are bounded out in this thesis. These situations may cause failures but do not result in the collapse of the structure.

The used safety factors for different loads are collected in Table 6-1. This thesis uses the same concept as ASME, i.e. all safety is on the load side.

Table 6-1. The used safety factors for different load cases.

Load Case	Pressure	Dead load	Live load
1. Normal	1.5	1.5	-
2. Abnormal	1.3	1.3	1.5
3. Yielding Order	1.1	1.1	1.1
4. Pressure adjustment	1.5	1.1	1.1
5. Maximum load	1.5	x	-

In the normal load case all loads are multiplied by the safety factor 1.5, which is the required level of safety in EN 12952-3 for DBF. In the abnormal load case only live load is multiplied by 1.5 but dead load and internal pressure have the safety factor of 1.3. This is the same concept as in ASME that an abnormal situation is uncommon and that is why it is improbable that these kinds of loads are affected at the same time.

The hanger rod capacity also has the safety factor of 1.1, because the material strength may be greater than guaranteed or the calculation temperature is lower and hence the strength is greater. In load case 4 the pressure is raised to the maximum and the load on the lug is constant. Thereby the load on the lug can be raised to reach the ultimate plastic capacity in which case the header yields. Therefore there is no need for an actual safety factor.

6.1.3 Design Stress

If all safety is on the load side and still, the safety factors are chosen to be according to EN 12952-3, a different safety factor is needed if the material is in the temperature area of creep rupture or in the temperature area of yield strength. This means that the safety factor depends on the material and the design temperature. This can be confusing when it is possible to have even five different material strengths in a FE-model of a header. Therefore it is logical to have just one safety factor on the load side and to modify the safety factors of materials.

In this context is used term maximum allowed working stress f_{MAWS}. It is defined as

$$f_{\mathrm{MAWS}} = min\left(\frac{R_{p0.2t}}{1.5}; \frac{R_{m20℃}}{2.4}; \frac{R_{mTt}}{1.25}\right) \quad . \tag{37}$$

This definition is according to EN 12952-3. These all correspond the nominal force on the load side. If the safety factor is on the load side and has the value of 1.5, the strength f_{MAWS} needs to expand with the same safety factor. The expansions of f_{MAWS} and the safety factor of the load is deduced Table 6-2.

Table 6-2. Expansion of f_{MAWS} and load. F_{nom} is the nominal force.

Material	Load
$f_{\mathrm{MAWS}} = min\left(\frac{R_{p0.2/t}}{1.5}; \frac{R_{m/20℃}}{2.4}; \frac{R_{m/T/t}}{1.25}\right)$	F_{nom}
${}^{1.5)}f_{\mathrm{MAWS}} = min\left({}^{1.5)}\frac{R_{p0.2/t}}{1.5}; {}^{1.5)}\frac{R_{m/20℃}}{2.4}; {}^{1.5)}\frac{R_{m/T/t}}{1.25}\right)$	${}^{1.5)}F_{\mathrm{nom}}$
$1.5 \cdot f_{\mathrm{MAWS}} = min\left(R_{p0.2/t}; \frac{R_{m20℃}}{1.6}; 1.2 \cdot R_{m/T/t}\right)$	$1.5\ F_{\mathrm{nom}}$

Even though the creep rupture stress $R_{m/T/t}$ is multiplied by 1.2, the same 1.2 is found on the load side. EN 12952-3 requires the safety factor 1.25 to be used when the material is on the temperature area of creep rupture.

$$\begin{aligned} &{}^{1.25)}\frac{R_{m/T/t}}{1.25} \sim {}^{1.25)}F_{nom} \\ &=> {}^{1.2)}R_{m/T/t} \sim {}^{1.2)}(1.25\ F_{nom}) \\ &=> 1.2R_{m/T/t} \sim 1.2 \cdot 1.25\ F_{nom} = 1.5F_{nom} \quad . \end{aligned} \tag{38}$$

These safety factors for yield stress $R_{m0.2/t}$ and creep rupture $R_{m/T/t}$ are clarified in Figure 6-1. First variable to be determined is f_{MAWS}, as in Equation (37). This is shown as a blue line. Then f_{MAWS} is expanded by the safety factor 1.5, which is shown as a red line. The red line is above the material creep rupture stress $R_{m/T/t}$, but that gap is covered on

the load side as explained before. The final material strength value added to FE-models and used in analytical solution is

$$f = 1.5 \cdot f_{\mathrm{MAWS}} \quad . \tag{39}$$

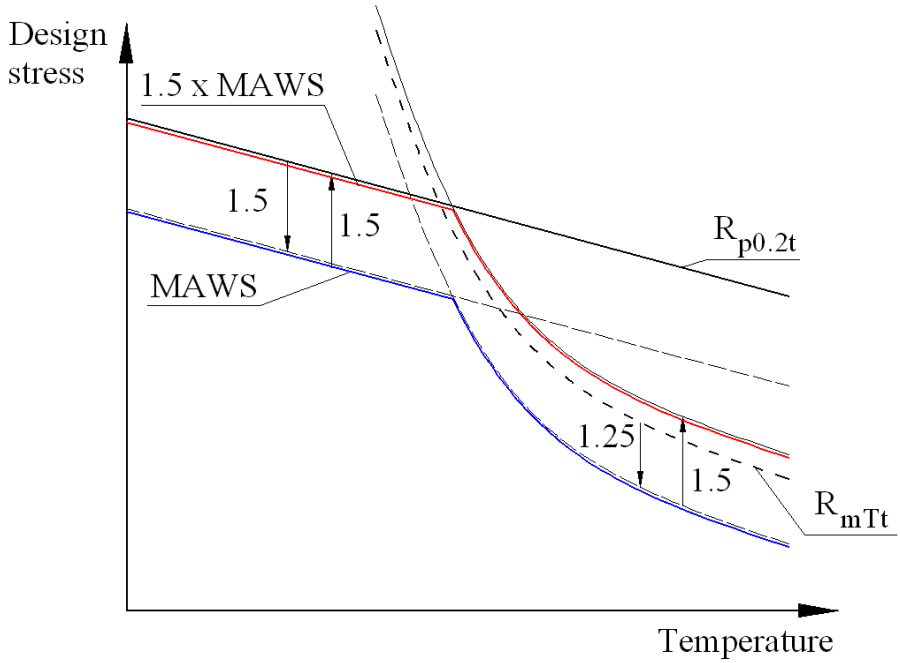

Figure 6-1. The principle for safety factors for materials when the safety factor is added to load.

Using all safety on the load side involves other advantages also. Nominal force multiplied by the safety factor 1.5 F_{nom} may be replaced by other combinations of loads. If only nominal force F_{nom} is used, cases where the required safety factor is less than 1.5, would lead to safety factors below one. Also buckling analyses may be calculated with the same models. If yield stress is reduced in a buckling analysis, true buckling shapes may not occur and in some cases analysis does not give true results.

In ASME 2010 section VIII-2 protection against plastic collapse is evaluated by elastic-plastic stress analysis method. The safety factor for load is 2.4 in normal load case, when it is 1.5 in limit load analysis method. This means that when there is even a little

possibility that instability occurs – i.e. some stress fields are in compressive stress – the safety factor increases 60% from 1.5 to 2.4. Increasing the safety factor by 60% seems exaggerated.

6.1.4 Boundary Conditions and Mesh

Boundary conditions vary in each model since the geometries are a bit different in every header. Internal pressure and force on the lug exist in every model but other boundary conditions vary. Symmetry is used whenever it is possible to reduce the calculation time.

Force from the hanger rod is added as a bearing load on the surface of the hole in the lug. Material model nonlinearity is turned off on the upper part of the lug so that local plastic deformations and instabilities do not disturb the calculation.

Internal pressure causes also longitudinal stress that is covered using pressure on the cross-section, modeling a plug or using frictionless support. Frictionless support may be used when the cross-section is parallel to the direction of the force; otherwise the support causes an unwanted support reaction. Pressure on the cross-section is used when the cross-section is symmetric and not parallel to the direction of the force. The value of the added pressure is the value of the internal pressure scaled with the ratio of the areas of the cross-section as

$$p_{\text{axial}} = \frac{A_1}{A_2} \cdot p_{\text{c}} \ , \tag{40}$$

where A_1 is the area of the hole on the header end and A_2 is the area of the ring area as shown in Figure 6-2.

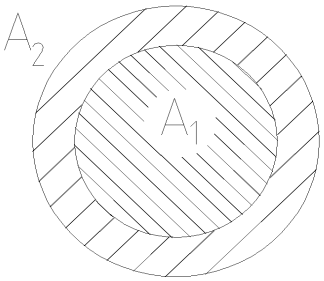

Figure 6-2. Areas A_1 and A_2 that are used when determining the longitudinal stress of the header.

When the cross-section is not symmetric – because of unsymmetrical corrosion allowances – and it is parallel to the direction of the force, a real plug is modeled. On the inner surface of this plug is set the same internal pressure as on the inner surface of the header.

In a real structure support reaction develops in the panel beneath the header. Only a relatively short length of the panel is modeled and frictionless support is added on the cross-sectional surface. This support allows deformation of the cross-section in the direction perpendicular to the tubes of the panel but does not allow deformation in the longitudinal direction of the tubes.

If it is not possible to use symmetry, frictionless support is added also in the other end of the header. This causes support reaction for the longitudinal stress caused by the pressure on the other end. The so called couplet set-command is used on the cross-section of the header – where longitudinal pressure is added. This requires all nodes on that surface to have the same displacement in the longitudinal direction of the header. This makes global rotation on that surface fixed. This represents the continuity of the header. The CP-command does not restrict the global longitudinal deformation.

The boundary conditions in a non-symmetric header are shown in Figure 6-3. Normal internal pressure, frictionless support on wall panel and force on the lug are added. There is a frictionless support on the right end. There is pressure on the left end and a

couplet set-command is used. Longitudinal stress in bigger nozzles is added as pressure because they have symmetrical cross-section, but in roof panel the plug is modeled because cross-section is not symmetric due to corrosion allowances.

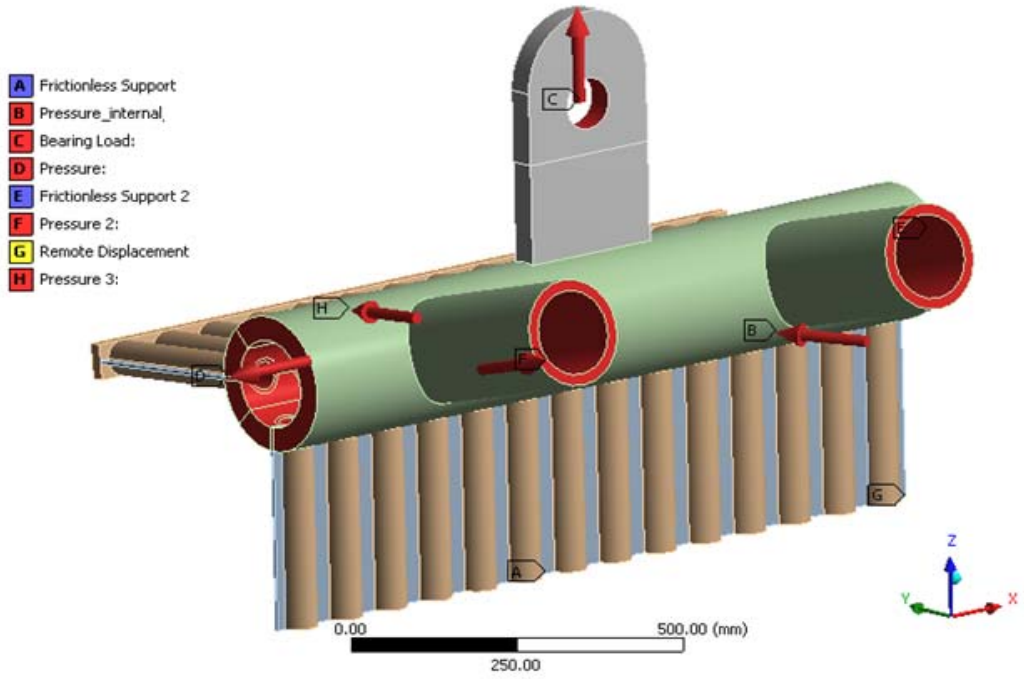

Figure 6-3. Boundary conditions in a non-symmetric header. The directions the arrows are not correct due to the used program.

A double symmetric header with relatively simple boundary conditions is shown in Figure 6-4; two symmetry planes, internal pressure, frictionless support on the wall panel, force on the lug and couplet set-command and pressure on the end.

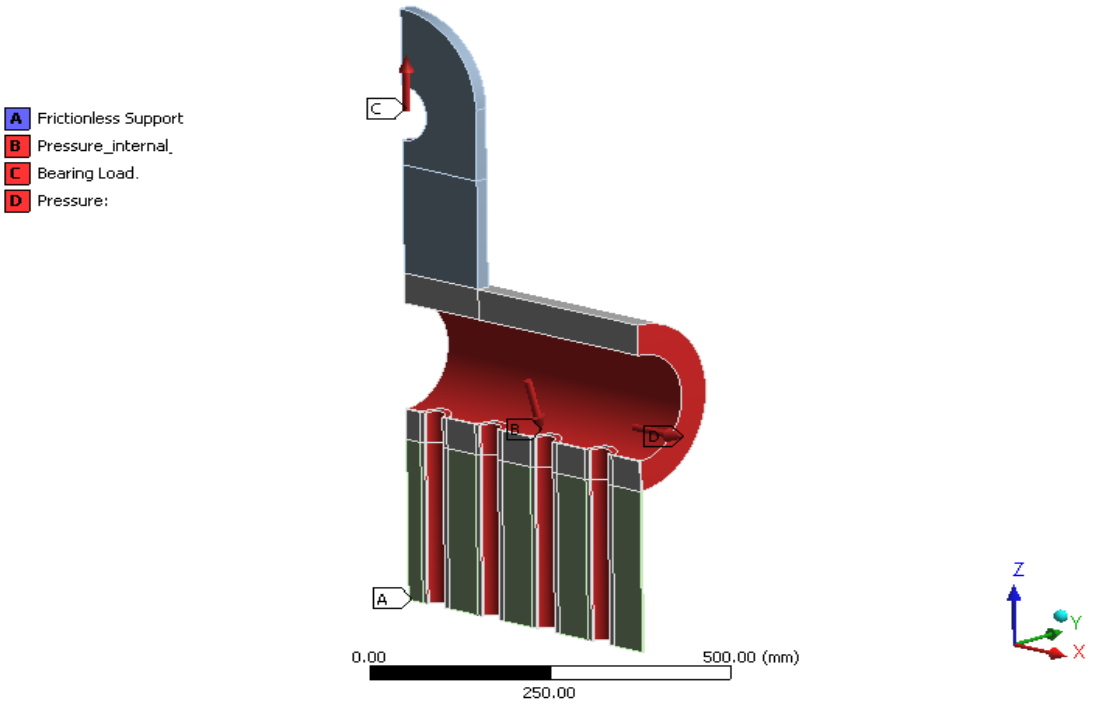

Figure 6-4. Boundary conditions in a double symmetric header.

Mesh had a relatively important role for the results. The used element type is a hex dominant solid element. Tetrahedrons may also be used, but the number of elements would increase. There should be at least five elements over the wall thickness of the header so that bending moment over the wall thickness is taken into account properly. In those cases, where the outside diameter of the connecting pipe is bigger than the inner diameter of the header, contact is used between the nozzle and the header. This eases meshing because slim bodies will not exist.

Used yield criterion is von Mises' yield criterion without the factor $\sqrt{3}/2$, which EN 13445-3 requires when gross plastic deformation is domineering. Because the different cases have to be separated whether the temperature is on creep rupture area or not, the aforementioned factor is not used. This is the same concept that is used with safety factors. Besides, when using a more accurate method, it is practical to take benefits out of it.

5 % of the equivalent plastic strain is the limit for maximum load. Elastic strain is included in the results, but the effects are not significant. The work that elastic deformation makes is much smaller than the work done by plastic deformation. This is shown in Figure 6-5. Hatched areas describe the work.

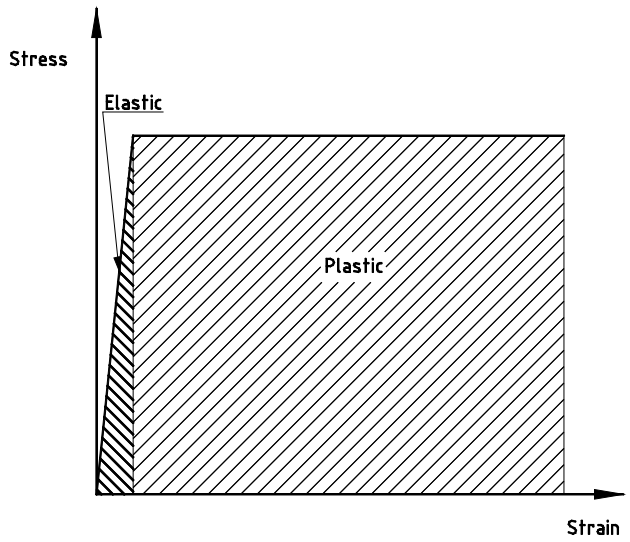

Figure 6-5. Work done by elastic and plastic deformation when the perfectly plastic material model is used.

6.2 Analytical Solution

Headers are loaded as an unusual way when considering headers as shells. The typical loadings for shells are normally for example as internal pressure or other distributed forces. The header is loaded locally on the lug side and longitudinally distributed on the wall side. Such loaded shells are challenging to find in literature and most like cases are circumferential hollow section beams and these are taken in comparison. Ready dimensioning equations are usually restricted to thin shells and do not take into account internal pressure.

The analytical solution is approached first by determining the circumferential strength of the headers since it is the most critical direction. After this the plastic moment is defined and it is used with the principle of virtual work to define the maximum load that can be applied to headers. The effect of branches is discussed in its own chapter. Another failure mode, punching shear, is also discussed in the same chapter.

6.2.1 Stresses caused by Internal Pressure

When a pressure vessel is loaded with internal pressure, the pressure causes three divergent stresses; circumferential stress σ_φ (also known as "hoop stress"), radial stress σ_r and longitudinal stress σ_z. These stresses are drawn in Figure 6-6.

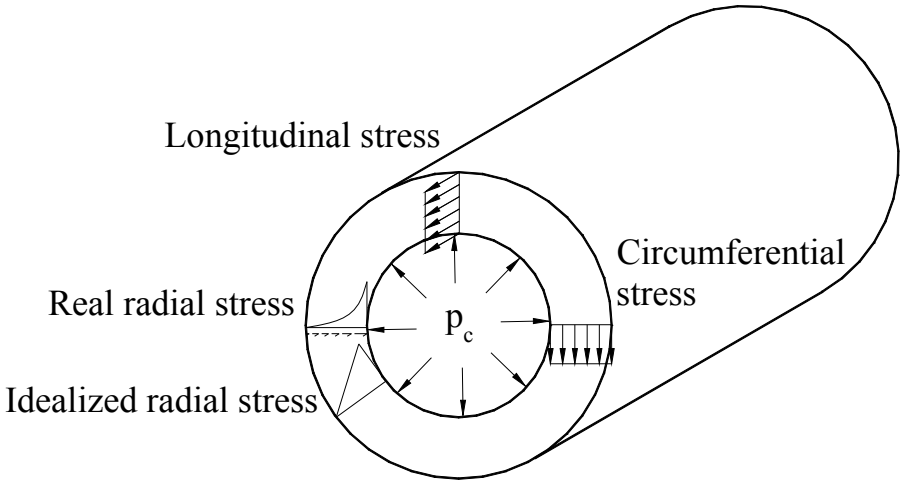

Figure 6-6. Stress components caused by internal pressure p_c.

If the wall thickness of a vessel is relatively big, the longitudinal and circumferential stresses cannot be considered uniform throughout the thickness of the wall and radial stress cannot be considered negligible. (Young, Budynas 2002, p.587.)

Radial stress is compression if the internal pressure is positive. In the inside surface of the vessel radial stress has the value of internal pressure and the stress reduces to the outside surface, where the radial stress has the value of zero. The true stress distribution is nonlinear with thick walled pressure vessels, but is usually assumed to be linearly distributed.

Circumferential stress has the greatest value of these three stress components. It is tension, when internal pressure is positive. The stress can be determined as

$$\sigma_\varphi = \frac{d_i}{2 \cdot e} p_c \,, \tag{41}$$

where d_i is the inside diameter of the vessel, e is the wall thickness and p_c is the calculation internal pressure (Pilkey 2005, p. 124).

Longitudinal stress is caused by for example a pipe bend or a header end and for thin walled pipe has the value of

$$\sigma_z = \frac{d_i}{4 \cdot e} p_c \tag{42}$$

(Pilkey 2005, p. 124). For thick walled pipe the longitudinal stress has the same value that is added in the FE-models as pressure in the headers end. This is presented in equation (40).

The values of these stress components are usually as $\sigma_\varphi \geq \sigma_z \geq \sigma_r$. For example the Tresca's yield criterion takes into account the biggest and the smallest of the three principal stresses as in Equation (5). Then the longitudinal stress is ignored in usual cases where internal pressure is positive and no significant external longitudinal compression occurs. It is natural to consider the plane stress situation in the σ_φ - σ_r –plane and consider the longitudinal stress negligible. Other reasoning to ignore the longitudinal stress is that it does not have to affect the area of the plastic hinge but the area that is still elastic.

6.2.2 Circumferential Strength and the Effects of Normal and Shear Forces

Headers may be imagined to be curved beams. If a curved beam is loaded with local force F, linear normal force N is

$$N(\theta) = \frac{F}{2} \cdot \sin\theta \ , \tag{43}$$

where θ is angle defined as in Figure 6-7. Shear force V is

$$V(\theta) = \frac{F}{2} \cdot \cos\theta \ . \tag{44}$$

Linear bending moment M is

$$M(\theta) = \frac{F}{2} \cdot R \cdot \sin\theta - \frac{F \cdot R}{\pi} \ , \tag{45}$$

where R is radius of the bar. (Pilkey 2005, p. 832, 834.)

Normal force, shear force and bending moment distributions from Equations (43), (44) and (45) are drawn in Figure 6-7.

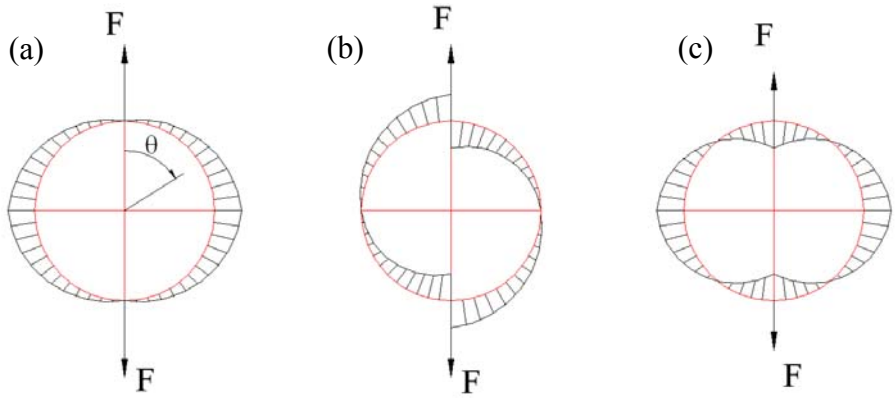

Figure 6-7. Linear-elastic a) normal force, b) shear force and c) bending moment distributions of a curved beam.

Shear force causes shear stress $\tau_{r\varphi}$ that approximately is

$$\tau_{r\varphi}(\theta) = \frac{V(\theta)}{A_\tau} \ , \tag{46}$$

where A_τ is the cross-sectional area that shear force V affects.

To evaluate the effect of shear forces, the von Mises' yield criterion is used, as previously in Equation (31). Using the three stress components caused by internal pressure, the criterion defined in Equation (8) may be written as

$$\sigma_{\mathrm{o}}(\theta)^2 = \frac{1}{2}\left[(\sigma_{\varphi} - \sigma_{\mathrm{r}})^2 + (\sigma_{\varphi} - \sigma_{\mathrm{z}})^2 + (\sigma_{\mathrm{z}} - \sigma_{\mathrm{r}})^2 + 6\tau_{\mathrm{r}\varphi}(\theta)^2\right] \quad . \tag{47}$$

Stress components caused by internal pressure are not depended on the angle θ. Normal force is a function of the angle θ and circumferential stress is not depended on the angle, these components are discussed separately. If the yield stress σ_0 has the value of design stress f, the circumferential stress can be solved from Equation (47)

$$\sigma_{\varphi} = \frac{\sigma_{\mathrm{r}}+\sigma_{\mathrm{z}}}{2} \pm \frac{\sqrt{4f^2 - 3\sigma_{\mathrm{r}}^2 + 6\sigma_{\mathrm{r}}\sigma_{\mathrm{z}} - 3\sigma_{\mathrm{z}}^2 - 12\tau_{\mathrm{r}\varphi}(\theta)^2}}{2} \quad . \tag{48}$$

This circumferential stress is the strength that is left after shear stress and radial stress reductions to carry the normal force caused by external load W and internal pressure p_{c}. If this is considered in the plane stress situation ($\sigma_{\mathrm{z}} = 0$) and the stress σ_{φ} is marked as f_{φ} the circumferential strength is

$$f_{\varphi}(\theta) = \frac{\sigma_{\mathrm{r}}}{2} \pm \frac{\sqrt{4f^2 - 3\sigma_{\mathrm{r}}^2 - 12\tau_{\mathrm{r}\varphi}(\theta)^2}}{2} \quad . \tag{49}$$

The radial stress has different values on the inner and on the outer surfaces of the header, so the circumferential strength has also different values. Also strength is different if the circumferential strength is positive or if it is negative. This is a pretty notable thing because the normal-circumferential stress caused by the bending moment is positive or negative. On the outer surface where radial stress is $\sigma_{\mathrm{r}} = 0$, circumferential strength is the same for both positive and negative normal stress. On the inner surface the strength for negative normal stress is higher, because radial stress $\sigma_{\mathrm{r}} \leq 0$. This difference appears also in Figure 6-8.

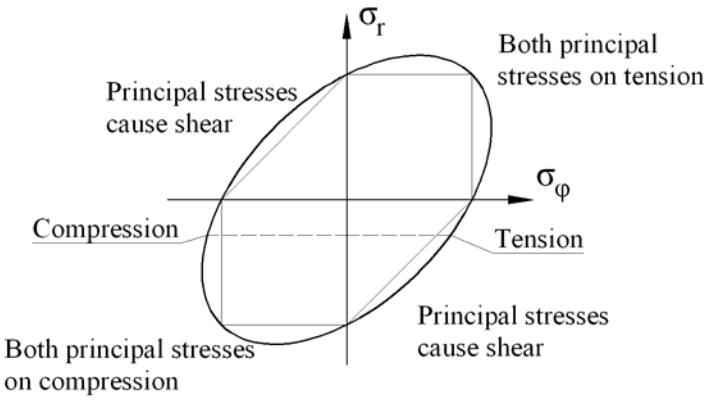

Figure 6-8. Von Mises' yield criteria and different values of circumferential stress σ_φ when $\sigma_r \leq 0$.

Plastic design usually assumes that the true cross-sectional area reaches true and constant yield stress. Now equivalent yield stress i.e. the circumferential strength is not constant. In this thesis it is assumed that the yield stress is constant but the equivalent area has the shape of parallelogram, see Figure 6-9. To simplify, in Figure 6-9, the different values of circumferential strength for tension and compression is ignored.

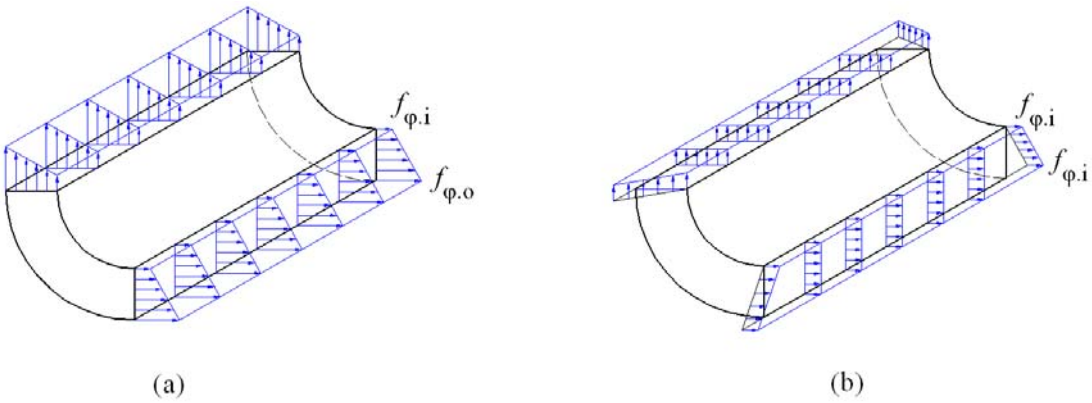

Figure 6-9. Transforming the circumferential strength to equivalent parallelograms; (a) the circumferential strength after pressure and shear stress reductions and original cross-sectional areas, (b) the circumferential stress has the value of the inner surface and cross-sectional area is modified.

When the header reaches the plastic limit state, normal force concentrates around the equal area axis and reserves some cross-sectional area. Bending moment takes areas on

sides, as in Figure 3-3. The cross-sectional areas are different for tension and compression in different segments of the header as shown in Figure 6-10.

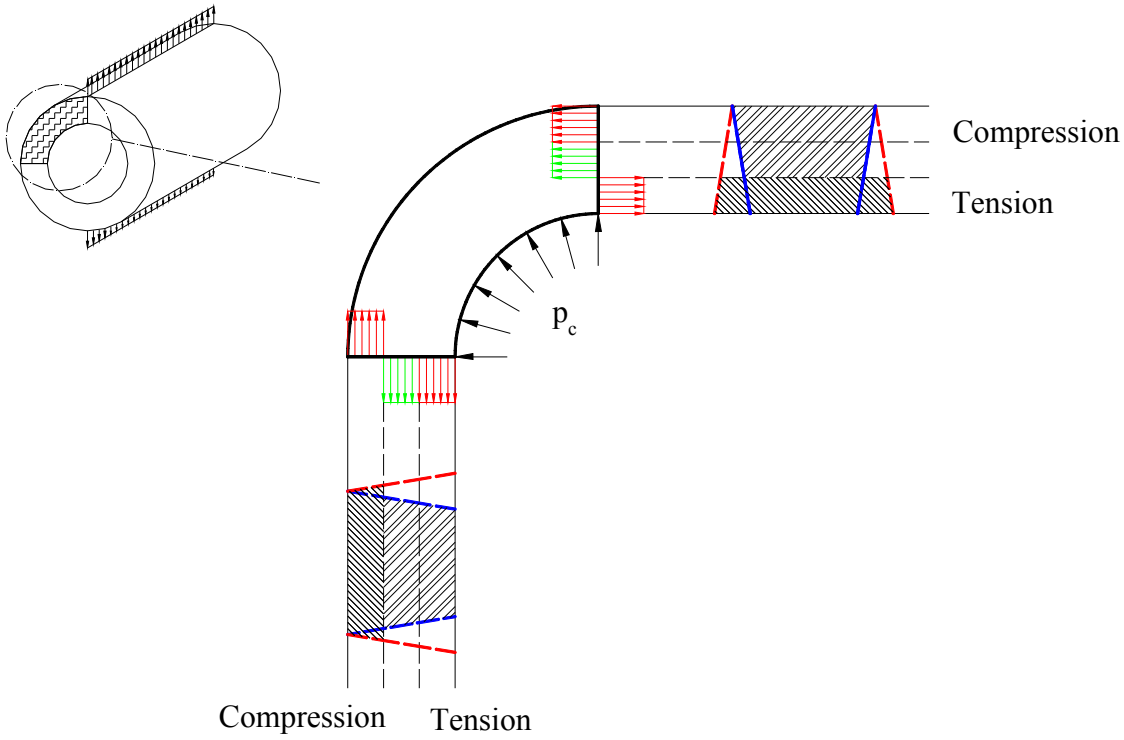

Figure 6-10. Effective areas for plastic dimensioning when difference in circumferential strength is taken into account.

Due to the nature of the loading it is practical to consider the circumferential stress caused by the internal pressure as a distributed force. This makes it easier to evaluate the cross-sectional area that the internal pressure requires in the plastic limit state. Normal force $N(\theta)$ caused by external load and normal force N_φ caused by internal pressure may be combined easily. Normal force N_φ can be solved from circumferential stress σ_φ by multiplying Equation (41) by wall thickness e as

$$N_\varphi = \frac{d_\mathrm{i}}{2} p_\mathrm{c} \quad . \tag{50}$$

Unit of normal force N_φ is N/mm and it is distributed to the length of the header. Normal force $N(\theta)$ caused by external load is distributed only to an effective length of the header which is determined later.

6.2.3 Plastic Moment

As written before, the yield stress is considered to be constant and the equivalent area has the shape of a trapezoid. To avoid complexity the higher yield strength on the inner surface for compression is ignored and the equivalent area has the shape of a simple trapezoid.

Normal force reserves area in the middle part of the cross-section while the stress blocks resisting the bending moment are reduced. The same phenomenon is shown in Figure 3-3. Because normal force, i.e. circumferential stress, caused by internal pressure is independent from the width of the lug, i.e. the effective length of the plastic hinge, these two components need to be united. The distributed normal force N_φ, as defined in Equation (50), is multiplied by the length of the plastic hinge and is then added to the normal force $N(\theta)$ caused by external loading, as defined in Equation (43). This sum of normal forces is then divided by design stress. Finally the area that normal force requires is

$$A_{\mathrm{N}}(\theta) = \frac{N(\theta) + N_\varphi \cdot L_{\mathrm{H.i}}(\theta)}{f_{\varphi.\mathrm{i}}(\theta)} \ , \tag{51}$$

where $A_{\mathrm{N}}(\theta)$ is the area for normal force, $L_{\mathrm{H.i}}(\theta)$ is the length of the plastic hinge on the inside surface and $f_{\varphi.\mathrm{i}}(\theta)$ is the design stress on the inner surface. True design stress on the area of normal force is between the stresses on the inner and outer surfaces. To make calculations simpler, the design stress has the same value than it has on the inner surface. When taking the design stress on the inner surface, the effective area is a bit conservative. How areas for normal force and bending moment are placed is shown in Figure 6-11.

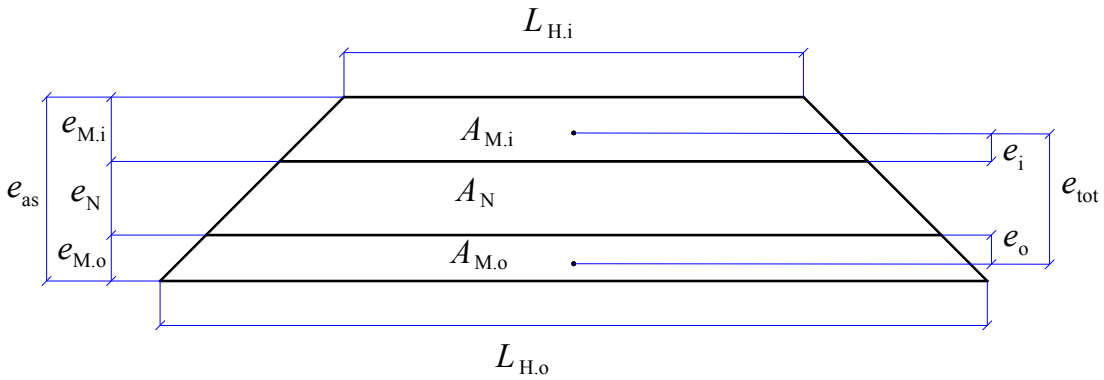

Figure 6-11. Effective areas for normal force A_N and bending moment $A_{M.i}$, $A_{M.o}$ in the plastic hinge.

The effective length of the plastic hinge is longer on the outer surface. The length on the outer surface is proportional to the ratio of the design stress on the inner and on the outer surface as

$$L_{H.o}(\theta) = \frac{f_{\varphi.o}(\theta)}{f_{\varphi.i}(\theta)} L_{H.i}(\theta) \ , \tag{52}$$

where $L_{H.o}(\theta)$ is the effective length of the plastic hinge on the outer surface and $f_{\varphi.o}(\theta)$ is the design stress on the outer surface.

The areas and wall thicknesses for plastic moments and the distance between centers of plastic moment areas are defined using simple equations of geometry of trapezoid. The deduction of these areas is in Appendix II. Effective wall thicknesses for moment carrying areas on the inner part are

$$e_{M.i}(\theta) = -B(\theta) \cdot L_{H.i}(\theta) + \sqrt{[B(\theta) \cdot L_{H.i}(\theta)]^2 + B(\theta)[A(\theta) - A_N(\theta)]} \ , \tag{53}$$

and for the outer part

$$e_{M.o}(\theta) = B(\theta) \cdot L_{H.o}(\theta) - \sqrt{[B(\theta) \cdot L_{H.o}(\theta)]^2 - B(\theta)[A(\theta) - A_N(\theta)]} \ , \tag{54}$$

where $e_{\mathrm{M.i}}$ is the equivalent wall thickness of the inner area for bending moment, $e_{\mathrm{M.o}}$ is the equivalent wall thickness of the outer area for bending moment, A(θ) is the whole area of the plastic hinge and $B(\theta)$ is auxiliary variable defined as

$$B(\theta) = \frac{e_{\mathrm{as}}}{L_{\mathrm{H.o}}(\theta) - L_{\mathrm{H.i}}(\theta)} \quad , \tag{55}$$

where e_{as} is calculation wall thickness of the header. Wall thickness that is left for normal force is

$$e_{\mathrm{N}}(\theta) = \ e_{\mathrm{as}} - e_{\mathrm{M.i}}(\theta) - e_{\mathrm{M.o}}(\theta) \quad . \tag{56}$$

where $e_{\mathrm{N}}(\theta)$ is the wall thickness for normal force. Note that the area for normal force is therefore reassigned. The area that is determined before must be smaller than the area determined latter. In other words there is a reservation made for the normal force earlier and now the normal force carrying capacity checked for being sufficient.

Distances from the center of areas to the edge of the area of normal force $A_{\mathrm{N}}(\theta)$ are

$$e_{\mathrm{i}}(\theta) = \frac{e_{\mathrm{M.i}}(\theta)}{3} \cdot \frac{3 \cdot L_{\mathrm{H.i}}(\theta) + \frac{e_{\mathrm{M.i}}(\theta)}{B(\theta)}}{2 \cdot L_{\mathrm{H.i}}(\theta) + \frac{e_{\mathrm{M.i}}(\theta)}{B(\theta)}} \tag{57}$$

and

$$e_{\mathrm{o}}(\theta) = \frac{e_{\mathrm{M.o}}(\theta)}{3} \cdot \frac{3 \cdot L_{\mathrm{H.o}}(\theta) - \frac{e_{\mathrm{M.o}}(\theta)}{B(\theta)}}{2 \cdot L_{\mathrm{H.o}}(\theta) - \frac{e_{\mathrm{M.o}}(\theta)}{B(\theta)}} \quad , \tag{58}$$

where $e_{\mathrm{i}}(\theta)$ is the distance from the inner area to the edge of $A_{\mathrm{N}}(\theta)$ and $e_{\mathrm{o}}(\theta)$ is the distance from the outer area to the edge of $A_{\mathrm{N}}(\theta)$. Finally distance between the centers of moment carrying areas is

$$e_{\mathrm{tot}}(\theta) = e_{\mathrm{i}}(\theta) + e_{\mathrm{o}}(\theta) + e_{\mathrm{N}}(\theta) \quad . \tag{59}$$

Now the moment carrying areas are for inner part

$$A_{\mathrm{M.i}}(\theta) = e_{\mathrm{M.i}}(\theta) \cdot \left[L_{\mathrm{H.i}}(\theta) + \frac{e_{\mathrm{M.i}}(\theta)}{2 \cdot B(\theta)} \right] \tag{60}$$

and for outer part

$$A_{\mathrm{M.o}}(\theta) = e_{\mathrm{M.o}}(\theta) \cdot \left[L_{\mathrm{H.o}}(\theta) - \frac{e_{\mathrm{M.o}}(\theta)}{2 \cdot B(\theta)} \right], \tag{61}$$

where $A_{\mathrm{M.i}}(\theta)$ is the inner part of the moment carrying area and $A_{\mathrm{M.i}}(\theta)$ is the outer part of the moment carrying area. These areas must be equal. Finally plastic moment of a hinge is

$$M_{\mathrm{p}}(\theta) = A_{\mathrm{M.o}}(\theta) \cdot e_{\mathrm{tot}}(\theta) \cdot f_{\varphi \mathrm{.i}}(\theta) \ , \tag{62}$$

where $M_{\mathrm{p}}(\theta)$ is the plastic moment.

6.2.4 Principle of Virtual Work

Now when the plastic moment $M_{\mathrm{p}}(\theta)$ is defined, it may be used to determine the header's load carrying capacity using the principle of virtual work. The principle of virtual work may be expressed as

$$F(\theta) \cdot \delta(\theta) = \sum_{j=1}^{n} M_{\mathrm{p}.j}(\theta) \cdot d\varphi_j(\theta) \, . \tag{63}$$

where F is applied force, $M_{\mathrm{p}.j}(\theta)$ is the plastic moment of a hinge and $\mathrm{d}\varphi_j(\theta)$ is the virtual rotation of a hinge, subscript j refers to the number of a hinge and n refers to the number of hinges. To simplify the calculation the header is considered as two halves

and only one half is examined at the time. This enables that header need not to be symmetric and for example the roof affects only one-sided.

The following equations are deduced in Appendix III. The used parameters are shown in Figure 6-12. The distances a and b between angles φ_1, φ_2 and φ_3 are supposed to be constant and elastic deformation is ignored. To make further calculations easier, only one half of the header is considered.

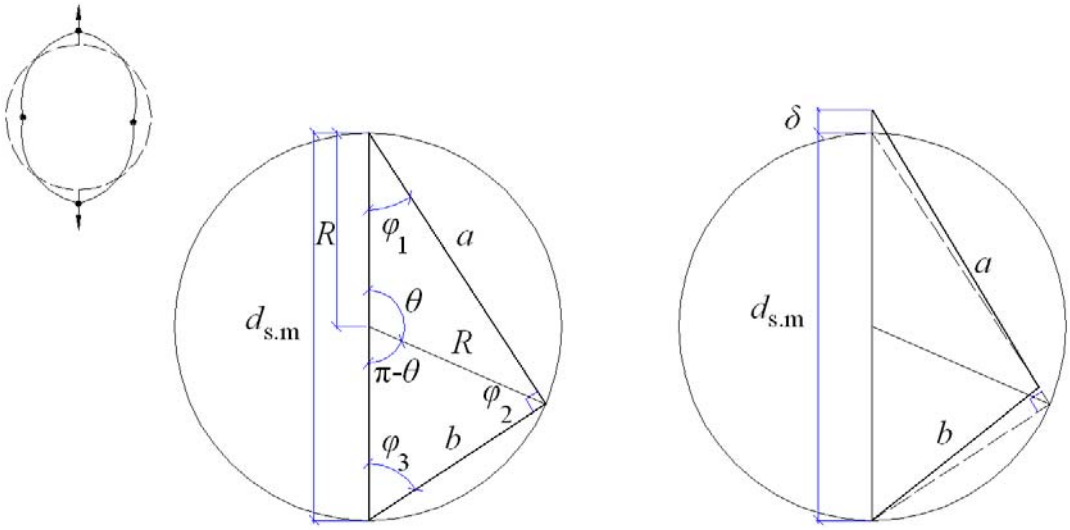

Figure 6-12. Parameters used to solve virtual displacement δ and rotations dφ_1, dφ_2 and dφ_3.

Dependence between virtual displacement $\delta(\theta)$ and angle d$\varphi_1(\theta)$ is

$$\delta(\theta) = [-a(\theta) \cdot sin(\varphi_1(\theta))] \cdot \left(1 + \frac{a(\theta) \cdot cos\,(\varphi_1(\theta))}{\sqrt{a(\theta) \cdot cos^2(\varphi_1(\theta)) - (a(\theta)^2 - b(\theta)^2)}}\right) \cdot d\varphi_1 . \quad (64)$$

Likewise dependence between virtual displacement $\delta(\theta)$ and angle d$\varphi_3(\theta)$ is

$$\delta(\theta) = [-b(\theta) \cdot sin(\varphi_3(\theta))] \cdot \left(1 + \frac{b(\theta) \cdot cos\,(\varphi_3(\theta))}{\sqrt{b(\theta) \cdot cos^2(\varphi_3(\theta)) - (b(\theta)^2 - a(\theta)^2)}}\right) \cdot d\varphi_3 . \quad (65)$$

Rotation d$\varphi_2(\theta)$ may be expressed using rotations d$\varphi_1(\theta)$ and d$\varphi_3(\theta)$

$$d\varphi_2(\theta) = -[d\varphi_1(\theta) + d\varphi_3(\theta)] \quad . \tag{66}$$

The dependence between virtual displacement and rotations is now defined, as are the plastic moments of hinges, the applied force F may be solved from Equation (63).

6.2.5 Effect of Branches

An essential part of a header is its branches and nozzles. These holes naturally weaken the plastic capacity, but then branches have a reinforcing influence –compared to holes – that may be difficult to define. This conflict is approached using effective cross-sectional areas as defined in EN 12952-3. The deduction of following equations and the principle of pressure areas are in Appendix IV. The goal is to have an equivalent wall thickness with the effect of branches and finally transform it to the effective length and to use the original wall thickness. The procedure may be divided in four steps and these are shown in Figure 6-13.

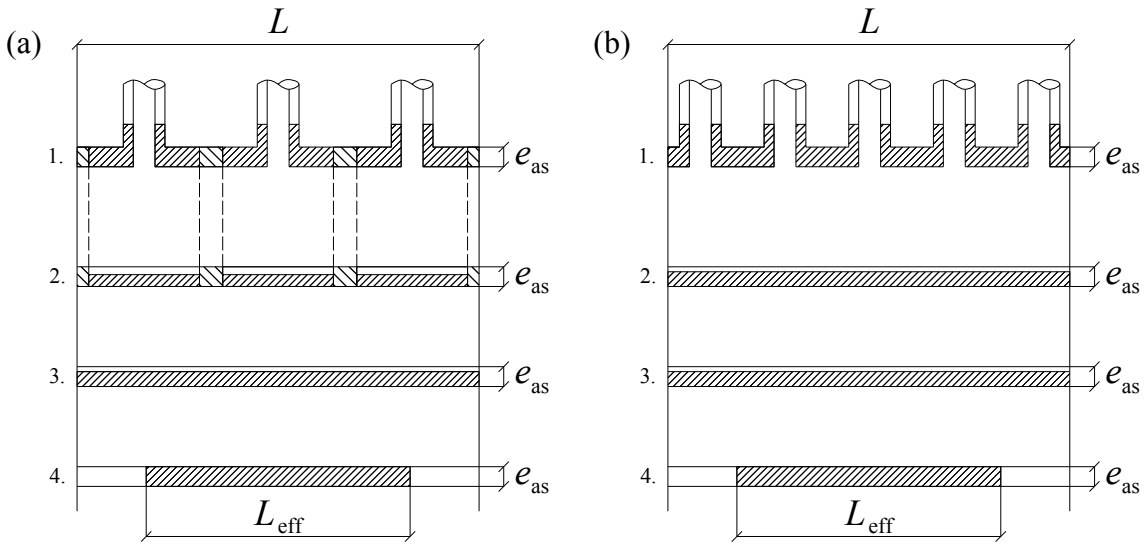

Figure 6-13. The effect of branches; (a) isolated openings, (b) adjacent openings.

The four steps are

1. Calculate effective cross-sectional areas according to EN 12952-3.
2. Reduce wall thickness on the nozzle area.
3. Calculate the final effective wall thickness for the whole header taking into account reinforcing effect of the areas between nozzle areas.
4. Transform the reduced wall thickness to the original by reducing the length of the header.

The step four enables the use of original wall thickness and makes calculations simpler. If pitch is sparse, i.e. openings are isolated, the step three takes into account the reinforcing effect of the areas between the nozzle areas. There again if pitch is dense, i.e. openings are adjacent, the step four is not deeded, because the nozzle areas cover the whole length of the header.

In case the design stress of the branch is less than that of the header; the effective area of the branch is reduced with the ratio of the design stresses. If the design stress of the branch is higher than that of the header, the calculation design stress is the same as the one of the header, i.e. following condition must be satisfied

$$\frac{f_{\mathrm{b}}}{f_{\mathrm{s}}} \leq 1 \,, \tag{67}$$

where f_{b} is the design stress of the branch and f_{s} is the design stress of the header. This condition is the same for design by formulas in EN 12953-2 in chapter 8.3.3.2.

The result from this procedure is an efficiency factor that may be used for a single plastic hinge. The efficiency factor reduces the equivalent length of the hinge.

The used areas are meant to be used when determining the headers capacity for internal pressure, not to be used when determining the plastic capacity for bending. Now it is possible to make good use of the angle variable θ; the wall panel is always downwards but the roof panel is sometimes at 90° angle and sometimes 95°, and the angle that oth-

er connecting pipes vary. Also the angle where the hinge at side locates is not always 90°. Using the variable θ provides a more fluent use of equations.

The effective areas of the cross-sections are defined to be equal to the effective cross-sectional area of the plain header. Stresses are supposed to be linearly distributed circumferential stresses – not secondary bending of the shell. If these areas are used for plastic capacity examination, the secondary bending is ignored. The cross-sectional area of the connecting branch is further of the equal area axis than it is now assumed. The true effect is now assumed conservative. Even though this method is simplified and a bit robust, the test results from FE-analyses support this method.

6.2.6 Punching Shear

Another possible failure type is punching shear. In this failure type the maximum shear is dominant and no plastic hinges are formed so the principal of virtual work is not useful as it was used earlier. A punching shear dominant header is presented in Figure 6-14.

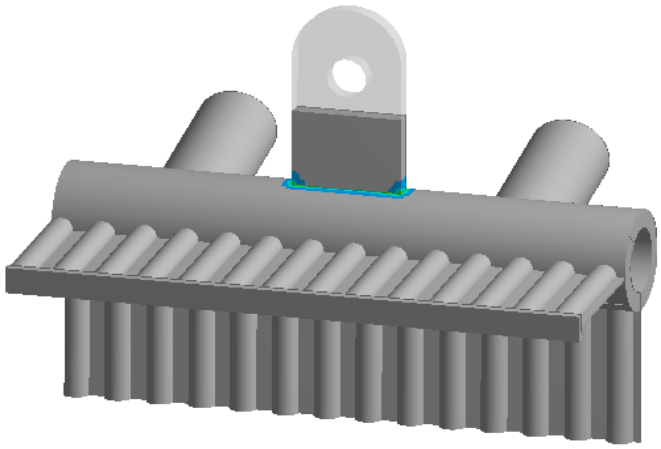

Figure 6-14. Plastic strain of a header when the punching shear failure type is dominant.

When analyzing the results from the FE-analyses, it was noted that internal pressure but also the bending moment decrease the shear capacity. This failure type is approached by reducing the equivalent height of the cross-sectional area for shear. The deduction of

the formulas is presented in Appendix V. Because solving these equations is easiest numerically, the used equations are presented only in Appendix V.

The cross sectional area is divided in three sections; two areas for bending moment $A_{M.\tau}$ and area for the shear force A_τ. These areas are shown in Figure 6-15. The cross-section is assumed to be a rectangle. The circumferential stress caused by internal pressure weakens the circumferential stress of the area for the shear force A_τ and the is no area specifically for normal force. External load do not cause normal force on the shearing area.

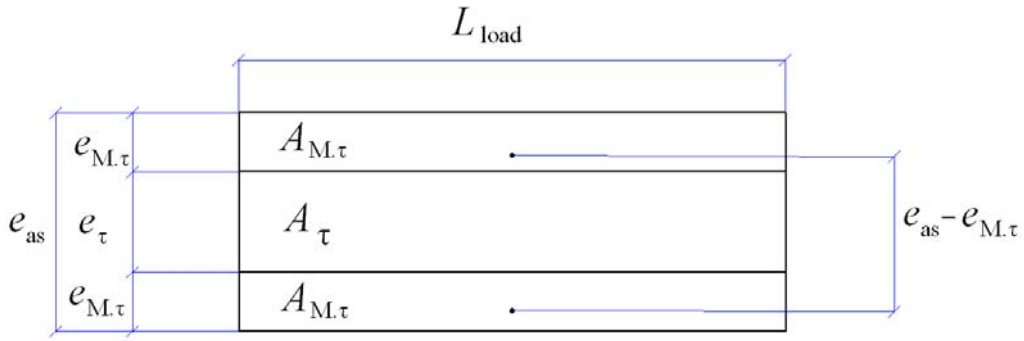

Figure 6-15. Cross-sectional areas when determining punching shear.

When punching shear is dominating, the bending moment distributes wider than the applied force and shear force. This is why the width of the normal stress caused by the bending moment is left as a variable $L_{M.\tau}$. This idea is shown in Figure 6-16.

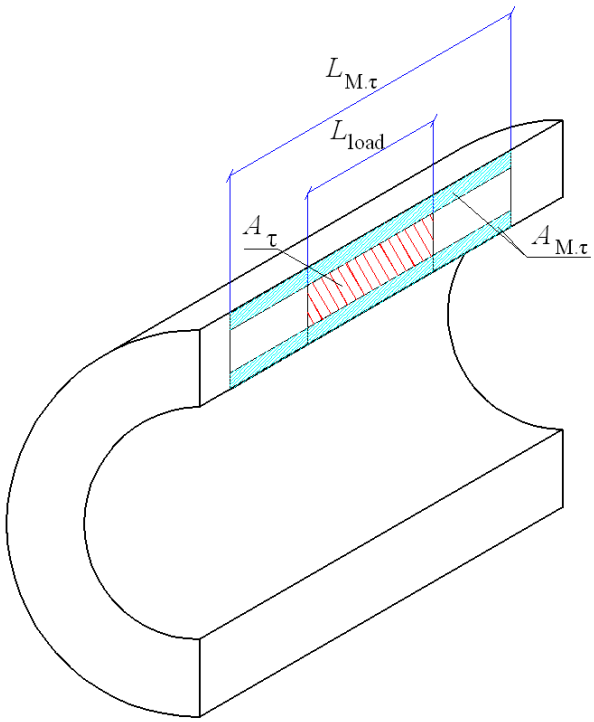

Figure 6-16. Different widths of the effective cross-sectional area for shear and bending moment.

The effective length $L_{M.\tau}$ is not the same as it is when determining the plastic capacity using the principle of virtual work because plastic hinges do not form. The length $L_{M.\tau}$ is determined later.

The area on the narrow side of the lug is not taken into account. It is not clear how the bending moment affects on that small area. The capacity of this area is left as an extra capacity.

7 RESULTS

As written before, the research begun by analyzing just the header without any branches or lug. Then the wall panel was added and later the roof panel and the other

connecting pipes. The same header was studied by using both the FE-analysis and analytical solution.

One header was chosen to be an example. Its dimensions were; outside diameter d_{os} = 219.1 mm, calculation wall thickness e_{as} = 37.375 mm and the length of the plain header L = 1000 mm and if branches are added L = 1056 mm to make the pitch fit in the FE-models. The dimensions of the wall panel and the roof panel are; outside diameter d_{ow} = d_{or} = 80 mm, calculation wall thickness e_{aw} = e_{ar} = 18.137 mm and pitch P_0 = 88 mm. The angle between roof and lug is α = 95°. Design strength of all parts are f_s = f_w = f_r = 150 MPa. The wall thickness and thereby the outside diameter of the tubes of the wall panel are larger than usual because the capacity of the header was wanted to be more critical than the longitudinal strength of the wall panel. In other words the wall panel should not be more critical than the header so that the true plastic capacity of the header could be reviewed. The lengths of the modeled tubes of panels are equal to the effective length of pressure areas so that the FE-analyses would give similar results than the analytical solution.

7.1 Results from the Finite Element Analyses

Results from the finite element analyses are discussed in this chapter.

7.1.1 Plain Header

Symmetry was utilized and one fourth of a header was analyzed and boundary conditions were added as two parallel and opposite direction forces. The force on the lower part was affecting on all the cross section and the width of the force on upper part was varied. The used widths of the upper force were; L_{load} = 100 mm, 200 mm, 400 mm, 600 mm, 800 mm and 1056 mm. One remote displacement support was added to prevent rigid body motion. The effect of internal pressure was also studied using different values of internal pressures.

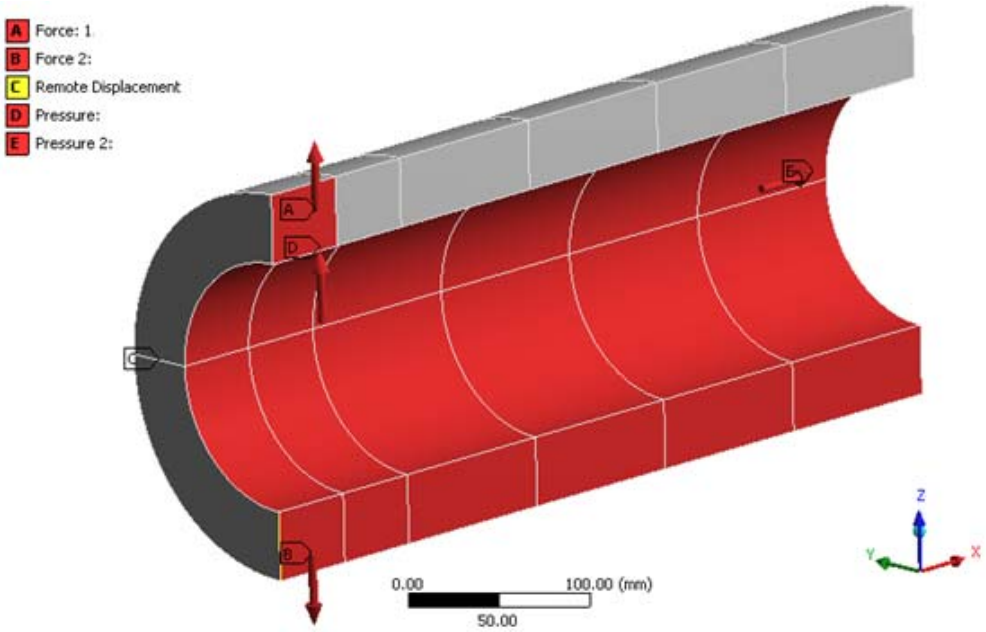

Figure 7-1. Boundary conditions of the plain header.

How the width of the force has notable effect on the failure mode is shown in Figure 7-2. The compiled results using different widths of force and different values of internal pressure are in Figure 7-3.

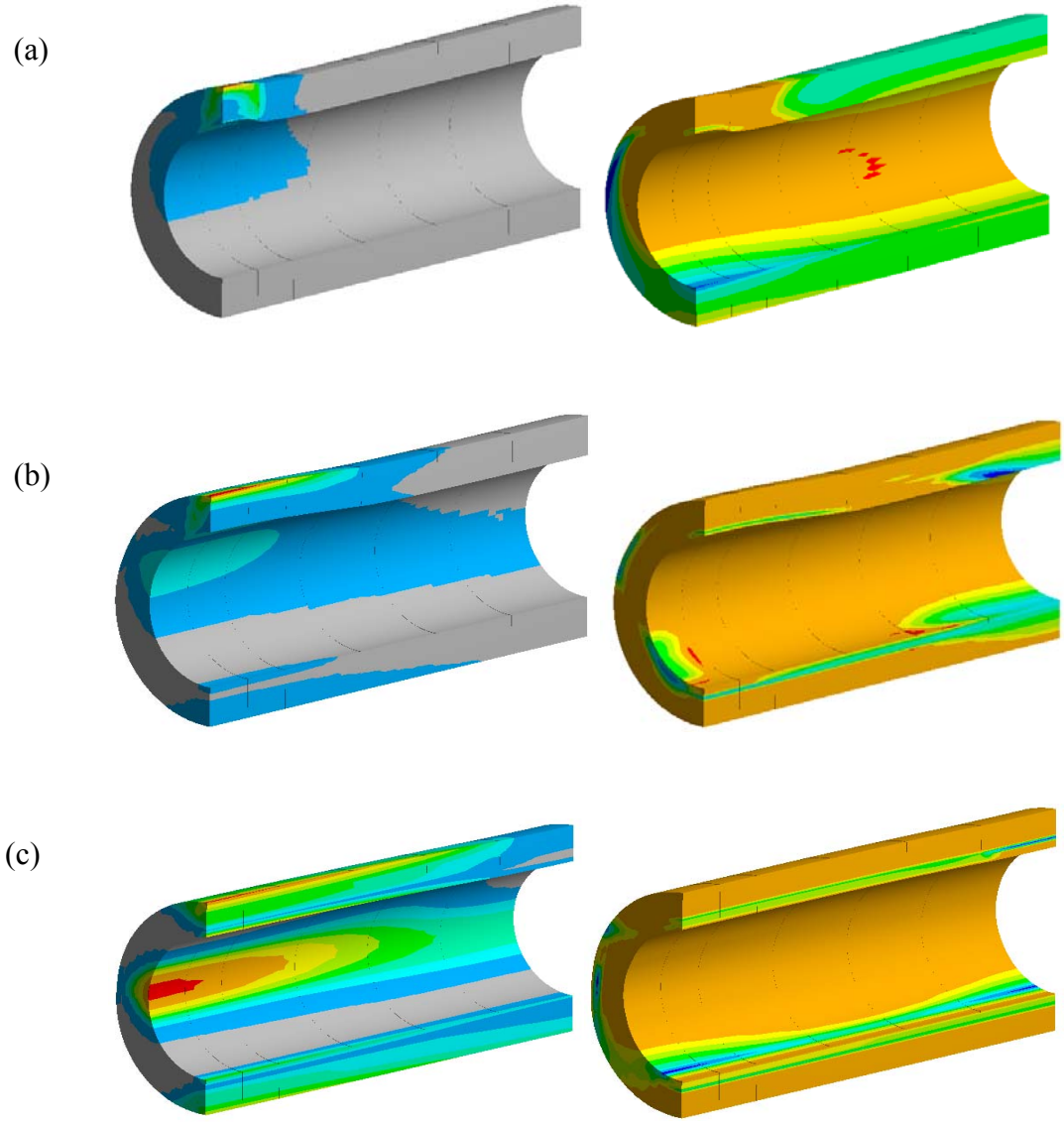

Figure 7-2. Plastic strains (left) and von Mises – equivalent stresses (right) when width of the load is (a) L_{load} = 100 mm, (b) L_{load} = 400 mm, (c) L_{load} = 800 mm.

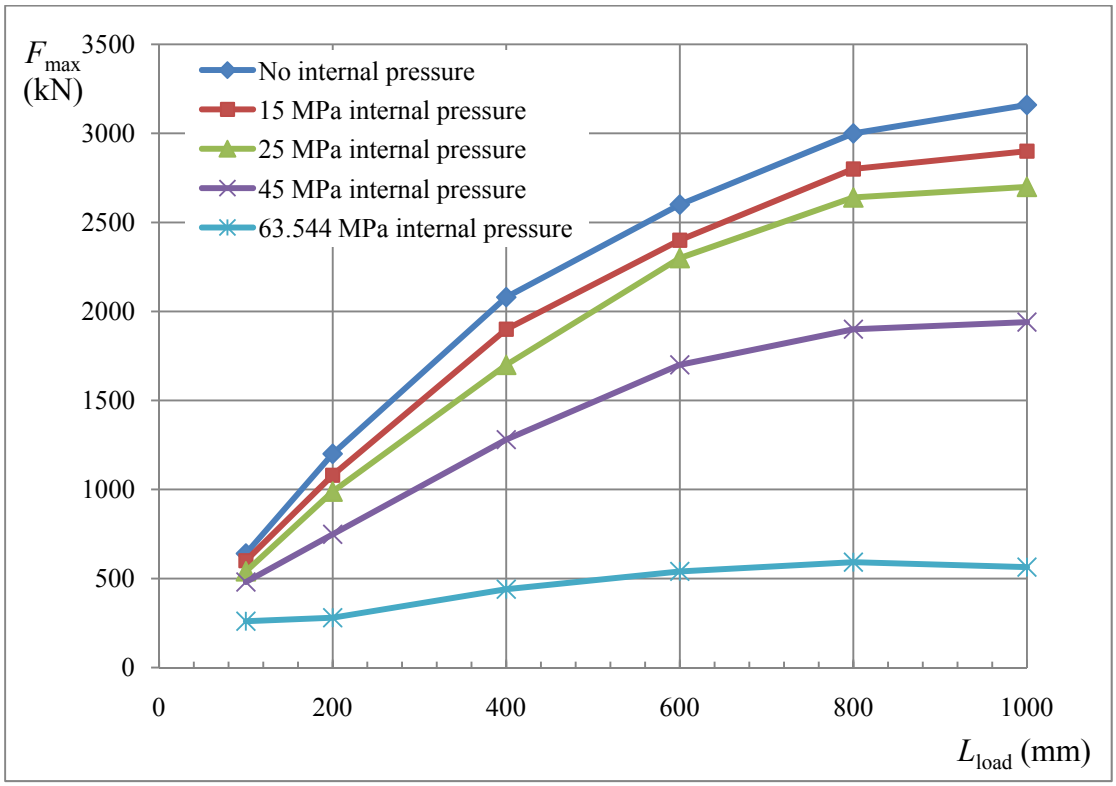

Figure 7-3. The comparison between FE-models with different width of force and different values of internal pressure.

The used internal pressure value of 63.5 MPa is the maximum value of internal pressure that normal pressure part calculations allow to use.

7.1.2 Header with Wall Panel and Roof Panel

The effects of wall and roof panels were approached by applying just wall panel and later on the roof panel. The effect of roof was also studied by applying roof on both sides so that the effect of roof was symmetric and later just on one side. The boundary conditions of these models are shown in Figure 7-4. The width of the load was modified as earlier. In the model where roof was only on one side, symmetry was used only once. The force was applied on a narrow strip on the outside surface to prevent local nodal dysfunction. This skews the punching shear results slightly.

(a)

(b)

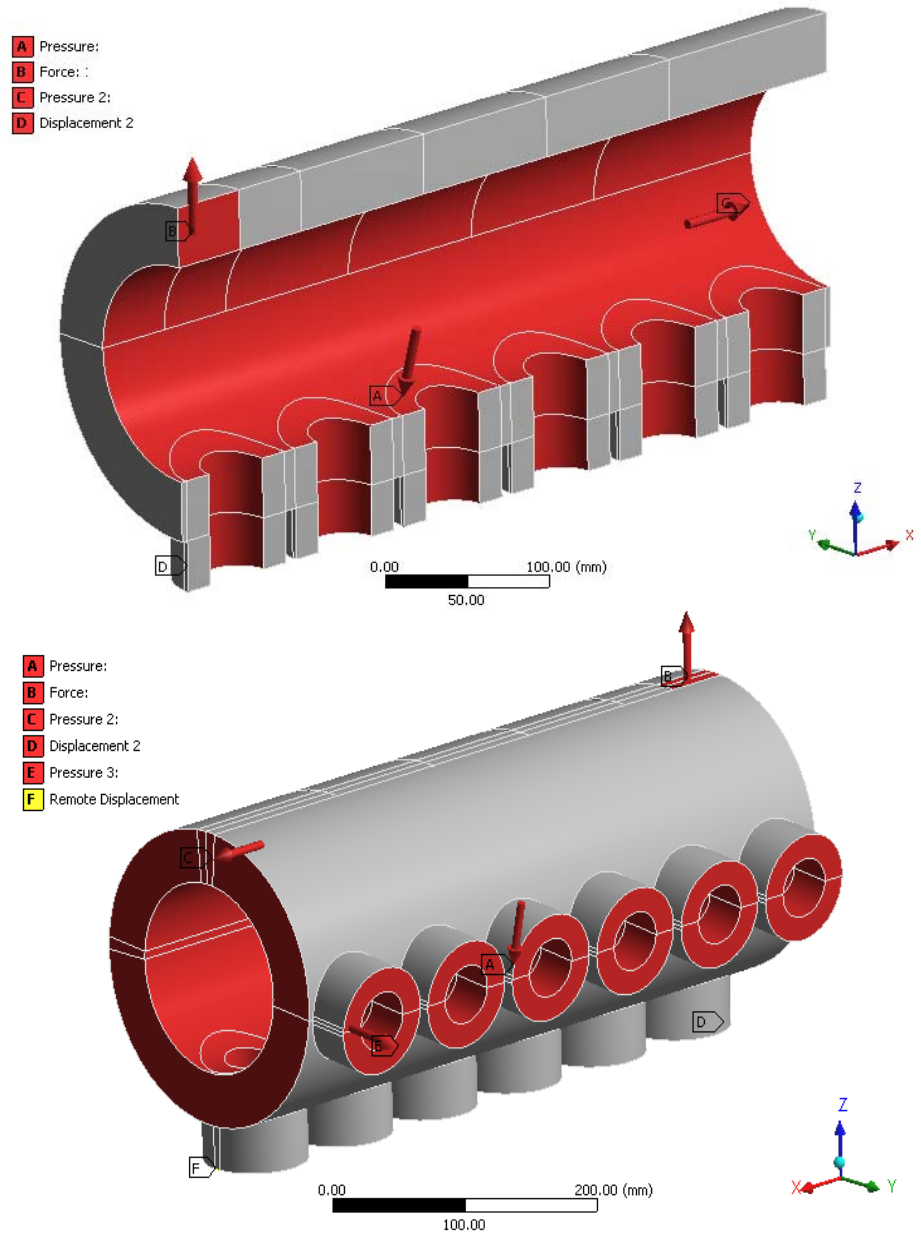

Figure 7-4. Boundary conditions when analyzing the effect of branches; (a) wall panel, (b) wall and roof panels.

Failure types were similar to the ones with the plain header and the location of the plastic hinge on the side did not significantly move. The plastic strain of a model with wall and roof panels when L_{load} = 400 mm is shown in Figure 7-5.

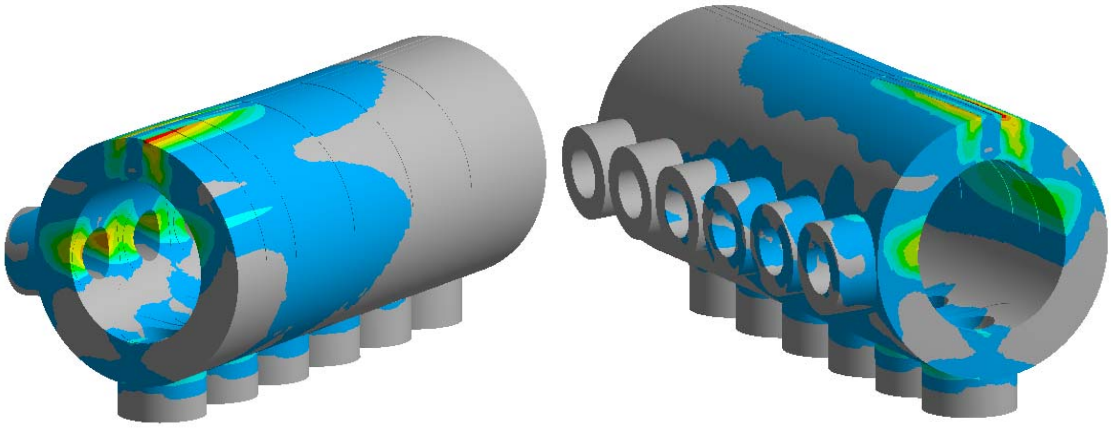

Figure 7-5. Plastic strains of a model with wall and roof panels when L_{load} = 400 mm.

Results from these FE-models are presented in Figure 7-6. The used internal pressure was 25 MPa.

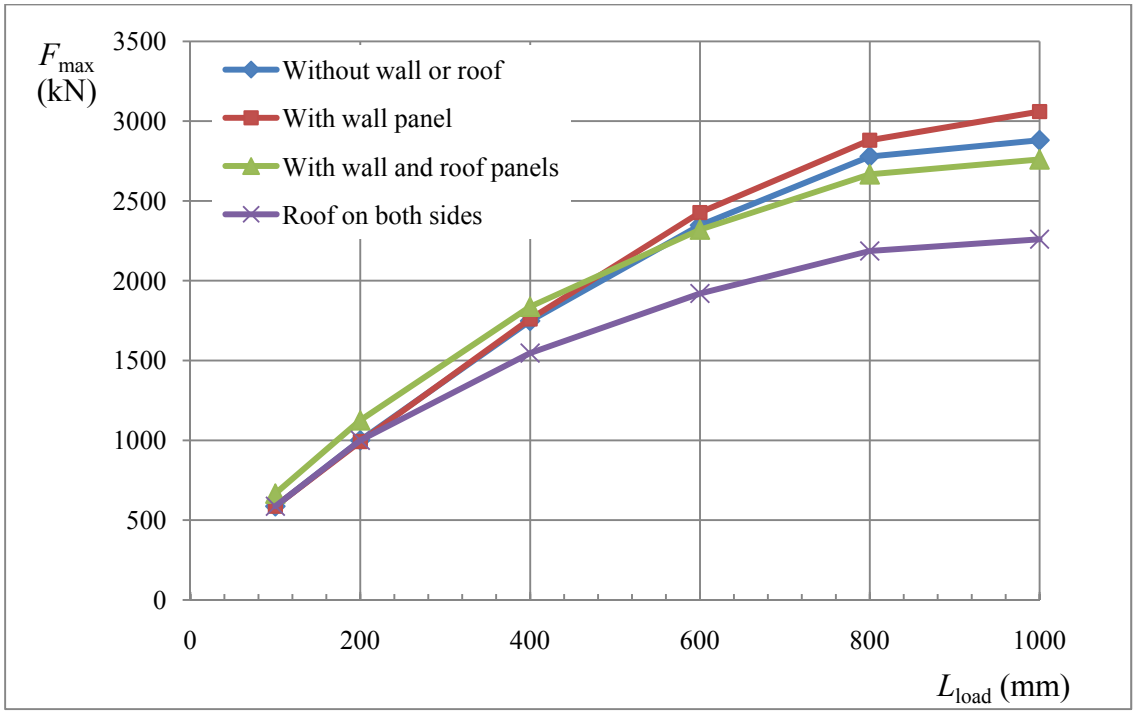

Figure 7-6. The effect of wall and roof panels and the width of the load when internal pressure is 25 MPa.

7.2 Results from Analytical Solutions

The length of the plastic hinge was left undetermined in chapter 6.2. The length of the plastic hinge is discussed in this chapter. The length of the plastic hinge is varied to fit best with the results from FE-analyses but also to be practical. Later the effect of roof and wall panels is studied.

7.2.1 Variable Length of the Plastic hinge

The first idea to approach the problem of the length of the plastic hinge was to assume the length on the upper hinge to have the length equal to the width of the load, i.e. $L_{Hi} = L_{load}$, similarly on the lower part. The length of the third hinge is assumed – using linear approximation – to have the length between the lengths mentioned earlier. This assumption is shown in Figure 7-7. The location of the plastic hinge is not yet defined but marked with the angle variable θ. This is why the length of the hinge is marked as a function $L_{H.i}(\theta)$.

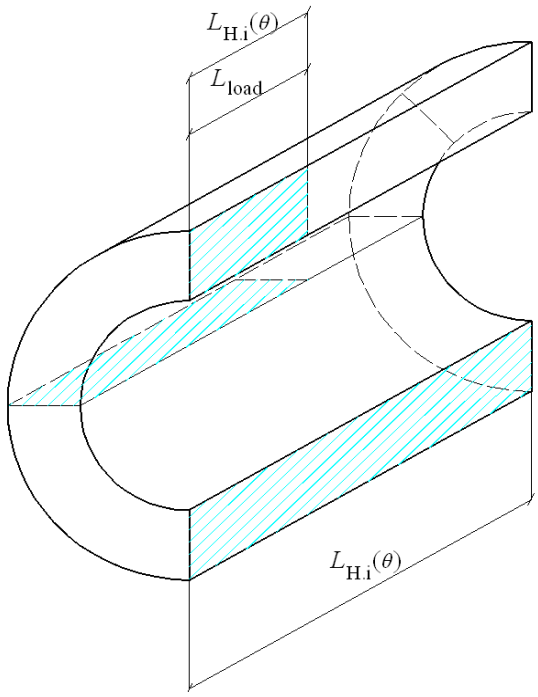

Figure 7-7. The variable lengths of the plastic hinges, one fourth of the header.

When the location of the third hinge is not fixed but is given by using angle variable θ, the location may be solved from the work-equation (63), finding the minimum of applied force $F(\theta)$. The forces corresponding to virtual work that each plastic hinge

makes and the sum of these forces as a function of angle variable θ, in other words $F_1(\theta)$, $F_2(\theta)$ $F_3(\theta)$ and $F(\theta)$ are plotted in Figure 7-8.

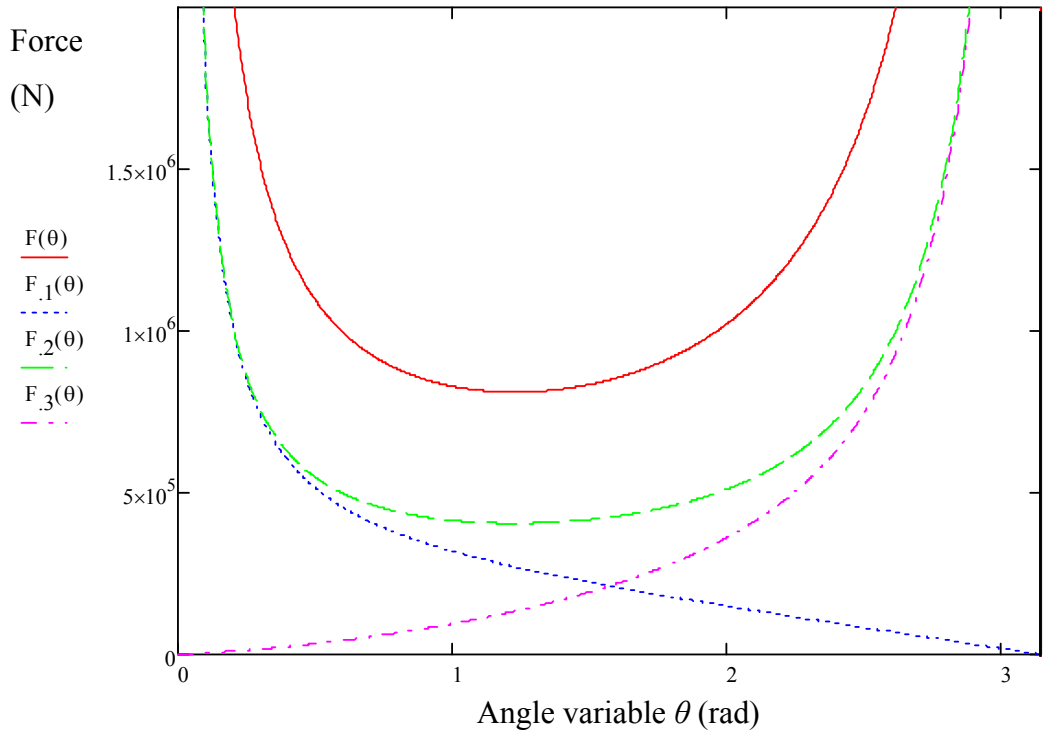

Figure 7-8. Applied forces corresponding to the work each hinge makes as a function of angle variable θ, when width of the force is 400 mm.

The minimum of the force $F(\theta)$ is when the angle variable has the value of 1.225 rad, i.e. 70.2°. This means that the smallest work is done when the location of the third hinge is at this angle. When the width of the force – as the length of the first hinge – decreases the angle of the hinge on side also decreases as well. If the load is applied to the whole length of the header, the third hinge is at 90° angle.

The lengths of plastic hinges in FE-models vary. The length of the lowest hinge is not equal to the length of the header if the width of the load is relatively narrow, see Figure 7-2(b). This is why other lengths of the plastic hinges were tested. This method turned out to be hard to define and the results did not quite match with the results from the FE-models.

7.2.2 Constant Length of the Plastic Hinge

To make calculations simpler it was assumed that all hinges have the same length, see Figure 7-9.

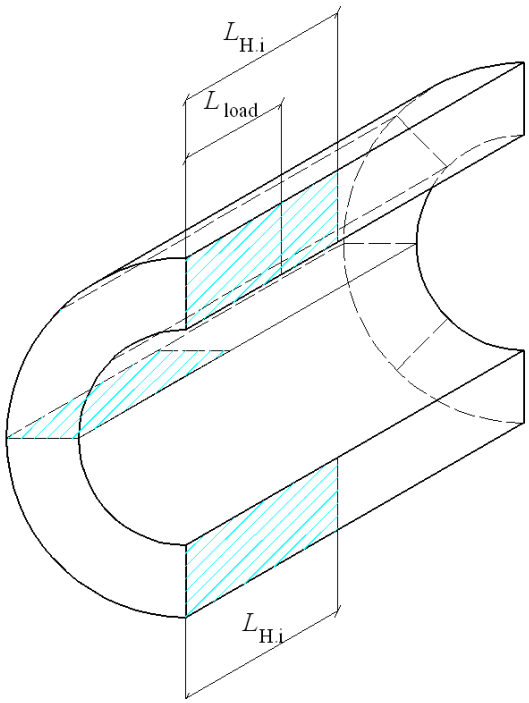

Figure 7-9. Constant lengths of plastic hinges, one fourth of the header.

To solve the equivalent lengths of the hinges, the length of the hinge in analytical solution was calculated. It gives the same force as FE-models. Equivalent length in some of the points was sorted out by this method. To make a formula from these points the method of least square was used. As a result from this procedure, it was noticed that if the effective length of the plastic hinge was $L_{H.i} = 1.5\ L_{load}$, the slope of the results from analytical solution is approximately the same as the results from the FE-models. This is shown in Figure 7-10. Lines are drawn in Figure 7-10 when the length of the plastic hinge is $L_{H.i} = 1.25\ L_{load}$ and $L_{H.i} = L_{load}$.

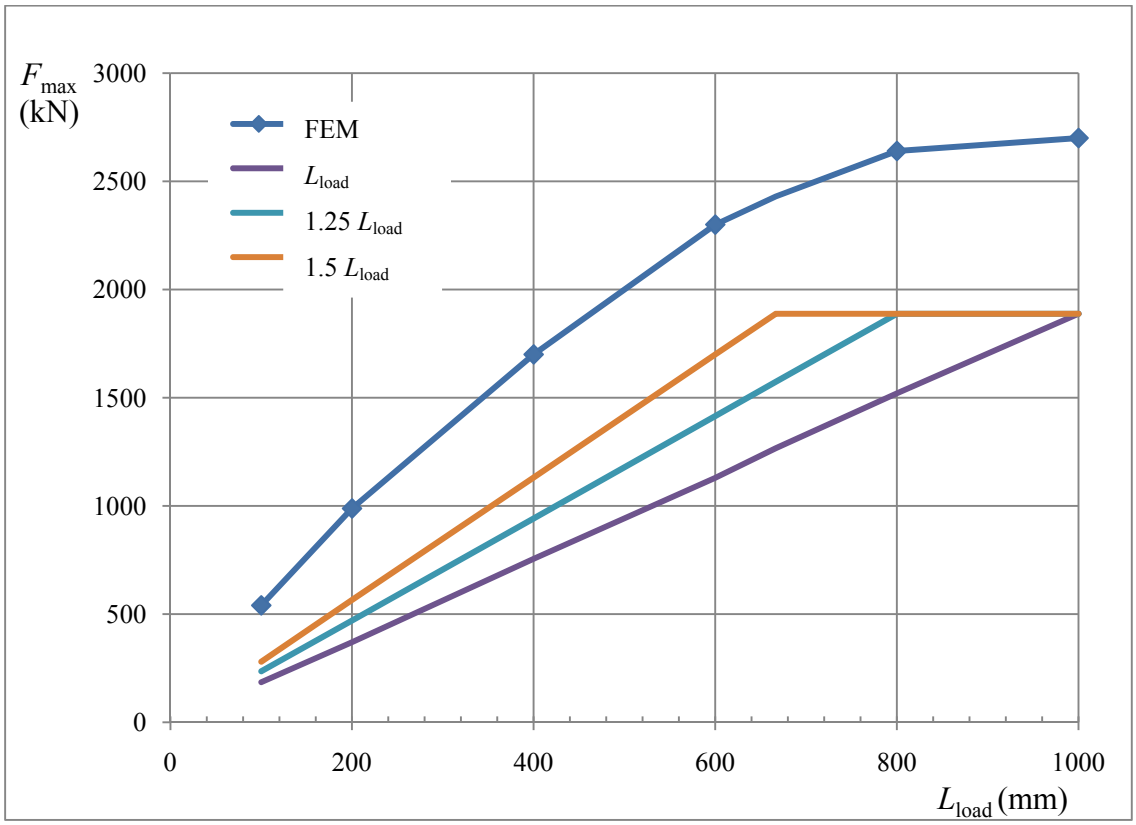

Figure 7-10. Load resistances with different length of plastic hinges compared to results from the FE-models.

The slopes of the curves in Figure 7-10 decrease as the length of the plastic hinge get closer to the length of the header. This is a natural limit value for the load resistance, because the theoretical length of the plastic hinge cannot be longer than the header.

The effective length of the plastic hinge is chosen to be $L_{H.i} = 1.25\ L_{load}$ because it reflects the slope of the curve of FEM on the area where the plastic capacity is dominant – not the punching shear – and it is properly conservative. The results are still a bit too conservative so a constant is added to the length of the plastic hinge. This constant is chosen to be a function of the outside diameter of the header. Therefore the diameter of the header is taken into account. Tester constants were d_{os}, 0.5 d_{os}, 1.5 d_{os} and 2 d_{os}. The results are in Figure 7-11.

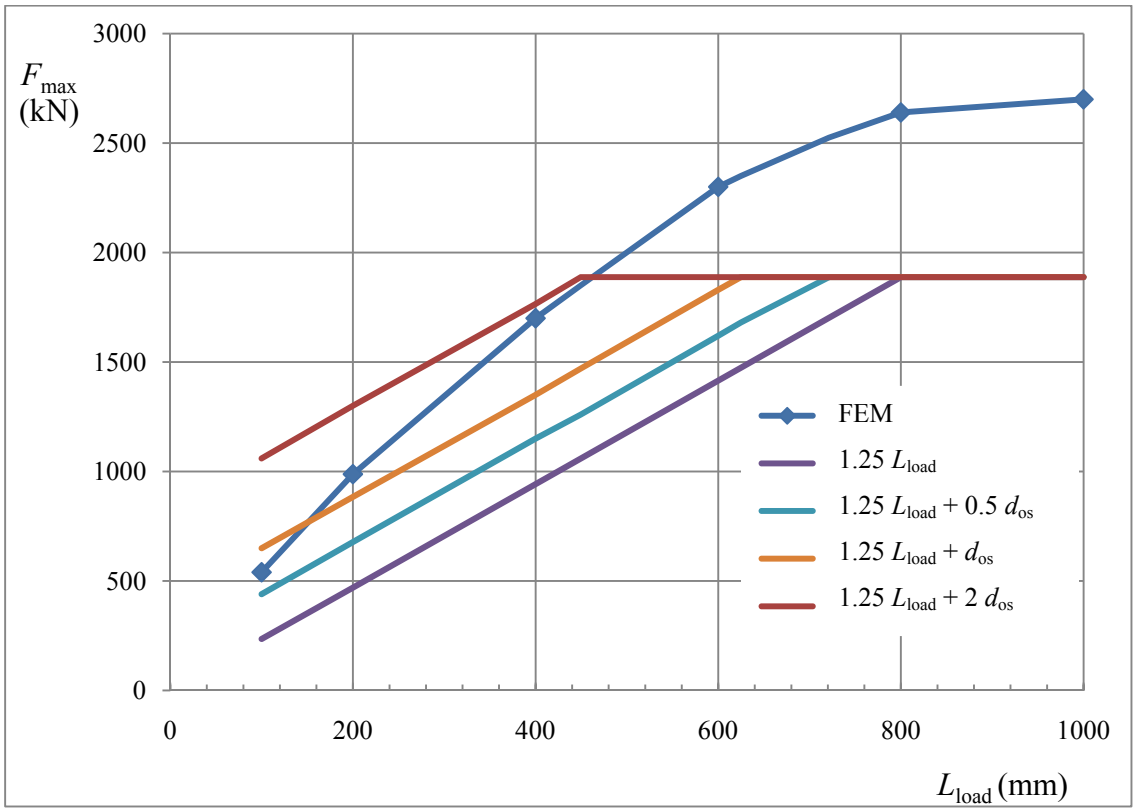

Figure 7-11. Load resistances with different length of plastic hinges when adding a constant to the length of the plastic hinge.

When using the constant term, results are less conservative, but if the constant term is chosen to be 2 d_{os} the results are on the risky side. For further research the effective length is chosen to be $L_{H.i}$ = 1.25 L_{load} + 0.5 d_{os}. These results are on the safe side. Because analyzed header is just one example it is not reasonable to make the length of the plastic hinge any longer.

7.2.3 Punching Shear

Because the cross-sectional area for shear stress A_τ is bordered only to the width of the load L_{load}, modified length is the length that bending moment affects $L_{M.\tau}$. This is shown previously in Figure 6-16. Analyzed lengths for bending moment were $L_{M.\tau}$ = L_{load}, $L_{M.\tau}$ = 2 L_{load} and $L_{M.\tau}$ = 3 L_{load}. The results from these analyses are plotted in Figure 7-12. For comparison the plastic capacity and results from FEM are also plotted.

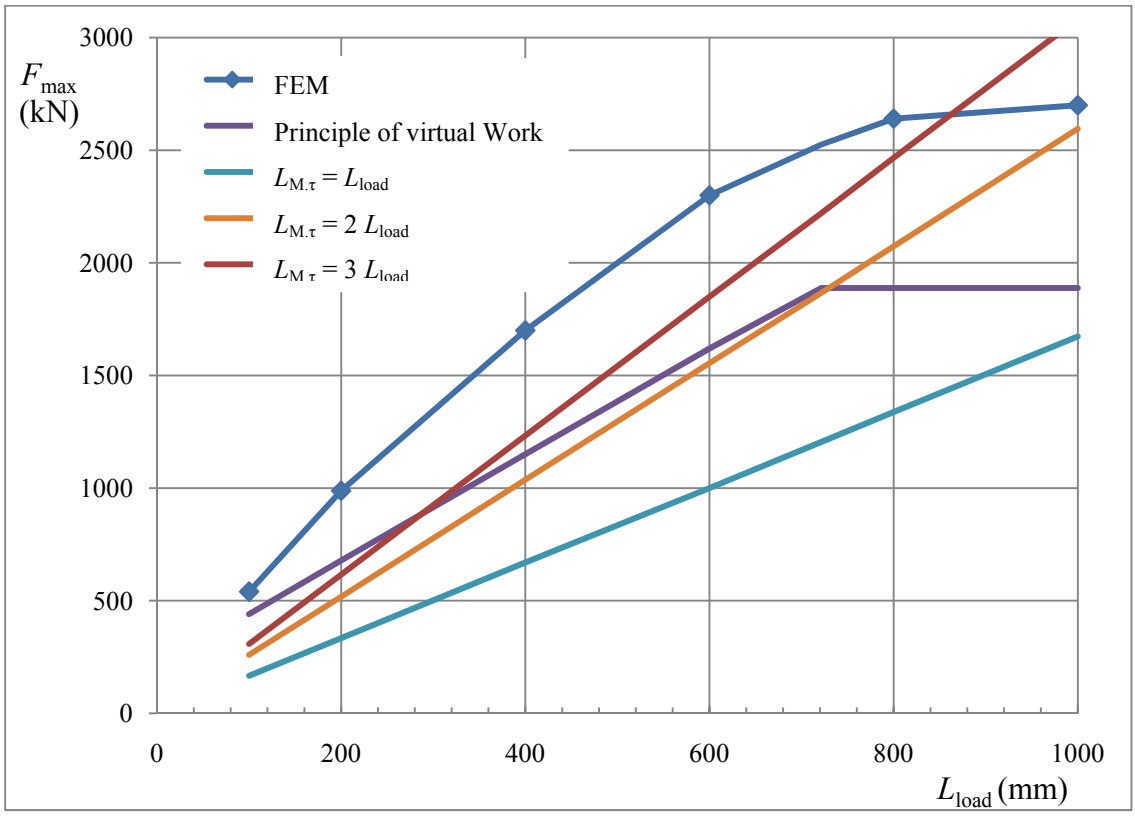

Figure 7-12. Capacities for punching shear with different length for bending moment.

It is notable that bending moment is spread on a wider area than shear force, because if the used length for bending moment is $L_{M.\tau} = L_{load}$, the results are remarkably smaller than the results from FEM. Only if the used length for bending moment is $L_{M.\tau} = 3\ L_{load}$, the curves of punching shear and the plastic capacity intercept and the slope of the punching shear capacity is closer to the slope of the curve of the FEM results on the area where punching shear is dominant.

7.2.4 Header with Roof and Wall Panels

The effects of the wall and roof panels are collected in Figure 7-13, Figure 7-14 and Figure 7-15. The results of the plastic capacity of the plain header and the punching shear are presented in these Figures. It is notable that neither the wall nor the roof panel affects on the capacity of punching shear.

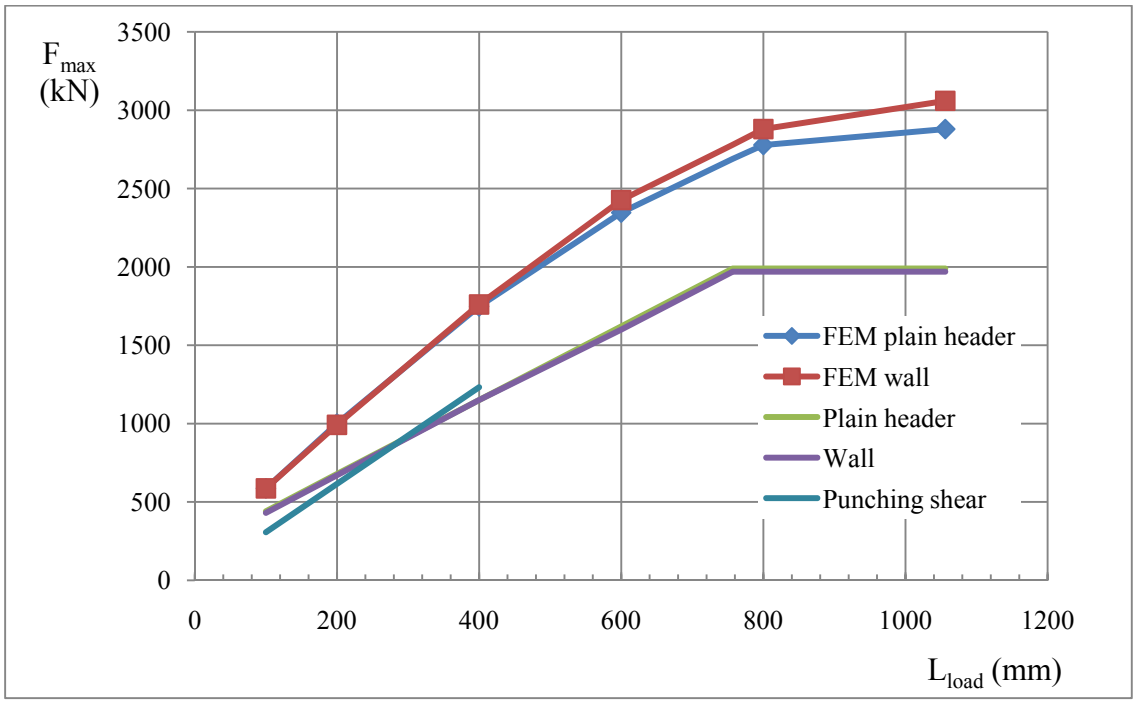

Figure 7-13. The effect of the wall panel.

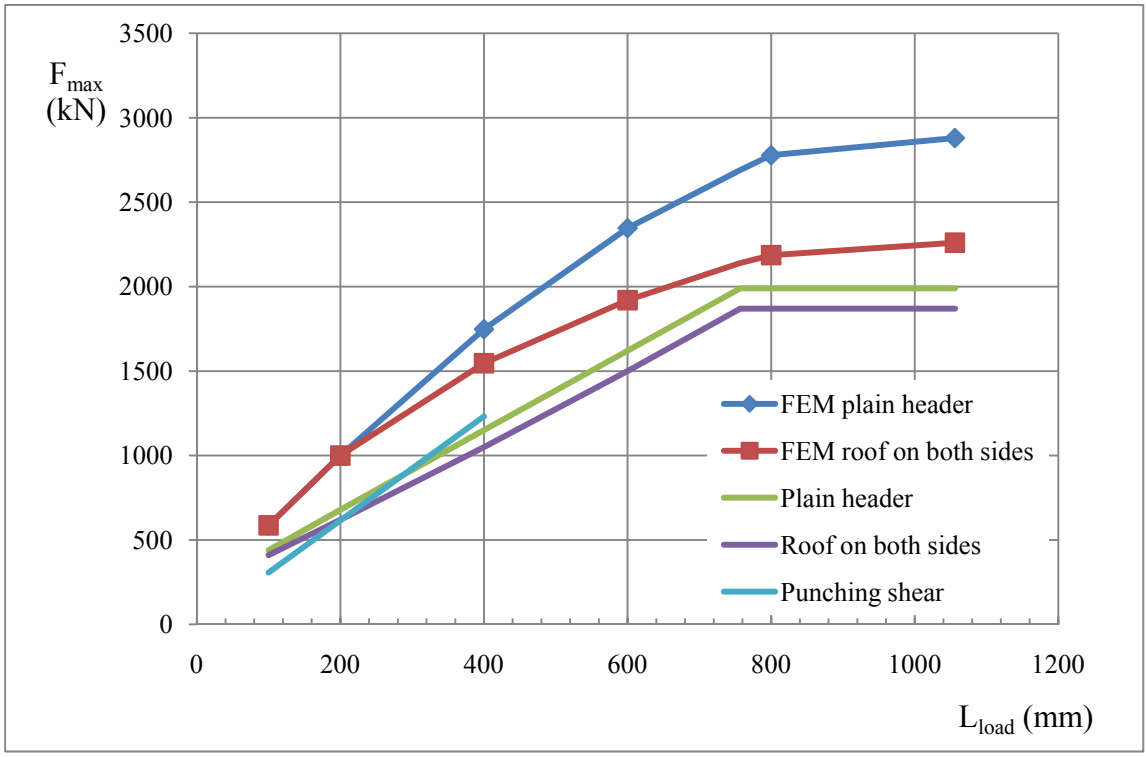

Figure 7-14. The effect of the wall panel and the roof panels added on both sides of the header.

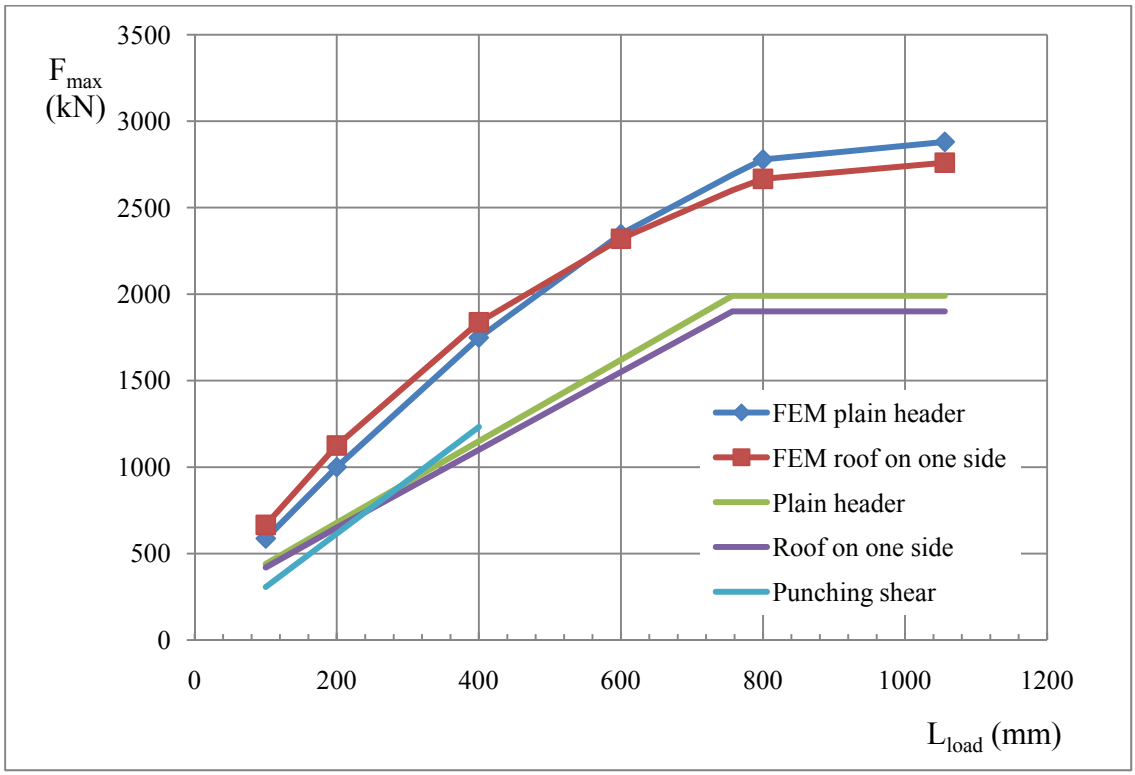

Figure 7-15. The effect of the wall panel and the roof panel added only on one side.

The corresponding force each plastic hinge makes in the case where only a wall panel is added and L_{load} is 400 mm is shown in Figure 7-16. The minimum capacity is when the second plastic hinge locates at the angle of 1.615 rad that is 92.5°.

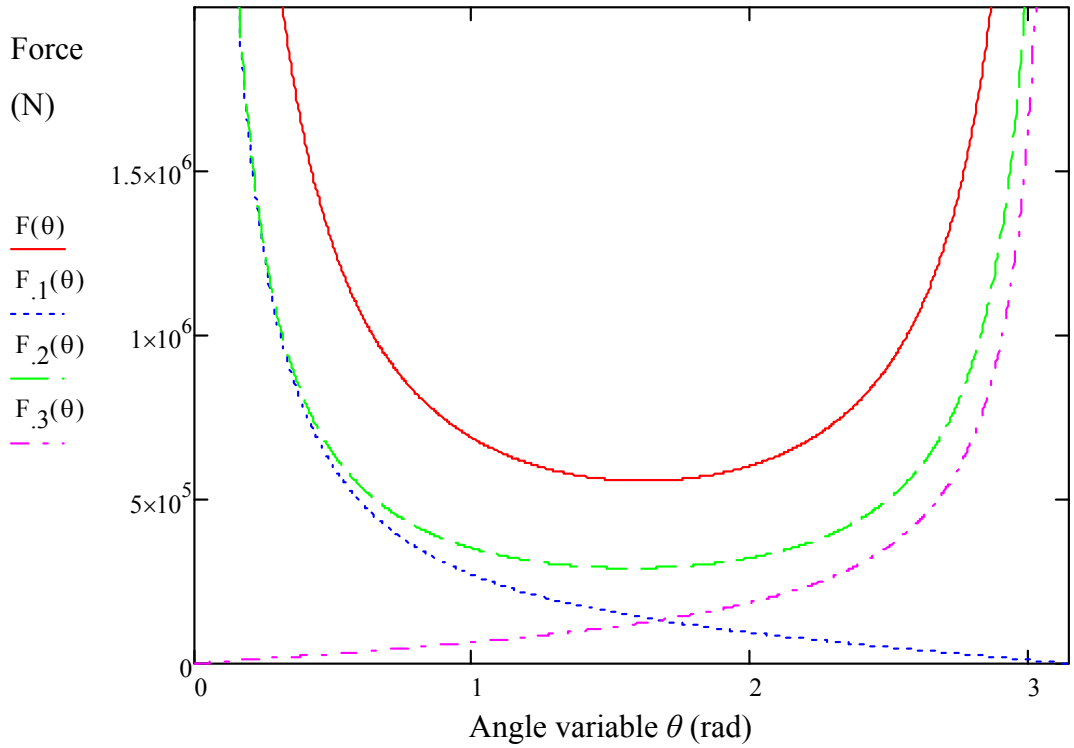

Figure 7-16. Applied forces corresponding to the work each hinge makes as a function of angle variable θ, when width of the force is 400 mm and the wall panel is added.

8 DISCUSSION

The results from the FE-analyses and the analytical solutions differ from each other. This chapter discusses the reasons of the differences and possible effects. Also the method for structural attachments is discussed.

8.1 Analyzing Headers According to Standards

If a header is analyzed by using the method of structural attachments presented in EN 12952-3 in chapter 11.5, the results are indefinable. The curves in Figure 5-2 are not logical. The angle α is given a rarely sharp decade and in those cases, where the angle α is not a decade, the figure is cumbersome. In addition, usage of this type of dimensioning is clumsy. The method is independent of the utilization rate of the internal pressure.

The conflicts in safety factors cause extra trouble when a more accurate method requires more safety. This is the most important reason why the used load cases are defined. The used load factors are in Table 6-1. The idea of load cases are from ASME but the level of safety is limited to the value of 1.5 as it is in EN 12952-3.

8.2 Differences in the FE-models and Analytical solution

This chapter discusses the differences in the FE-models and analytical solution.

8.2.1 Differences in Analyzing Plain Header

First simplification was that the radial stress caused by the internal pressure was assumed to be linearly distributed over the wall thickness. In thick walled vessels the radial stress distribution is parabolic and the linear assumption is conservative. This simplification causes first differences between the FE-models and the analytical solution.

The biggest difference between the FE-models and the analytical solution was the failure types. In the analytical solution failure type changes from punching shear to plastic capacity, but in the FE-analyses there was a third failure type as shown Figure 7-2(b). In this model there are three plastic hinges but the one on the side is not at the right angle but slightly higher. Also the uppermost and this side hinge unite at the end of the lug. This failure type is familiar from rectangular hollow sections. This area where the two hinges unite is troublesome to define and that is the reason why in analytical solutions this area is bounded put and left as an extra capacity.

The plastic hinge on side and its location was the idea why the length of the plastic hinges was first thought as variables. This made it possible to consider the location of the plastic hinge on side as a variable. Finally the location of the plastic hinge was solved and the result corresponded to the results from the FE-models. The reason why the side hinge moves higher is that shear stress is different in all hinges and the plastic moment is smaller in uppermost hinges and biggest on the lowermost hinge.

The effective lengths of the plastic hinges were hard to define if the lengths of the hinges were variable compared to each other. Also the length of the lowermost hinge is not equal to the width of the load at the lower part and it was not justified to assume the length of the lowermost hinge to be equal to the length of the header. There could be a conflict where a long header with just one lug would have relatively long plastic hinges and therefore too much capacity. This led to the decision where all hinges have equal lengths. Now the lengths of the hinges were simpler to define. If all hinges have equal lengths the location of the side hinge is at the right angle.

The effective length of the plastic hinge was chosen to be a function of the width of the lug, i.e. the width of the load, and of the outside diameter. Therefore the dimensions of the lug and the header are taken into account.

8.2.2 Differences in punching shear

The analytical results of punching shear were also conservative. It is likely that in the FE-models the bending moment takes effect outside the area of shear force. A part of the bending moment naturally affects on the area of the shear if not the results from the FE-models would give exactly the shear capacity of the simplified cross-section without shear or pressure reductions.

The reason why a constant term is not added in the length where bending moment affects – as it is in plastic capacity – is that the equations would not give zero capacities even though the width of the load would decrease to zero. In other words the curves of punching shear in Figure 7-12 would not go through the origin.

In these calculations the small cross-sectional area of the lug is not taken into account but it is left as an extra capacity. This means that the width of the lug is the effective length of the load L_{load} not the front area of the lug.

Branches have no effect on the shear capacity. In the FE-models if the roof is only on one side of the header, as shown in Figure 7-4, the force is applied on narrow strip on the surface of the header. This slightly skews the results presented in Figure 7-6.

8.2.3 Effect of Branches

When analyzing the effect of the wall using FE-analysis, the wall panel seems to give extra capacity comparing to the plain header. This extra capacity is an error caused by the boundary condition placed on the cross-section of the pipes. This support caused longitudinal stress on the tubes of the wall panel and thereby supports the header. The roof panel reduces the plastic capacity like the wall panel would do if the longitudinal displacement was free. This extra capacity affects all models with the wall panel and that is why the results are considered with caution.

The wall thicknesses of the tubes of the wall panel were thickened so that the capacity of the wall panel was no more critical. This made the outside diameter of the tubes relatively big and the nozzles are close to each other. This kind of structure is not used but the outside diameters and so the wall thicknesses of the connecting tubes are smaller.

In manual calculations the location of the plastic hinge on the side moves slightly lower when the wall panel is added. This phenomenon is caused by the weakened plastic moment of the lowermost plastic hinge. The plastic hinge on the side did not move in the FE-analyses. In all analytical solution where the plastic hinges have equal lengths the location of the side hinge is approximately at 90° angle and the slope near the minimum work, i.e. the plastic capacity. If the hinge is assumed to be exactly at 90° angle, the approximate error is not significant.

Naturally, one source of an error is the effect of branches when implemented in the same way as in determining the headers capacity for internal pressure. The used method does not give true results but the weakening effect is close enough when taken into account other sources of error.

8.3 Suggestions for Further Research

The results from the analytical solutions should be closer to the results from the FE-analysis. Also a true scale test in a laboratory could help the calibration of both the analytical and the FE-solutions. The real distribution of the radial and circumferential stresses caused by the internal pressure should be taken into account especially when

the wall thickness of the header is thick. The linear assumption of the radial stress and the circumferential stress assumed as constant are both conservative.

Probably the biggest effect in the results is the equivalent length of the plastic hinge. The used parameter for the length $L_{H.i} = 1.25\ L_{load} + 0.5\ d_o$ is conservative. More different sized headers should be tested to calibrate these parameters. Similarly the equivalent length for the bending moment in punching shear needs more testing for calibration.

The true effect of branches is much more complicated and more research is needed. The weakening effect of the holes could be easily determined. This is probably too conservative approach and the branch gives extra – and more close to the actual – capacity. The branch itself affects the capacity in a more complicated way. First the effective length, which the plastic moment affects, should be determined. Then the final plastic moment could be determined using these effective areas.

In punching shear the width of the area bending moment affects is also left parametric and may be later modified. The width of the lug determines the shearing area. Also the small side should be taken into account, in other words more capacity could be taken into account if the whole perimeter of the lug is analyzed. The small cross-sectional area is not taken into account in the thesis because the effect of the bending moment on this area is not known and it needs more research.

The shape of the header transforms from a circle to an ellipse like shape when it is loaded. When the roof is added and the modeled length of the tubes is relatively long the roof starts to resist the transformation of the header. The roof operates as a supporting spring. This effect is ignored in this thesis but it should be studied more. The roof may be dozens of meters wide and the tubes are several meters long so the roof is a relatively stiff structure to carry loads parallel to the roof. This phenomenon may give extra capacity for the header.

The headers capacity to resist and distribute loads as a beam was bounded out in this thesis. This is still a significant load carrying method and should be studied. If the capacity to distribute loads from the lug to the wall panel is confirmed, the pitch of the lugs may be spaced. However, this requires a limit value for the capacity to distribute loads.

The lugs are usually placed parallel to the header. This causes loads in unwanted directions when the boiler is in operation and thermal expansion is significant. One solution in this could be to place the lug perpendicularly to the header in some headers depending of the location in the boiler. The studied issue is how the rotation would affect the failure type and thereby the plastic capacity. Also the manufacturing point of view should be considered.

9 CONCLUSIONS

The ready equations provided in standard EN 12952-3 in chapter 11.5 are clumsy. This type of dimensioning does not give reliable results when the utilization rate of the internal pressure, the effects of branches or corrosion allowances are not taken into account. This is the main reason why the design by formulas is replaced by design by analysis.

The given guidelines – especially the safety factors – for DBA differ significantly from the ones given for DBF. In EN 13445-3 for creep rupture the required level of safety in DBF is 1. 5 when it is in DBA 1.25. EN 13445-3 requires in the gross plastic deformation design check that the materials strength is to be multiplied by $\sqrt{3}/2$ if the von Mises yield criterion is used. This reduces the capacity by 15.5 %. On the other hand ASME uses load cases and requires the level of safety to be 1.7 in some load cases for some loads. Due to this confusion loadings are divided in load cases and the used load factors are in Table 6-1. The level of safety is similar to EN 12952-3 so when a more accurate analysis is made no extra safety is required.

When determing the plastic capacity of the header the effective lengths of the plastic hinges were challenging to define. The variable lengths of the hinges turned out to be complex and the hinges decided to have equal lengths. The length in final calculations was $L_{H.i} = 1.25\ L_{load} + 0.5\ d_o$. This curve fitted properly to the results from the FE-analyses and still was on safe side. Because only a few models were analyzed using FEM, the used parameters for the length of the hinges are conservative. The parameters may be fixed later on the grounds of future research.

The location of the plastic hinge on the side was undefined. When the lengths of the plastic hinges were equal in the analytical solution, the plastic hinge was at the right angle. If the wall panel was added, the hinge moved slightly lower. This movement is not taken into account to keep the calculation simple and because the movement did not occur in FE-models. If the roof panel was added, the panel weakened the plastic capacity and the plastic hinge locates at the angle of the roof, which is not at the right angle.

The bending moment reduced the shear capacity notably and a more accurate method was required than pure shear stress. The bending moment was assumed to affect on inner and outer surfaces and the mid area was left for shear stress, as shown in Figure 6-16. The analytical results fitted the best with the results from the FE-analysis when the effective length of the areas carrying the bending moment was $2\ d_o$. The slopes of the result curves were similar. The effective length of the moment carrying areas may be fixed later on the grounds of future research as well as the length of the plastic hinges. Branches did not have an effect on the punching shear capacity in the FE-analyses or in the analytical solution.

The effect of branches was examined using pressure areas. Even though these effective areas are to determine the pressure carrying capacity, the results were promising. If the effect of the branches was analyzed using just the effect of holes, the results would be too careful. Extra capacity was needed and the strengthen effect of the branches was taken into account.

10 SUMMARY

The goal of the thesis was to make a dimensioning tool to define the plastic capacity of boiler supporting headers. Plastic capacity is needed because the elastic solution is too conservative. The material may yield even when only internal pressure is affecting and no external loads are added. The dimensioning tool is needed in proposal phase so that no FE-analysis is needed in project phase.

The FE-models were the starting point for the study. The study began by analyzing the headers of ongoing projects. For the analytical solution only plain header without any braches or lug was analyzed. Therefore the parameter of analytical solution could be calibrated. When determing the analytical solution, several simplifications had to be made.

The supposed failure type is presented in Figure 10-1. To define the plastic capacity of the header the plastic moments of hinges have to be defined. The internal pressure weakens the plastic capacity. The radial stress caused by the internal pressure has different value on the inside surface of the header than it has on the outside surface on the header. Because of the radial stress, there is extra capacity on the outer parts of the header to carry external loading.

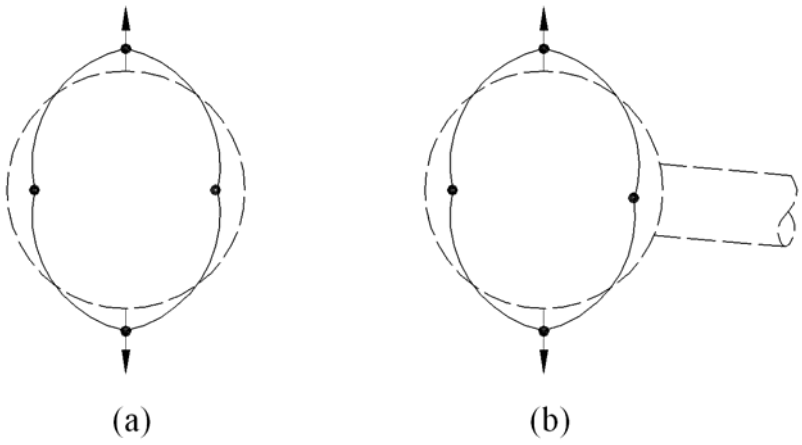

Figure 10-1. The supposed failure type of (a) plain header, (b) header with branch.

To make the formation of the analytical solution easier the extra capacity on outer parts of the header is taken as an extra cross-sectional area and the circumferential stress is kept as constant. In other words the effective length of the plastic hinge is longer on the outside surface than it is on the inside surface and the effective cross-sectional area has the shape of trapezoid. The internal pressure causes also circumferential stress that weakens the plastic moment. The weakening effects of shear and normal stresses caused by external loading are taken into account.

The effective lengths of the plastic hinges were significant point of research. Variable lengths were studied but the calculation model with equal lengths of the hinges fitted better in the results from the FE-models. The final capacity of the header is defined using the principle of virtual work. The effect of branches was analyzed using pressure areas. This method is not intended for plastic capacity but for the capacity for internal pressure. However, the results from analytical solution correlated with the results from the FE-models.

The internal pressure and the bending moment, caused by the external load, weaken the capacity of punching shear. The capacity is defined by reducing the equivalent wall thickness for shear. The widths of the areas for bending moment are growing while the shear stress affects only on the width of the applied load. The affecting bending moment is assumed to be elastic. The principle of virtual work is not used.

As a result of the research done for this thesis a simplified dimensioning tool for the plastic capacity of boiler supporting headers is established. Some parameter may be modified based on future research.

REFERENCES

ASME Boiler & Pressure Vessel Code 2010. Section II Part D. Properties (Metric) Materials. Addenda 2009b.

ASME Boiler & Pressure Vessel Code 2010. Section VIII Division 2. Alternative Rules: Rules for Construction of Pressure Vessels. Addenda 2009b.

Baylac, G. & Koplewicz, D. 2004. EN 13445 "Unfired pressure vessels" Background to the rules in Part 3 Design. Union de Normalisation de la Mécanique.

Chakrabarty, J. 1987. Theory of Plasticity. McGraw-Hill. 791 p. ISBN 0-07-010392-5

Chen, W.F. & Han, D.J. 1988. Plasticity for Structural Engineers. New York: Springer-Verlag. 606 p. ISBN 0-387-96711-7

Chen, W.F. & Zhang, H. 1991. Structural Plasticity: Theory, Problems, and CAE Software. New York: Springer-Verlag. 250 p. ISBN 0-387-96789-3

Davies, J.M. & Brown, B. A. 1996. Plastic Design to BS 5950. United Kingdom: Blackwell Science. 326 p. ISBN 0-632-04088-2

Hakala, M. 1980. Lujuusopin Elementtimenetelmä. 5. ed. Espoo: Otatieto. 490 p. ISBN 951-671-395-5

Horne M. R. & Morris L. J. 1981. Plastic Design of Low-Rise Frames. London: Granada Publishing. 238 p. ISBN 0-246-11199-2

Häkkilä, Juha. Welding Coordinator. Foster Wheeler Energy Oy. [Conversation] 9.3.2011

Kaliszky, S. 1989. Studies in Applied Mechanics 21; Plasticity: Theory and Engineering Applications. Amsterdam: Elsevier Science Publishers and Budapest: Akadémiai Kiadó. 505 p. ISBN 0-444-98891-2

Ohnami, M. 1988. Plasticity and High Temperature Strength of materials, Combined Micro- and Macro-Mechanical Approaches. London: Elsevier Applied Science. 525 p. ISBN 1-85166-199-0

Pilkey, W. 2005. Formulas for Stress, Strain and Structural Matrices, 2nd edition. New Jersey, Hoboken, John Wiley & Sons. 1511 p. ISBN 0-471-03221-2

prEN 12952-3 Water-tube boilers and auxiliary installations. Part 3: Design and calculation of pressure parts. 2008 september.

SFS-EN 10028-2 Flat products made of steels for pressure purposes – Part 2: Non-alloy and alloy steel tubes with specified elevated temperature properties. 2009.

SFS-EN 10216-2 Seamless steel tubes for pressure purposes – Technical delivery conditions – Part 2: Non-alloy and alloy steel tubes with specified elevated temperature properties. 2002.

SFS-EN 12952-3 Water-tube boilers and auxiliary installations. Part 3: Design and calculation of pressure parts. 2002.

SFS-EN 13445-3 Unfired pressure vessels – Part 3: Design. 2009.

Spyrakos, C. & Raftoyiannis, J. 1997. Linear and Nonlinear Finite Element Analysis in Engineering and Practice. Pittsburgh, PA: Algor Publish Division. 497 p. ISBN 0-9652806-2-4

Szilard, R. 2004. Theories and Applications of Plate Analysis: Classical, numerical and engineering methods. Hoboken, New Jersey: John Wiley & Sons. 1024 p. ISBN 0-471-42989-9

Timoshenko. S. 1956. Strength of Materials, Part II: Advanced Theory and Problems. 3rd ed. Malabar, Florida: Robert E. Krieger Publishing Company. ISBN 0-88275-421-1

Young, W.C. & Budynas, R. G. 2002. Roak's Formulas for Stress and Strain, 7th edition. McGraw-Hill. 852 p. ISBN 0-07-072542-X

APPENDIX I. EXAMPLE CALCULATIONS ACCORDING TO EN 12952-3, CHAPTER 11.5

Header's dimensions: d_o = 216.1 mm, e_t = 45 mm, c_1 = 5.625 mm.
Lug's dimensions: w_{lug} = 200 mm and wall thickness e_{lug} = 40 mm.
The design stress of the tube material is f_{MAWS} = 150 N/mm^2.

The angle subtended by the attachment at the header center in degrees

$$\alpha = 2 \cdot \arcsin\left(\frac{e_{\mathrm{lug}}}{d_{\mathrm{o}}}\right) = 21.038°$$

Ratio

$$\frac{e_{\mathrm{t}} - c_1}{d_0} = 0.18$$

From Figure 5-2, ratio

$$\frac{q}{f_{\mathrm{MAWS}} \cdot (e_{\mathrm{t}} - c_1)} = 0.47$$

Greatest intensity of radial force is

$$q = 0.47 \cdot f_{\mathrm{MAWS}} \cdot (e_{\mathrm{t}} - c_1) = 2776\ kN/mm^2.$$

Finally the maximum load is

$$F = q \cdot w_{\mathrm{lug}} = 555\ kN.$$

APPENDIX II. DEDUCION OF PLASTIC MOMENT

For clearness angle variable θ is not marked.

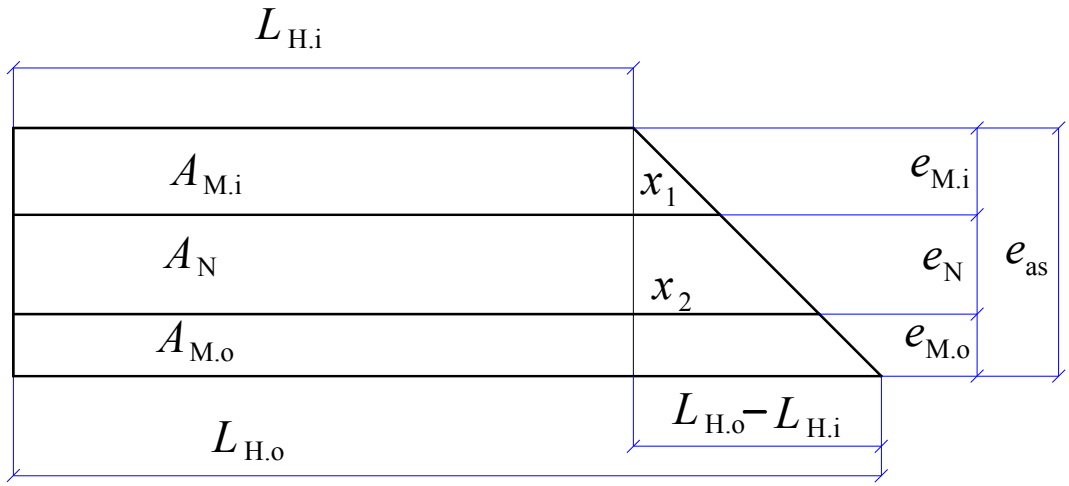

Figure II-1. Equivalent areas of the plastic hinge. For clearness areas are thought to be one side trapeziums.

Whole area of the plastic hinge is

$$A = \frac{e_{as}(L_{H.i} + L_{H.o})}{2} \quad . \tag{II-1}$$

Area is divided areas for normal force and plastic moment

$$A = A_{M.i} + A_{M.o} + A_N \tag{II-2}$$

and because $A_{M.i} = A_{M.o}$

$$A = 2 \cdot A_{M.i} + A_N$$

$$\Leftrightarrow A_{M.i} = \frac{A - A_N}{2} \quad . \tag{II-3}$$

Area for normal force is

$$A_{\mathrm{N}} = \frac{N + N_{\varphi} \cdot L_{\mathrm{H.i}}}{f_{\varphi.\mathrm{i}}} \quad . \tag{II-4}$$

Auxiliary variables x_1 and x_2 are

$$\frac{x_1}{L_{\mathrm{H.o}} - L_{H.i}} = \frac{e_{\mathrm{M.i}}}{e_{\mathrm{as}}} \Leftrightarrow x_1 = \frac{e_{\mathrm{M.i}}}{e_{\mathrm{as}}} \cdot \ (L_{\mathrm{H.o}} - L_{\mathrm{H.i}}) \tag{II-5}$$

$$\frac{x_2}{L_{\mathrm{H.o}} - L_{\mathrm{H.i}}} = \frac{e_{\mathrm{as}} - e_{\mathrm{M.2}}}{e_{\mathrm{rs}}} \Leftrightarrow x_2 = \frac{e_{\mathrm{as}} - e_{\mathrm{M.2}}}{e_{\mathrm{as}}} \cdot \ (L_{\mathrm{H.o}} - L_{\mathrm{H.i}})$$

$$\Leftrightarrow x_2 = \left(1 - \frac{e_{\mathrm{M.2}}}{e_{\mathrm{rs}}}\right) \cdot \ (L_{\mathrm{H.o}} - L_{\mathrm{H.i}})$$

$$\Leftrightarrow x_2 = L_{\mathrm{H.o}} - L_{\mathrm{H.i}} - \frac{e_{\mathrm{M.2}}}{e_{\mathrm{rs}}} \cdot \ (L_{\mathrm{H.o}} - L_{\mathrm{H.i}}) \quad . \tag{II-6}$$

Now may the inner part of the moment carrying area be determined

$$A_{\mathrm{M.i}} = \frac{1}{2} \cdot e_{\mathrm{M.i}} \left[L_{\mathrm{H.i}} + \frac{e_{\mathrm{M.i}}}{e_{\mathrm{rs}}} \cdot (L_{\mathrm{H.o}} - L_{\mathrm{H.i}}) + L_{\mathrm{H.i}} \right]$$

$$= \frac{1}{2} \cdot e_{\mathrm{M.i}} \left[2 \cdot L_{\mathrm{H.i}} + \frac{e_{\mathrm{M.i}}}{e_{\mathrm{rs}}} \cdot (L_{\mathrm{H.o}} - L_{\mathrm{H.i}}) \right]$$

$$\Leftrightarrow A_{\mathrm{M.i}} = e_{\mathrm{M.i}} \left[L_{\mathrm{H.i}} + \frac{e_{\mathrm{M.i}}}{2 \cdot e_{\mathrm{rs}}} \cdot (L_{\mathrm{H.o}} - L_{\mathrm{H.i}}) \right] . \tag{II-7}$$

Same for the outer part of the moment carrying area

$$A_{\mathrm{M.o}} = \frac{1}{2} \cdot e_{\mathrm{M.o}} \left[L_{\mathrm{H.o}} + L_{\mathrm{H.i}} + L_{\mathrm{H.o}} - L_{\mathrm{H.i}} - \frac{e_{\mathrm{M.i}}}{e_{\mathrm{rs}}} \cdot (L_{\mathrm{H.o}} - L_{\mathrm{H.i}}) \right]$$

$$= \frac{1}{2} \cdot e_{\mathrm{M.o}} \left[2 \cdot L_{\mathrm{H.o}} - \frac{e_{\mathrm{M.i}}}{e_{\mathrm{rs}}} \cdot (L_{\mathrm{H.o}} - L_{\mathrm{H.i}}) \right]$$

$$\Leftrightarrow A_{\mathrm{M.o}} = e_{\mathrm{M.o}} \left[L_{\mathrm{H.o}} - \frac{e_{\mathrm{M.i}}}{2 \cdot e_{\mathrm{rs}}} \cdot (L_{\mathrm{H.o}} - L_{\mathrm{H.i}}) \right] . \qquad \text{(II-8)}$$

These moment carrying areas must be equal $A_{\mathrm{M.i}} = A_{\mathrm{M.o}}$. Equivalent wall thicknesses for moment carrying areas are

$$A_{M.i} = \frac{A - A_N}{2} = e_{M.i} L_{H.i} + \frac{{e_{M.i}}^2}{2 \cdot e_{as}} \cdot (L_{H.o} - L_{H.i})$$

$$\Leftrightarrow {e_{\mathrm{M.i}}}^2 \cdot \frac{(L_{\mathrm{H.o}} - L_{\mathrm{H.i}})}{2 \cdot e_{\mathrm{as}}} + e_{\mathrm{M.i}} L_{\mathrm{H.i}} - \frac{A - A_{\mathrm{N}}}{2} = 0 \qquad \left| \cdot \frac{2 \cdot e_{\mathrm{as}}}{(L_{\mathrm{H.o}} - L_{\mathrm{H.i}})} \right.$$

$$\Leftrightarrow {e_{\mathrm{M.i}}}^2 + e_{\mathrm{M.i}} \frac{2 \cdot e_{\mathrm{rs}} \cdot L_{\mathrm{H.i}}}{L_{\mathrm{H.o}} - L_{\mathrm{H.i}}} - \frac{2 \cdot e_{\mathrm{as}} \cdot (A - A_{\mathrm{N}})}{2 \cdot (L_{\mathrm{H.o}} - L_{\mathrm{H.i}})} = 0 \quad .$$

(II-9)

Solving this using quadratic equation

$$e_{\mathrm{M.i}} = -\frac{e_{\mathrm{rs}} \cdot L_{\mathrm{H.i}}}{L_{\mathrm{H.o}} - L_{\mathrm{H.i}}} + \sqrt{\left(\frac{e_{\mathrm{as}} \cdot L_{\mathrm{H.i}}}{L_{\mathrm{H.o}} - L_{\mathrm{H.i}}} \right)^2 + \frac{e_{\mathrm{as}}}{L_{\mathrm{H.o}} - L_{\mathrm{H.i}}} \cdot (A - A_{\mathrm{N}})} \quad . \qquad \text{(II-10)}$$

Likewise for outer part

$$A_{\mathrm{M.o}} = \frac{A - A_{\mathrm{N}}}{2} = e_{\mathrm{M.o}} L_{\mathrm{H.o}} - \frac{{e_{\mathrm{M.o}}}^2}{2 \cdot e_{\mathrm{as}}} \cdot (L_{\mathrm{H.o}} - L_{\mathrm{H.i}}) \tag{II-11}$$

$$\vdots$$

$$e_{\mathrm{M.o}} = -\frac{e_{\mathrm{as}} \cdot L_{\mathrm{H.o}}}{L_{\mathrm{H.o}} - L_{\mathrm{H.i}}} + \sqrt{\left(\frac{e_{\mathrm{as}} \cdot L_{\mathrm{H.o}}}{L_{\mathrm{H.o}} - L_{\mathrm{H.i}}}\right)^2 - \frac{e_{\mathrm{as}}}{L_{\mathrm{H.o}} - L_{\mathrm{H.i}}} \cdot (A - A_{\mathrm{N}})} \quad . \tag{II-12}$$

To simplify equations (II-12) and (II-10) an auxiliary variable *B* is defined

$$B = \frac{e_{\mathrm{as}}}{L_{\mathrm{H.o}} - L_{\mathrm{H.i}}} \quad . \tag{II-13}$$

Now equivalent wall thicknesses for moment are

$$\begin{cases} e_{\mathrm{M.i}} = -BL_{\mathrm{H.i}} + \sqrt{(BL_{\mathrm{H.i}})^2 + B(A - A_{\mathrm{N}})} \\ e_{\mathrm{M.o}} = BL_{\mathrm{H.o}} - \sqrt{(BL_{\mathrm{H.o}})^2 - B(A - A_{\mathrm{N}})} \end{cases} . \tag{II-14}$$

Wall thickness left for normal force is

$$e_{\mathrm{N}} = e_{\mathrm{as}} - e_{\mathrm{M.i}} - e_{\mathrm{M.o}} \quad . \tag{II-15}$$

Next are defined the distanced from the centers of moment carrying areas to the edge of the area for normal force.

The distanced from the centers of moment carrying areas to the edge of the area for normal force are in Figure 6-11.

For the inner part

$$e_{\mathrm{i}} = \frac{e_{\mathrm{M.i}}}{3} \cdot \frac{L_{\mathrm{H.i}} + \frac{e_{\mathrm{M.i}}}{e_{\mathrm{as}}} \cdot (L_{\mathrm{H.o}} - L_{\mathrm{H.i}}) + 2 \cdot L_{\mathrm{H.i}}}{L_{\mathrm{H.i}} + \frac{e_{\mathrm{M.i}}}{e_{\mathrm{as}}} \cdot (L_{\mathrm{H.o}} - L_{\mathrm{H.i}}) + L_{\mathrm{H.i}}}$$

$$\Leftrightarrow e_{\mathrm{i}} = \frac{e_{\mathrm{M.i}}}{3} \cdot \frac{3 \cdot L_{\mathrm{H.i}} + \frac{e_{\mathrm{M.i}}}{e_{\mathrm{as}}} \cdot (L_{\mathrm{H.o}} - L_{\mathrm{H.i}})}{2 \cdot L_{\mathrm{H.i}} + \frac{e_{\mathrm{M.i}}}{e_{\mathrm{as}}} \cdot (L_{\mathrm{H.o}} - L_{\mathrm{H.i}})} \quad . \tag{II-16}$$

And for the outer part

$$e_{\mathrm{o}} = \frac{e_{\mathrm{M.o}}}{3} \cdot \frac{2 \cdot L_{\mathrm{H.o}} + L_{\mathrm{H.o}} - \frac{e_{\mathrm{M.o}}}{e_{\mathrm{as}}} \cdot (L_{\mathrm{H.o}} - L_{\mathrm{H.i}})}{L_{\mathrm{H.o}} + L_{\mathrm{H.o}} - \frac{e_{\mathrm{M.o}}}{e_{\mathrm{as}}} \cdot (L_{\mathrm{H.o}} - L_{\mathrm{H.i}})}$$

$$\Leftrightarrow e_{\mathrm{o}} = \frac{e_{\mathrm{M.o}}}{3} \cdot \frac{3 \cdot L_{\mathrm{H.o}} - \frac{e_{\mathrm{M.i}}}{e_{\mathrm{as}}} \cdot (L_{\mathrm{H.o}} - L_{\mathrm{H.i}})}{2 \cdot L_{\mathrm{H.o}} - \frac{e_{\mathrm{M.i}}}{e_{\mathrm{as}}} \cdot (L_{\mathrm{H.o}} - L_{\mathrm{H.i}})} \quad . \tag{II-17}$$

These equations may also be simplified using the auxiliary variable B

$$\begin{cases} e_{\mathrm{i}} = \frac{e_{\mathrm{M.i}}}{3} \cdot \frac{3 \cdot L_{\mathrm{H.i}} + \frac{e_{\mathrm{M.i}}}{B}}{2 \cdot L_{\mathrm{H.i}} + \frac{e_{\mathrm{M.i}}}{B}} \\ e_{o} = \frac{e_{\mathrm{M.o}}}{3} \cdot \frac{3 \cdot L_{\mathrm{H.o}} - \frac{e_{\mathrm{M.i}}}{B}}{2 \cdot L_{\mathrm{H.o}} - \frac{e_{\mathrm{M.i}}}{B}} \end{cases} \quad . \tag{II-18}$$

Then distance between these two centers of areas is

$$e_{\mathrm{tot}} = e_{\mathrm{i}} + e_{\mathrm{o}} + e_{\mathrm{N}} \quad . \tag{II-19}$$

APPENDIX III. PRINCIPLE OF WIRTUAL WORK

Parameters used to solve virtual displacement δ and rotations $d\varphi_1$, $d\varphi_2$ and $d\varphi_3$ are in Figure 6-12.

For clearness in this appendix mid-diameter of the header $d_{s.m}$ is marked as D. Distances a and b between angles are supposed to be constant. First angles φ_1, φ_2 and φ_3 are determined as a function of angle θ

$$\begin{cases} \varphi_1 = \dfrac{\pi - \theta}{2} \\ \varphi_2 = \dfrac{\pi}{2} \\ \varphi_3 = \dfrac{\theta}{2} \end{cases} . \tag{III-1}$$

Distances between angles comes from sine law

$$\frac{a}{\sin \varphi_3} = \frac{D}{\sin \varphi_2}$$

$$\Leftrightarrow a = \frac{D}{\sin \varphi_2} \cdot \sin \varphi_3 \tag{III-2}$$

$$\frac{b}{\sin \varphi_1} = \frac{D}{\sin \varphi_2}$$

$$\Leftrightarrow b = \frac{D}{\sin \varphi_2} \cdot \sin \varphi_1 \quad . \tag{III-3}$$

Using angles from Equation (III-1)

$$\begin{cases} a = D \cdot \sin \dfrac{\theta}{2} \\ b = D \cdot \sin \dfrac{\pi - \theta}{2} \end{cases} . \tag{III-4}$$

Dependence between the virtual displacement δ and rotations $\mathrm{d}\varphi_1$, $\mathrm{d}\varphi_2$ and $\mathrm{d}\varphi_3$ is solved using cosine law and quadratic equation

$$b^2 = a^2 + D^2 - 2 \cdot a \cdot D \cdot \cos\varphi_1$$

$$\Leftrightarrow D^2 - 2 \cdot a \cdot D \cdot \cos\varphi_1 + (a^2 - b^2)$$

$$\Leftrightarrow D = a \cdot \cos\varphi_1 \pm \sqrt{a \cdot \cos\varphi_1{}^2 - (a^2 - b^2)}\,. \qquad \text{(III-5)}$$

To calculate virtual displacements and rotations the Equation (III-5) must be differentiate

$$\delta = \mathrm{d}D = -a \cdot \sin\varphi_1 \cdot \mathrm{d}\varphi_1 + \frac{2 \cdot (a \cdot \cos\varphi_1) \cdot (-a \cdot \sin\varphi_1)}{2 \cdot \sqrt{a \cdot \cos\varphi_1{}^2 - (a^2 - b^2)}} \cdot \mathrm{d}\varphi_1$$

$$\Leftrightarrow \delta = (-a \cdot \sin\varphi_1)\left(1 + \frac{a \cdot \cos\varphi_1}{\sqrt{a \cdot \cos\varphi_1{}^2 - (a^2 - b^2)}}\right) \cdot \mathrm{d}\varphi_1 \,. \qquad \text{(III-6)}$$

Likewise for

$$a^2 = b^2 + D^2 - 2 \cdot b \cdot D \cdot \cos\varphi_3$$

$$\vdots$$

$$\Rightarrow \delta = (-b \cdot \sin\varphi_3)\left(1 + \frac{b \cdot \cos\varphi_3}{\sqrt{b \cdot \cos\varphi_3{}^2 - (b^2 - a^2)}}\right) \cdot \mathrm{d}\varphi_3 \,. \qquad \text{(III-7)}$$

Finally the virtual rotation $\mathrm{d}\varphi_2$

$$\mathrm{d}\varphi_2 = -(\mathrm{d}\varphi_1 + \mathrm{d}\varphi_3)\,. \qquad \text{(III-8)}$$

APPENDIX IV. THE EFFECT OF BRANCHES.

Used parameters are shown in Figure IV-1.

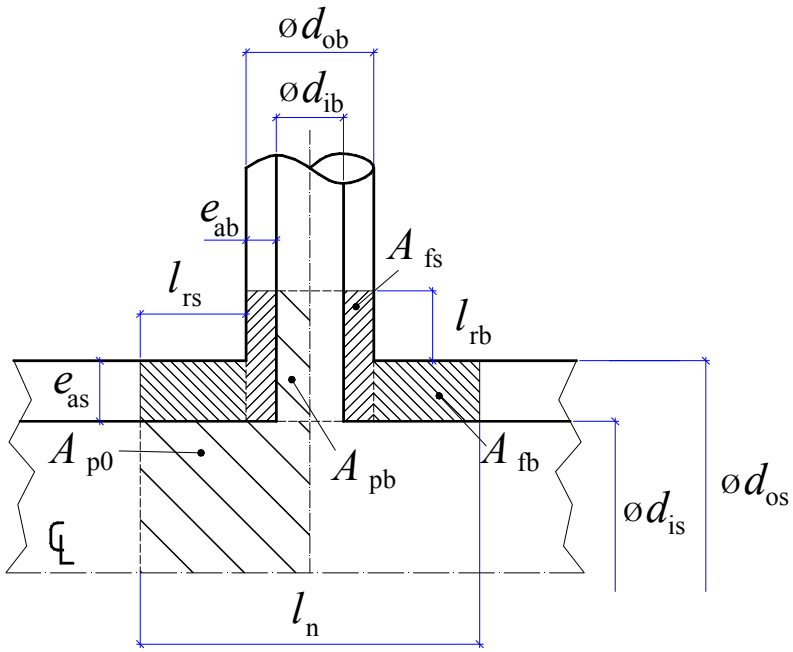

Figure IV-1.Used parameters and pressure areas.

Effective length for opening is defined as

$$l_{\mathrm{rs}} = \min\left\{\begin{matrix}\sqrt{(d_{\mathrm{is}} + e_{\mathrm{as}})e_{\mathrm{as}}} \\ \dfrac{P_0 - d_{\mathrm{ob}}}{2}\end{matrix}\right\} , \qquad \text{(IV-1)}$$

where P_0 is pitch. Likewise for the nozzle

$$l_{\mathrm{rb}} = \min\left\{\begin{matrix}\sqrt{(d_{\mathrm{ib}} + e_{\mathrm{ab}})e_{\mathrm{ab}}} \\ l_{b1}\end{matrix}\right\} . \qquad \text{(IV-2)}$$

The length of the nozzle area is

$$l_{\mathrm{n}} = d_{\mathrm{ob}} + 2 \cdot l_{\mathrm{rs}} \quad . \tag{IV-3}$$

Pressurized areas referred to header

$$A_{\mathrm{p0}} = (0.5 \cdot d_{\mathrm{ow}} + l_{\mathrm{rs}}) \cdot 0.5 \cdot d_{\mathrm{is}} \tag{IV-4}$$

and referred to branch

$$A_{\mathrm{pb}} = (0.5 \cdot e_{\mathrm{as}} + l_{\mathrm{ab}}) \cdot d_{\mathrm{ib}} \quad . \tag{IV-5}$$

Effective cross-sectional area of header

$$A_{\mathrm{fs}} = e_{\mathrm{as}} \cdot l_{\mathrm{rs}} \tag{IV-6}$$

and of branch

$$A_{\mathrm{fb}} = e_{\mathrm{ab}} \cdot (l_{\mathrm{rb}} + e_{\mathrm{as}}) \quad . \tag{IV-7}$$

The ligament efficiency for branches

$$v_{\mathrm{m}} = \frac{d_{\mathrm{is}}}{e_{\mathrm{as}}} \cdot \frac{A_{\mathrm{fs}} + \frac{f_{\mathrm{b}}}{f_{\mathrm{s}}} \cdot 2 \cdot A_{\mathrm{fb}}}{2 \cdot A_{\mathrm{p0}} + 4 \cdot A_{\mathrm{pb}} + 2 \cdot A_{\mathrm{fb}} - 2 \cdot \frac{f_{\mathrm{b}}}{f_{\mathrm{s}}} \cdot A_{\mathrm{fb}}} \quad . \tag{IV-8}$$

Final ligament efficiency that takes the possible areas between nozzle areas into account

$$v_{\mathrm{eff}} = \frac{l_{\mathrm{n}} \cdot v_{\mathrm{m}} + (P_0 - l_{\mathrm{n}})}{P_0} \quad . \tag{IV-9}$$

APPENDIX V. PUNCHING SHEAR.

The effective cross-sectional areas are shown in Figure 6-15, if $L_{M.\tau} = L_{load}$. The different widths for areas for bending moment and shear are presented in Figure 6-16.

Circumferential stress for bending moment

$$f_{\varphi.m} = \frac{\sigma_{r.m}}{2} + \frac{\sqrt{4 \cdot f_s^2 - 3 \cdot \sigma_{r.m}^2}}{2} \quad . \tag{V-1}$$

Circumferential stress for shear with the effect of circumferential stress caused by internal pressure

$$f_{\varphi.\tau} = \frac{\sigma_{r.m}}{2} - \sigma_{\varphi} + \frac{\sqrt{4 \cdot f_s^2 - 3 \cdot \sigma_{r.m}^2}}{2} \quad . \tag{V-2}$$

The bending moment as in equation (45) when $\theta = 0$ and force is marked as $F = F_M$ is

$$M(0) = \frac{F_M \cdot R}{\pi} \quad . \tag{V-3}$$

Now radius of the "bar" R comes from the mean diameter of the header

$$R = \frac{d_{m.s}}{2} \quad . \tag{V-4}$$

The cross sectional area $A_{M.\tau}$ is

$$A_{M.\tau} = L_{M.\tau} \cdot e_{M.\tau}. \tag{V-5}$$

This area is used to determine the plastic moment corresponding to the moment determined in equation (V-3). The plastic moment is

$$M_{\mathrm{p}.\tau} = A_{\mathrm{M}.\tau} \cdot f_{\varphi.\mathrm{m}} \cdot (e_{\mathrm{as}} - e_{\mathrm{M}.\tau}) \,. \tag{V-6}$$

The effective wall thickness for bending moment is solved combining the equations (V-3) and (V-6)

$$M_{\mathrm{p}.\tau} = M(0)$$

$$\Leftrightarrow L_{\mathrm{M}} \cdot e_{\mathrm{M}.\tau} \cdot f_{\varphi.\mathrm{m}} \cdot (e_{\mathrm{as}} - e_{\mathrm{M}.\tau}) = \frac{F_{\mathrm{M}} \cdot R}{\pi}$$

$$\Leftrightarrow e_{\mathrm{M}.\tau}^2 - e_{\mathrm{as}} \cdot e_{\mathrm{M}.\tau} + \frac{F_{\mathrm{M}} \cdot R}{\pi \cdot f_{\varphi.\mathrm{m}} \cdot L_{\mathrm{M}}} = 0$$

$$\Leftrightarrow e_{\mathrm{M}.\tau} = \frac{e_{\mathrm{as}}}{2} - \sqrt{\frac{e_{\mathrm{as}}^2}{4} - \frac{F_{\mathrm{M}} \cdot R}{\pi \cdot f_{\varphi.\mathrm{m}} \cdot L_{\mathrm{M}}}} \quad . \tag{V-7}$$

The wall thickness left for shear force is

$$e_{\tau} = e_{\mathrm{as}} - 2 \cdot e_{\mathrm{M}.\tau} \,. \tag{V-8}$$

Maximum shear capacity for the applied force is

$$F_{\tau} = \frac{f_{\varphi.\tau}}{\sqrt{3}} \cdot 2 \cdot e_{\tau} \cdot L_{\tau} \quad . \tag{V-9}$$

The maximum allowed force may be solved easily numerically by setting

$$F_{\tau} = F_{\mathrm{M}} \,. \tag{V-10}$$